Battery Degradation-Aware Electric Airline Planning

MSc Thesis

Duncan Lucas George Martin van Woerkom

TU Delft

Battery Degradation-Aware Electric Airline Planning

MSc Thesis Report

by

Duncan Lucas George Martin van Woerkom

to obtain the degree of Master of Science
at the Delft University of Technology
to be defended publicly on December 18, 2025 at 09:00

Thesis committee:

Chair:	Dr. M.J. (Marta) Ribeiro
Supervisors:	Dr. I.I. (Ingeborg) de Pater
	Dr.ing. P. (Pieter-Jan) Proesmans
External examiner:	Ir. P.C. (Paul) Roling
Place:	Hall N, Faculty of Aerospace Engineering, Delft
Project Duration:	February, 2025 - December, 2025
Student number:	4878914

An electronic version of this thesis is available at `http://repository.tudelft.nl/`.

Faculty of Aerospace Engineering · Delft University of Technology

Preface

This thesis marks the end of my studies at the Delft University of Technology, and with that my time as a student comes to a close. I have truly enjoyed these years and have grown along the way. I have had the chance to meet many different and inspiring people, and these experiences have helped shape me as both a person and a professional. I now feel ready for the years ahead and look forward to the challenges that will come.

The past ten months of my life has been dedicated to this work. The topic quickly drew me in, and I genuinely enjoyed the time I spent working on it and will treasure the experience it has given me. I am very happy with the final result and hope the enthusiasm behind it is reflected throughout this thesis.

I would like to express my sincere gratitude to all the people who supported me along the way. I am especially grateful to my supervisors, Ingeborg and Pieter-Jan, whose guidance, support, and thoughtful feedback helped shape the direction and quality of this work. I also want to thank my friends and family for being there to discuss ideas, offer advice, and share many moments of fun.

Duncan van Woerkom
Delft, December 2025

Summary

Aviation is a major contributor to global warming and so pathways for decarbonization need to be explored. As battery technology advances, electric regional aviation emerges as a viable option. A key challenge, however, is that the aircraft batteries degrade over time, progressively restraining the operational capability of electric aircraft. Current approaches do not account for this effect. To address this gap, this research presents the Battery Degradation-Aware Electric Fleet Assignment framework that enables the integration of battery ageing into tactical scheduling. It does this by combining a rolling-horizon fleet assignment model with a battery degradation module that predicts and updates each aircraft's state of health based on its flown missions, with battery replacement scheduled according to designated strategies to ensure continuity of operations. This framework is evaluated with five distinct experiments, tested on the *KLM Cityhopper* network and complemented by an additional case study for validation. The experiments validate the framework's operational and degradation dynamics and demonstrate that battery degradation has a significant impact, with depreciation costs amounting to 0.91 €/km flown. Degradation reduces fleet range capability, lowering ASKs by 0.96%, revenue by 0.76%, and increasing total operating costs by 9.1% as battery replacements become necessary. The sensitivity analysis indicates that future battery price scenarios can make or break profitability. Consequently, operational models that ignore degradation effects will overstate the profitability of electric aircraft.

Contents

1

Research Proposal

This section discusses the research proposal that guides the remainder of the research. It begins by identifying the research gap based on the preceding literature study, after which the central research question is formulated along with several sub-questions and a final research objective. The proposed work aims to integrate battery degradation modeling with uncertainty quantification into a rolling horizon fleet assignment framework for battery-electric aircraft. The outcomes of this research are expected to provide a foundational methodology for battery degradation-aware electric fleet planning, supporting future developments in sustainable and efficient airline operations.

Research Gap Analysis

A wide range of literature was examined to identify the current state of research on battery-electric aviation. While many studies address either battery degradation or airline operations, few attempt to combine these domains, particularly in the context of electric passenger aircraft. As summarized in Table 1.1, each of the most relevant studies contributes to specific areas, but none jointly capture the dynamic interaction between battery ageing and operational decision-making at the fleet level.

Table 1.1: Coverage of Key Topics Across Literature and the Research. Symbols indicate: ✓ = addressed, – = mentioned or partially adressed, no mark = not adressed.

	Electric Aviation	**Battery Degradation**	**Uncertainty in Degradation**	**Operational Airline Modelling**	**Range Estimation**
van Oosterom et al. (2023) [1]	✓	–		✓	
Paek et al. (2019) [2]	✓	✓			–
He et al. (2022) [3]		✓	✓		
Hoogreef et al. (2023) [4]	✓			✓	✓
Chan et al. (2024) [5]	✓			✓	
Wolleswinkel et al. (2024) [6]					
de Vries et al. (2024) [7]	✓	–		–	✓
This Research	✓	✓	✓	✓	✓

The papers by *Wolleswinkel et al. (2024)* [6] and *de Vries et al. (2024)* [7], authored by members of Elysian, who are also collaborators in this research, lay the foundation for the technical feasibility and conceptual design of large battery-electric aircraft. Their work highlights several design and performance challenges but does not address these predictive operational models that account for battery degradation over time in detail. To date, no research integrates both degradation modeling and operational planning in a manner that systematically propagates battery degradation effects into aircraft performance metrics, such as range, within fleet optimization or scheduling frameworks. While recent advances validate the

technical feasibility of large battery-electric passenger aircraft, a critical gap remains in modeling how battery degradation with its uncertainty quantification impacts aircraft performance and fleet-level operational decisions. Addressing this gap is essential to unlock the full environmental and economic potential of electric aviation.

Research Proposal

Taking the complete Literature Study into consideration, the overarching research question is:

> *"How can battery degradation and ageing be systematically incorporated into an electric fleet assignment model to optimize realistic operational and economic performance over time?"*

This study aims to develop a fleet assignment framework for battery-electric aircraft that explicitly accounts for battery degradation and ageing processes over time. The resulting model will support strategic and operational decision-making regarding aircraft deployment, battery replacement, and long-term performance forecasting. A rolling horizon methodology will be employed to adjust fleet assignments based on the evolving battery health of the aircraft, thereby enabling ageing-aware optimization of future electric airline operations.

To address this research question, the following research (sub-)questions are proposed:

1. **How can battery degradation be modeled to accurately estimate electric aircraft performance and range over time?**
   Metrics: State of Health (SoH), Achievable Range

2. **What are the main cost drivers of battery systems in electric aircraft, and how do different replacement strategies impact their lifecycle cost per flight hour?**
   Metrics: Lifecycle Cost per Flight Hour (LCC/FH)

3. **What are optimal battery replacement thresholds based on aircraft mission profiles and economic trade-offs?**
   Metrics: End-of-Life (EoL) Threshold

4. **How can predictive models of battery degradation, including uncertainty quantification, be optimally integrated into a rolling horizon fleet assignment framework?**
   Metrics: Computational Performance, Optimal Prediction Horizon, Planning Outcomes

5. **What is the impact of ageing-aware electric fleet assignment on airline-level performance metrics CASK and RASK?**
   Metrics: Revenue per Available Seat Kilometer (RASK), Cost per Available Seat Kilometer (CASK)

6. **How do utilization strategies affect battery longevity and long-term fleet economics in electric operations?**
   Metrics: Battery Cycle Life, % of Flights with >70% DoD, Long-Term Cost Efficiency

Together, these questions span the data-driven modelling of battery degradation, its integration into operational optimization, and the evaluation of system-level and economic impacts. The scope is aligned with the context of electric regional aircraft operations, with specific reference to the 90-passenger concept developed by Elysian Aircraft.

Research Objective

On the basis of the identified research gap and literature study, the objective of this thesis is:

> *"To develop a rolling horizon fleet assignment model for battery-electric aircraft that integrates battery degradation and ageing. The model aims to support optimal and realistic operational planning and battery replacement strategies, with a focus on maintaining aircraft performance and maximizing long-term profits."*

References for Research Proposal

[1] Simon van Oosterom et al. “Optimizing the Battery Charging and Swapping Infrastructure for Electric Short-Haul Aircraft—The Case of Electric Flight in Norway”. In: *Transportation Research Part C: Emerging Technologies* 155 (2023), p. 104313. DOI: 10.1016/j.trc.2023.104313. URL: https://doi.org/10.1016/j.trc.2023.104313.

[2] Sung Wook Paek et al. “Impact of Battery Degradation on Lifetime Ranges of Electric Aircraft and Unmanned Underwater Vehicles”. In: *2019 IEEE Conference on Control Technology and Applications (CCTA)*. IEEE. Hong Kong, China, Aug. 2019.

[3] Haowei He et al. “EVBattery: a Large-Scale electric vehicle dataset for battery health and capacity estimation”. In: *arXiv (Cornell University)* (Jan. 2022). DOI: 10.48550/arxiv.2201.12358. URL: https://arxiv.org/abs/2201.12358.

[4] M. F. M. Hoogreef et al. “Coupled Hybrid & Electric Aircraft Design and Strategic Airline Planning”. In: *AIAA AVIATION 2023 Forum*. AIAA 2023-3869. American Institute of Aeronautics and Astronautics (AIAA), 2023. DOI: 10.2514/6.2023-3869.

[5] Ben Chan et al. “Optimizing Fleet Assignment Decisions for Regional Airlines with Hybrid Electric Aircraft Uptake”. In: (2024). Preprint.

[6] Rob E. Wolleswinkel et al. “A New Perspective on Battery-Electric Aviation, Part I: Reassessment of achievable range”. In: *AIAA SCITECH 2022 Forum* (Jan. 2024). DOI: 10.2514/6.2024-1489. URL: https://doi.org/10.2514/6.2024-1489.

[7] R. de Vries et al. “A New Perspective on Battery-Electric Aviation, Part II: Conceptual Design of a 90-Seater”. In: *Proceedings of the AIAA SciTech 2024 Forum*. Article AIAA 2024-1490. Orlando, Florida, United States: American Institute of Aeronautics and Astronautics (AIAA), 2024. DOI: 10.2514/6.2024-1490.

2

Research Trajectory

The development of this research was not a linear process. Its direction and focus evolved significantly as my understanding of the topic deepened and the possibilities of the research became clearer. The initial aim was clear: to find a methodology to integrate battery degradation into electric airline planning. Early work therefore focused on understanding, developing, and testing advanced battery degradation prognostics, while in parallel exploring the basics of electric airline planning to understand how such predictions could be used operationally and what battery degradation would mean for electric airline operations.

As the degradation prognostics improved, it became clear that the main challenge of this research was shifting. The large uncertainty surrounding future electric-aircraft batteries meant that highly detailed prediction techniques were not always meaningful. Instead, the role of electric airline operation modelling grew in importance. Understanding how degradation influences scheduling, utilisation, and fleet-level decisions proved far more relevant to the problem at hand.

This shift in focus broadened the study. New components such as maintenance strategies, battery depreciation and synthetic physics-based battery data generation were introduced, gradually bringing together elements that were not anticipated at the start. As these pieces aligned, the methodology became increasingly advanced, to the point where it no longer only structured the problem but also enabled a practical solution. In this process, a second goal of the research emerged: not only to develop the framework itself, but also to use it to evaluate the broader implications of degradation-aware planning. This strengthened the overall framework and ultimately led to a more complete and integrated study than originally envisioned.

In the end, the research advanced far beyond its initial scope, bringing together technical, operational, and economic elements into a unified whole. This evolution not only strengthened the findings but also provides a foundation for future work on electric airline operations as the technology continues to develop.

3

Scientific Article

Battery Degradation-Aware Electric Airline Planning

D.L.G.M. van Woerkom

MSc. Student, Faculty of Aerospace Engineering, Delft University of Technology

Abstract

Aviation is a major contributor to global warming and so pathways for decarbonization need to be explored. As battery technology advances, electric regional aviation emerges as a viable option. A key challenge, however, is that the aircraft batteries degrade over time, progressively restraining the operational capability of electric aircraft. Current approaches do not account for this effect. To address this gap, this research presents the Battery Degradation-Aware Electric Fleet Assignment framework that enables the integration of battery ageing into tactical scheduling. It does this by combining a rolling-horizon fleet assignment model with a battery degradation module that predicts and updates each aircraft's state of health based on its flown missions, with battery replacement scheduled according to designated strategies to ensure continuity of operations. This framework is evaluated with five distinct experiments, tested on the *KLM Cityhopper* network and complemented by an additional case study for validation. The experiments validate the framework's operational and degradation dynamics and demonstrate that battery degradation has a significant impact, with depreciation costs amounting to 0.91 €/km flown. Degradation reduces fleet range capability, lowering ASKs by 0.96%, revenue by 0.76%, and increasing total operating costs by 9.1% as battery replacements become necessary. The sensitivity analysis indicates that future battery price scenarios can make or break profitability. Consequently, operational models that ignore degradation effects will overstate the profitability of electric aircraft.

1 Introduction

The aviation industry plays a vital role in global connectivity. Over the last century our modern society has become immensely reliant on air travel, and this trend is expected to continue to grow in the coming decades [1]. However, this reliance takes a significant toll on the environment. Aviation is a top global warming contributor with roughly 2–3% of global CO_2 emissions [2], and its climate footprint is further amplified by nitrogen oxides, water vapour, and contrail-induced cloud formation. This underscores the necessity to reduce emissions in line with international climate targets, such as the Paris Agreement [3].

In response, researchers and industry leaders are searching for more sustainable decarbonization pathways for aviation. Some of these, such as sustainable aviation fuels, are already in use, while others remain in early stages of development or concept phases and still have significant hurdles to overcome. Among these pathways battery-electric aviation emerges as an option, with the potential to electrify a large share of global flights [4, 5]. Yet, substantial hurdles remain. Most notably the low specific energy, which severely constrains the potential range of aircraft. Jet A-1 fuel holds a specific energy around 12,000 Wh/kg, while the highest lithium-ion cells only reach 250-300 Wh/kg. Additionally, there are durability trade-offs and safety requirements for aviation which can limit battery capacity [6].

Fortunately, battery technology is developing rapidly and their specific energy has increased by fivefold over the past 30 years [7], mostly due to lithium-ion batteries, with improvements still expected to come in lithium-ion and also other novel compositions. Although future trajectories are unlikely to match past advances, even modest gains could alleviate the energy density limitation and bring regional aviation closer to mirroring the rapid transition of electric cars from a niche to a dominant market segment [6].

However, the limited energy density of batteries is additionally strained by battery degradation, which reduces the amount of usable capacity over time. With any rechargeable device, the usage patterns and time-based factors wear down the usable energy density. This effect could be very consequential in electric aviation, where an aircraft can undergo numerous deep-discharges a day. As a result, an electric aircraft that had sufficient range for certain routes one week might no longer meet those requirements the next week due to reduced range.

Battery degradation primarily affects both battery capacity and power, and arises from electrochemical and mechanical processes inside the cell, where repeated lithium intercalation gradually induces material strain and long-term structural changes [6, 8, 9]. To cope with this degradation, many battery-reliant systems use mathematical, physical or machine learning models to predict how the battery State of Health (SoH) evolves over time and impacts its usable capacity [10]. A wide variety of methods exist, which are each applicable to numerous different situations depending on the required level of detail and data availability, ranging from electrochemical models at the cell level, to high level SoH forecasting based on operational history [11–13]. This diversity gives a broad range of methods to support the SoH prediction of electric aircraft battery capacity and bring insights on the effect on aircraft range.

For electric aviation, battery SoH becomes an operationally limiting factor because each aircraft's range decreases as its battery ages. This creates a fleet with heterogeneous capabilities over time, meaning that the set of feasible flights can change from week to week. As a result, schedules that are optimal for a fresh fleet may no longer be feasible once degradation accumulates, for example when simultaneous long-range flights require more high-SoH aircraft than are available. This directly conflicts with conventional fleet assignment models, which assume constant and uniform aircraft performance [14, 15]. This raises new questions about routing and battery replacement maintenance strategies for an ageing fleet.

While electric aircraft operations have been studied in several recent works [16, 17], the effects of battery degradation within these models remain underexplored. Studies predict the high-level impacts of battery degradation costs and replacement necessities [4, 5, 18], but current approaches do not capture integration of battery degradation effects throughout tactical planning, limiting their capacity to create realistic schedules and flight assignments or measure the degradation consequences in detail.

Therefore, this research aims to address the gap in electric airline operations modelling by developing the Battery Degradation-Aware Electric Fleet Assignment (BDAEFA) framework, which systematically integrates battery ageing into tactical airline planning. With the framework established, the second objective is to quantify how battery degradation shapes the long-term operations and economics of electric aviation. This work is carried out in collaboration with *Elysian Aircraft* [19], who offered insights into their conceptual *E9X* aircraft and contributed their expertise on the subject.

The remainder of this paper is organized as follows. The methodology of the BDAEFA framework is presented in Chapter 2. Chapter 3 elaborates on the economic formulation of the research. Chapter 4 introduces the case study used to evaluate the model, and Chapter 5 presents and interprets the results of the experiments. Finally, the conclusions and future research recommendations are discussed in Chapter 6.

2 Methodology

This chapter presents the methodology of the BDAEFA framework. Beyond describing the current implementation, the framework is also intended as a blueprint for future research. It outlines a generalizable modelling structure that can incorporate more advanced degradation models, operational strategies, or maintenance policies as technological understanding evolves.

The following sections describe the framework in detail. Section 2.1 introduces the overarching system architecture using the rolling-horizon methodology. Section 2.2 elaborates on the Electric Fleet Assignment Model (EFAM). Section 2.3 and Section 2.4 describe the degradation prediction and range estimation components. Section 2.5 presents the battery replacement maintenance strategies.

2.1 Battery Degradation-Aware Electric Fleet Assignment Framework

This section outlines the high-level structure of the BDAEFA framework. It starts by introducing the framework architecture in Subsection 2.1.1 and the high-level assumptions made for its design in Subsection 2.1.2.

2.1.1 BDAEFA Architecture

The BDAEFA framework is executed as an iterative simulation running in discrete weekly horizons H_t following a rolling-horizon structure, which allows the model to update aircraft states between horizons and capture the effects of battery degradation over time. The overall model architecture is shown in Figure 1, which visualises the sequence of steps performed during each horizon. Each component in the flowchart corresponds to a dedicated section discussed later in this chapter.

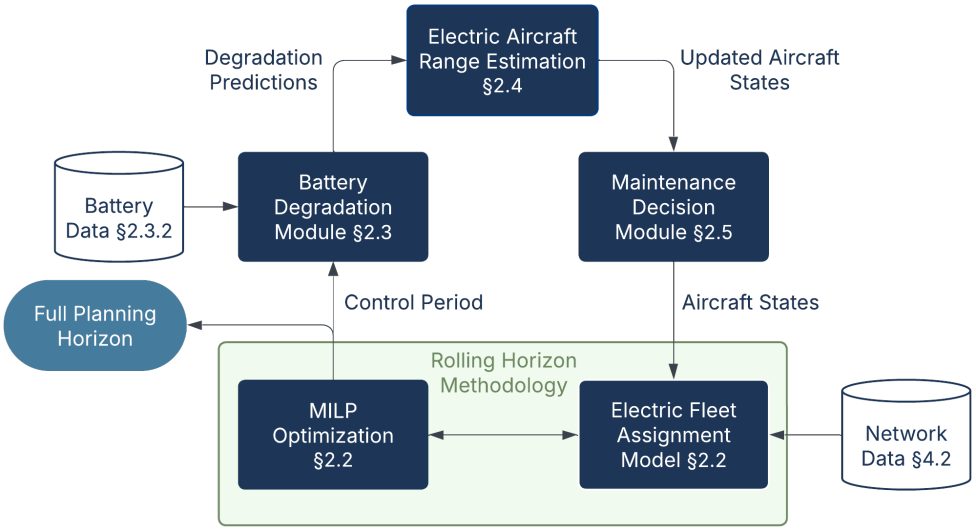

Figure 1: *Simplified overview of the system, illustrating the interaction between components.*

At the start of each horizon the model initializes the fleet using the updated aircraft states from the previous horizon or the initial fleet state provided at the beginning of the simulation. The EFAM is then solved for one full horizon, assigning specific aircraft to the selected flights. In the first horizon, the model selects from a dense schedule the set of flights that form the tactical base schedule for the simulation. In all subsequent horizons, the optimizer receives this fixed set of flights and assigns aircraft to them based on their evolving battery states,

though the optimizer may leave flights unassigned if necessary due to battery health. The resulting plan for each horizon is used to compute mission-level metrics, after which aircraft states are updated through degradation predictions based on the flights operated. Following this update, the aircraft's maximum range is recalculated and the chosen maintenance policy evaluates whether a battery replacement should be carried out. These updated states form the input to the next horizon, and the process repeats, as displayed in Figure 2, until the full simulation period has elapsed.

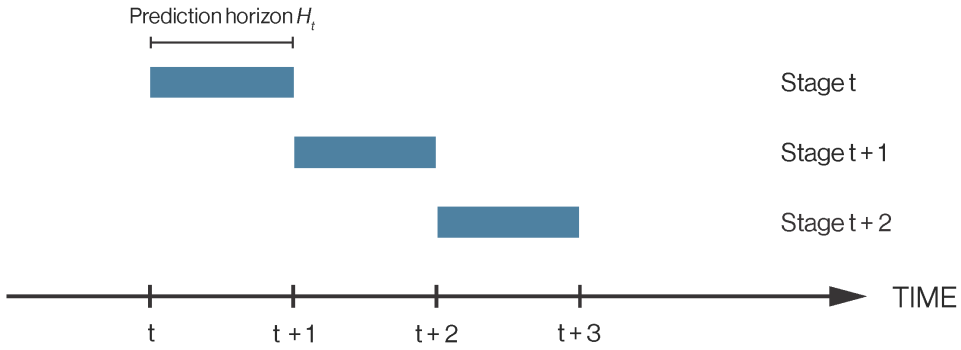

Figure 2: *Illustration of the rolling-horizon methodology.*

2.1.2 Framework Assumptions and Simplifications

This subsection presents the general modelling assumptions and simplifications in Table 1 that enable the framework to represent realistic electric aviation operations in an efficient and generalizable manner. These were chosen to support the first integrated design of a battery degradation–aware electric airline model.

Table 1: *Overview of general modelling assumptions and simplifications.*

ID	Description
A1	Each simulation horizon represents one operational week with fixed demand patterns.
A2	The operational schedule is discretized into 20-minute time buckets with departures between 06:00–22:00.
A3	Range degradation is fully determined by battery SoH.
A4	The battery is fully charged to 100% during each turnaround.
A5	Battery replacement removes the aircraft from operation for one full planning week.
A6	During battery replacement downtime, regular maintenance is performed.
A7	Maintenance decisions follow designated rule-based maintenance policies rather than optimisation.
A8	Flights operate under nominal conditions with no wind effects.

2.2 Electric Fleet Assignment Model

This section formulates the EFAM as a Mixed Integer Linear Programming (MILP) problem that determines aircraft-to-flight assignments and passenger allocations within each planning horizon. The formulation integrates operational, physical, and economic constraints and is solved iteratively within the rolling-horizon methodology. Its objective, presented in Subsection 2.2.3, maximizes total profit by balancing itinerary revenues against operating, lease, and battery-related costs. The remainder of this section introduces the notation, describes the model structure, and outlines the constraint set.

2.2.1 EFAM Notation

This section defines the sets, decision variables, and parameters with Table 2 used throughout the EFAM.

Electric Fleet Assignment Model Notation	
Sets	
N	Set of airports, indexed by $n \in N$
F	Set of candidate flights, indexed by $f \in F$
T	Set of aircraft tails, indexed by $t \in T$
$\mathcal{T}$	Set of time buckets, indexed by $\tau \in \mathcal{T}$
OD	Set of valid origin–destination pairs (i, j) with $i, j \in N,\ i \neq j$
R	Set of passenger itineraries, indexed by r
$\mathcal{D}$	Set of days in the week, indexed by d
Decision and State Variables	
$y_{ft} \in \{0, 1\}$	1 if flight f is operated by tail t
$p_r \in \mathbb{R}_+$	Passengers assigned to itinerary r
$S_{n,\tau,t} \in \{0, 1\}$	1 if aircraft t is at airport n in time bucket τ
Parameters	
$D_{ij} \in \mathbb{Z}_+$	Weekly passenger demand between airports i and j
$LF \in [0, 1]$	Target load factor
$s_f \in \mathbb{Z}_+$	Seat capacity of flight f
$\bar{y}_{ij} \in \mathbb{R}_+$	Yield between i and j (€/RPK)
p_{elec}, $p_{\text{CO}_2} \in \mathbb{R}_+$	Energy and carbon price parameters
$\hat{E}_f \in \mathbb{R}_+$	Nominal energy of flight f (kWh)
$E_{f,t} \in \mathbb{R}_+$	SoH-adjusted energy use of flight f by tail t (kWh)
$\text{SoH}_t \in (0, 1]$	State of Health of tail t
$\kappa \in \mathbb{R}_+$	Degradation multiplier calibration parameter
$d_f \in \mathbb{R}_+$	Distance of flight f (km)
o_f, $dest_f$	Origin and destination of flight f
τ_f^{dep}, τ_f^{arr}	Departure and arrival time buckets
$\text{dur}_f \in \mathbb{Z}_+$	Duration of flight f (time buckets)
$R_t \in \mathbb{R}_+$	Maximum range of tail t (km)
$S_{n,t}^{\text{init}} \in \{0, 1\}$	Initial location of aircraft t at the start of the horizon
$H \subseteq N$	Subset of designated hub airports
$\pi_r \in \mathbb{R}_+$	Revenue per passenger for itinerary r (€)
$c_{f,t}^{op}$, $c_{f,t}^{en}$, $c_{f,t}^{CO_2} \in \mathbb{R}_+$	Operating, electricity, and carbon costs of flight f by tail t (€)
$c^{\text{lease}} \in \mathbb{R}_+$	Lease cost per planning period (€)
$\delta_t \in \mathbb{R}_+$	Battery depreciation rate for tail t (€/km)
$\beta,\ \alpha,\ \gamma \in \mathbb{R}_+$	Yield–distance model parameters
$\text{Cap}_{ij}(d) \in \mathbb{Z}_+$	Daily passenger cap for OD pair (i, j) on day d

Table 2: *Notation used in the EFAM*

2.2.2 Model Overview

The EFAM formulates the aircraft-to-flight assignment problem as a MILP operating on a space–time network defined over the set of airports N, candidate flights F, aircraft tails T, and discrete time buckets $\mathcal{T}$. The assignment is made from a pre-generated schedule, where for each 20-minute time bucket $\tau \in \mathcal{T}$ and origin airport $n \in N$, all feasible destination options are considered as candidate flights.

This time–space network, illustrated in Figure 3, captures the progression of aircraft positions over time. Nodes represent specific airport–time combinations $(n, \tau) \in N \times \mathcal{T}$, and arcs indicate either flight movements, ground operations, or overnight stays between nodes. This structure enables explicit tracking of aircraft positions for each tail $t \in T$ across airports and time periods, ensuring that only feasible flight sequences are assigned. In this formula-

tion an itinerary represents an Origin–Destination (OD) connection offered to passengers and corresponds to a single direct flight in the networks analysed in this work, while the general framework also allows itineraries to contain multiple legs in larger or more complex networks. A flight is the individual leg in the time–space network on which the model evaluates aircraft movements and their associated operating costs.

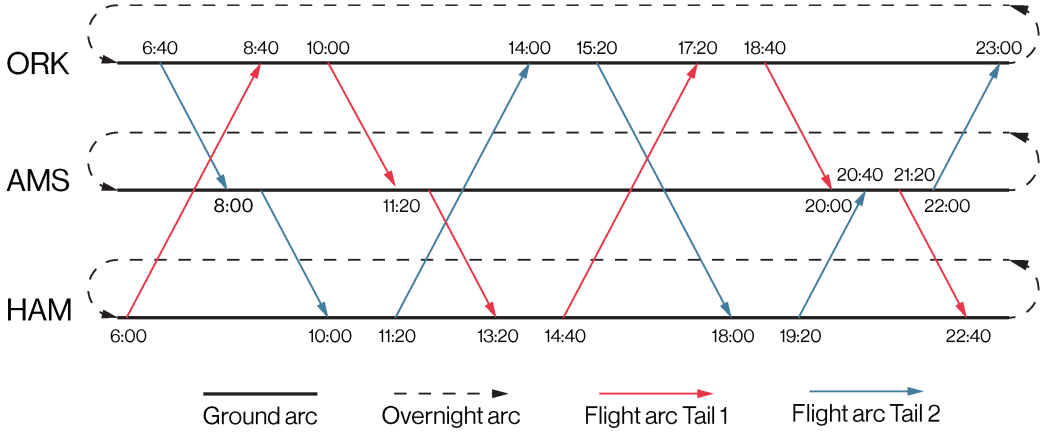

Figure 3: *Illustration of a time-space network with two separate aircraft tails.*

2.2.3 Objective Function

This subsection introduces the objective function that determines the EFAM decisions. The model aims to maximize total profit. The objective function in Equation 1 integrates revenues, operating costs, lease expenses, and battery depreciation to identify the most efficient passenger and aircraft assignments within each simulation horizon.

$$\max \underbrace{\sum_{r \in R} \pi_r \, p_r}_{\text{Revenue}} - \underbrace{\sum_{f \in F} \sum_{t \in T} \left(c^{\text{op}}_{f,t} + c^{\text{en}}_{f,t} + c^{\text{CO}_2}_{f,t} \right) y_{ft}}_{\text{Operating Costs}} - \underbrace{c^{\text{lease}} \, |T|}_{\text{AC Lease Costs}} - \underbrace{\sum_{f \in F} \sum_{t \in T} \delta_t \, d_f \, y_{ft}}_{\text{Battery Depreciation}} \tag{1}$$

The first term in Equation 1 represents the total revenue gained from passenger itineraries. Each itinerary $r \in R$ connects an OD pair and carries an associated passenger flow p_r. The total revenue is determined by multiplying the number of passengers assigned to each itinerary by its corresponding fare π_r using Equation 2, which depends on travel distance and yield.

$$\pi_r = \bar{y}_{o_r d_r} \cdot d_{o_r d_r} \qquad \forall r \in R \tag{2}$$

Here, $d_{o_r d_r}$ denotes the total itinerary distance, and $\bar{y}_{o_r d_r}$ is the average yield per revenue passenger-kilometer. The yield follows the relation in Equation 3, which decreases with distance to reflect that shorter flights generally exhibit higher fares per kilometer, since fixed costs and a larger share of non-cruise time are spread over fewer flown kilometers [20].

$$\bar{y}_{ij} = \beta \, d_{ij}^{-\alpha} + \gamma \qquad \forall (i,j) \in OD \tag{3}$$

Parameters β, α, and γ define the scale, distance sensitivity, and minimum yield level, respectively. The values are calibrated using real flight cost data from the *KLM Cityhopper*

network described in Section 3.1. The resulting function does not aim to reproduce exact fares for each OD pair but provides a consistent and sufficiently accurate approximation of average yields across the network.

The second term in the objective function captures the operating costs associated with assigning flight f to aircraft t. These costs are decomposed into three components: a general operating cost $c^{\text{op}}_{f,t}$, an electricity cost $c^{\text{en}}_{f,t}$, and a carbon allowance cost $c^{\text{CO}_2}_{f,t}$. The three components are given in Equation 4–Equation 6.

$$c^{\text{op}}_{f,t} = c_{\text{fixed}} + c_{\text{time}} \cdot \text{dur}_f \qquad \forall f \in F,\, t \in T \tag{4}$$

$$c^{\text{en}}_{f,t} = p_{\text{elec}}\, E_{f,t} \qquad \forall f \in F,\, t \in T \tag{5}$$

$$c^{\text{CO}_2}_{f,t} = p_{\text{CO}_2}\, E_{f,t} \qquad \forall f \in F,\, t \in T \tag{6}$$

The general operating cost $c^{\text{op}}_{f,t}$ aggregates all non-energy expenses associated with flight f, including crew, navigation, airport, and ground handling. The electricity and carbon allowance components scale with the SoH-adjusted energy requirement $E_{f,t}$ shown in Equation 7. The values p_{elec} and p_{CO_2} denote the electricity price per kWh and the carbon allowance price per ton of CO_2 emissions. All economic parameters are specified in Chapter 3.

$$E_{f,t} = \hat{E}_f\, \phi(\text{SoH}_t) \qquad \phi(\text{SoH}_t) = 1 + \kappa(1 - \text{SoH}_t) \tag{7}$$

The term $\hat{E}_f$ represents the nominal mission energy demand for a fresh battery, and the multiplier $\phi(\text{SoH}_t)$ captures the additional energy required as the battery state decreases. The parameter κ is set such that 90% SoH corresponds to a 6% increase in required charge energy, providing a conservative efficiency adjustment [21, 22].

The third term represents aircraft lease costs and appears as a constant, since the model assumes a fleet of fixed size throughout all simulations. As outlined in Appendix A, an adjustment can be made when fleet activation is modelled endogenously.

The final term accounts for battery depreciation. As aircraft operate, cumulative distance flown contributes to gradual capacity loss and reduced residual value. This is represented in the objective function through a per-kilometer depreciation rate δ_t applied to each operated flight $f \in F$. The calculated depreciation is used for the funding of battery replacement maintenance events. A more detailed description of the underlying depreciation mechanism is provided in Subsection 2.5.2.

2.2.4 Constraints

This subsection introduces the full set of mathematical constraints that define the feasible space of the MILP model. They govern aircraft routing, resource utilisation, timing, and passenger flow to ensure operational, physical, and commercial consistency.

The routing logic begins by tracking each aircraft's position throughout the planning horizon. The binary state variable $S_{n,\tau,t}$ indicates whether aircraft $t \in T$ is at airport $n \in N$ in time bucket $\tau \in \mathcal{T}$. Initial locations are specified by the parameter $S^{\text{init}}_{n,t}$, which equals 1 when aircraft t starts at airport n. The initial conditions in Equation 8 and Equation 9 ensure that each aircraft begins at exactly one valid airport.

$$S_{n,0,t} = S^{\text{init}}_{n,t} \qquad \forall n \in N,\, t \in T \tag{8}$$

$$\sum_{n \in N} S_{n,0,t} = 1 \qquad \forall t \in T \tag{9}$$

The stock of each aircraft throughout the planning horizon is tracked using flow-balance constraints. Flights are represented by the binary assignment variable y_{ft}. Each flight f has an origin o_f, a destination dest_f, and departure and arrival time buckets τ_f^{dep} and τ_f^{arr}.

Equation 10 updates aircraft presence across airports and time buckets by adding arrivals and subtracting departures.

$$S_{n,\tau,t} = S_{n,\tau-1,t} + \sum_{\substack{f \in F \\ \text{dest}_f = n \\ \tau_f^{\text{arr}} = \tau - 1}} y_{ft} - \sum_{\substack{f \in F \\ o_f = n \\ \tau_f^{\text{dep}} = \tau - 1}} y_{ft} \qquad \forall n \in N,\, \tau \in \mathcal{T} \setminus \{0\},\, t \in T \tag{10}$$

Together, Equation 8–Equation 10 define aircraft initialisation and movement in the time–space network. The model then applies several operational constraints that govern aircraft sequencing, utilisation, range feasibility, and end-of-week positioning.

Equation 11 enforces the minimum turnaround time between consecutive flights operated by the same aircraft $t \in T$. If two flights f_1 and f_2 share the same airport ($\text{dest}_{f_1} = o_{f_2}$) and their scheduled arrival–departure interval is shorter than the required turnaround time TAT, both flights cannot be assigned to the same aircraft.

$$y_{f_1,t} + y_{f_2,t} \leq 1 \qquad \forall f_1, f_2 \in F,\, t \in T :\ \text{dest}_{f_1} = o_{f_2},\ 0 \leq \tau_{f_2}^{\text{dep}} - \tau_{f_1}^{\text{arr}} < TAT \tag{11}$$

Equation 12 limits the total scheduled block time for each aircraft over the planning horizon. The cumulative block time, calculated as the sum of operated flight durations dur_f, cannot exceed the aircraft-specific maximum threshold $BT^{\max}$. Here, dur_f represents the duration of flight f, expressed in time buckets, and includes airborne time derived from distance and cruise speed as well as fixed taxi, take-off, and landing components.

$$\sum_{f \in F} \text{dur}_f\, y_{ft} \leq BT^{\max} \qquad \forall t \in T \tag{12}$$

Battery degradation directly affects aircraft range and thus constrains flight feasibility. To ensure that degraded aircraft are not assigned to routes beyond their capability, Equation 13 restricts the assignment variable y_{ft} such that a flight $f \in F$ can only be operated by aircraft t if its route distance d_f does not exceed the current degradation-adjusted range limit R_t.

$$y_{ft} = 0 \qquad \forall f \in F,\, t \in T :\ d_f > R_t \tag{13}$$

At the end of each planning horizon, every aircraft must return to a designated hub airport. This requirement ensures operational continuity across subsequent horizons and prevents aircraft from being stranded at remote locations, which could occur if their degradation-reduced range R_t no longer allows any feasible outbound flights. To enforce this, Equation 14 requires that each aircraft $t \in T$ is positioned at one of the designated hub airports $H \subseteq N$ during the final time bucket τ^{final}.

$$\sum_{n \in H} S_{n,\tau^{\text{final}},t} = 1 \qquad \forall t \in T \tag{14}$$

Together, the constraints from Equation 11-Equation 14 ensure operationally feasible aircraft sequencing, range compliance, and end-of-horizon recoverability.

Equation 15 enforces that each flight $f \in F$ can be operated by at most one aircraft, ensuring exclusivity in the assignment and avoiding duplicate scheduling.

$$\sum_{t \in T} y_{ft} \leq 1 \qquad \forall f \in F \tag{15}$$

Ideally, passenger assignment would be constrained by *daily* demand data to capture day-specific travel patterns. As only weekly OD demand data is available for the case studies in this research, the model applies a *weekly* demand limit through Equation 16, complemented by daily caps in Equation 17 to approximate a realistic temporal distribution of passengers.

Equation 16 limits the total number of passengers assigned to each origin–destination pair $(i, j) \in OD$ across all itineraries $r \in R$. Here, p_r denotes the passenger flow assigned to itinerary r, and D_{ij} is the total weekly passenger demand between airports i and j provided as model input. The constraint ensures that passenger assignments for an OD market remain within the available demand.

$$\sum_{\substack{r \in R \\ o_r = i,\, d_r = j}} p_r \;\leq\; D_{ij} \qquad \forall (i,j) \in OD \tag{16}$$

To prevent the optimizer from concentrating weekly demand on a single day, daily cap constraints are introduced in Equation 17. These caps limit the number of passengers that can be assigned to each origin–destination pair $(i, j) \in OD$ on day $d \in \mathcal{D}$. They are calibrated so that the tiered caps spread both low- and high-demand OD markets across the week, preventing concentration on a single day or, for higher-demand markets, only a few days. In this constraint, p_r denotes the passenger flow on itinerary r, $\mathrm{day}(r)$ maps each itinerary to its departure day, the left-hand side aggregates all passengers departing on day d, and $\mathrm{Cap}_{ij}(d)$ specifies the maximum permitted.

$$\sum_{\substack{r \in R \\ o_r = i,\, d_r = j,\, \mathrm{day}(r) = d}} p_r \;\leq\; \mathrm{Cap}_{ij}(d) \qquad \forall (i,j) \in OD,\, d \in \mathcal{D} \tag{17}$$

The daily cap $\mathrm{Cap}_{ij}(d)$ is determined by a tiered rule based on the total weekly OD demand D_{ij}:

$$\mathrm{Cap}_{ij}(d) = \begin{cases} 0.333\, D_{ij}, & \text{if } D_{ij} \geq 500, \\ 160, & \text{if } 320 \leq D_{ij} < 500, \\ 80, & \text{if } D_{ij} < 320. \end{cases}$$

The tier values were calibrated through trial and error to reflect realistic daily passenger loads for regional jets of roughly 90 seats with a load factor of 85%.

Equation 18 limits passenger assignments to the available seat capacity of each operated flight. Here, $\mathrm{flights}(r)$ denotes the set of flight legs composing itinerary r. The left side counts all passengers using flight f, while the right side applies the available capacity based on the target load factor LF, seat capacity s_f, and the number of times flight f is operated.

$$\sum_{\substack{r \in R \\ f \in \mathrm{flights}(r)}} p_r \;\leq\; LF \cdot s_f \cdot \sum_{t \in T} y_{ft} \qquad \forall f \in F \tag{18}$$

Together, Equation 15–Equation 18 ensure coherent passenger routing and consistent use of aircraft capacity across the network.

2.3 Battery Degradation Module

This section introduces the battery degradation module used to predict capacity loss for the flights operated in the simulation. The module is developed in three parts. First, the modelling approach is outlined. Second, a physics-based degradation dataset is generated. Third, a machine learning model is trained to estimate degradation throughout the simulation.

2.3.1 Degradation Modelling Overview

This subsection provides an overview and the design rationale of the battery degradation module. Because empirical battery degradation datasets that reflect the expected operational characteristics of electric aviation do not yet exist, a synthetic dataset is generated using general physics-based degradation relations. This approach provides physically interpretable training data while allowing the predictive component to be updated or replaced when empirical data becomes available. The module focuses on capacity degradation, as power-loss degradation is not expected to limit performance and available power margins remain sufficient throughout service life.

To represent the uncertainty in future battery durability, three calibrated degradation scenarios are defined: *fast*, *medium*, and *slow*. These correspond to 1,000, 1,500, and 2,000 cycles to 90% SoH. The scenarios reflect an operational usage pattern in which roughly 30 % of cycles are deep discharges (DoD $>$ 70 %). These assumptions are based on existing literature as well as discussions with *Elysian Aircraft* [4, 5]. For each scenario, degradation trajectories are generated and used to train a predictive model that estimates the incremental capacity loss per flight, as illustrated in Figure 4. These scenarios are later used during the experiments to explore the effects of uncertainty in future battery characteristics.

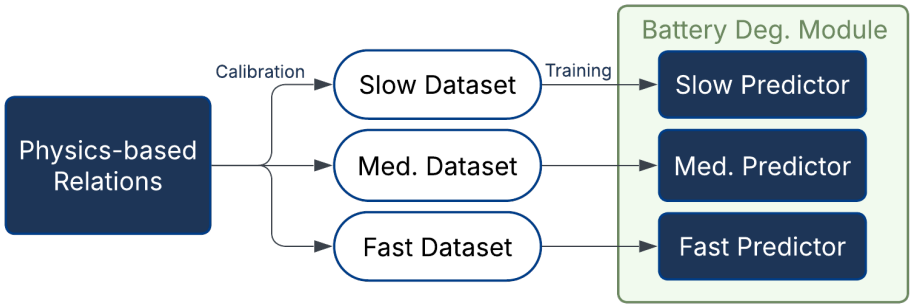

Figure 4: *Overview of the degradation module. Physics-based relations generate synthetic datasets for three scenarios, which are used to train the predictors in the BDAEFA framework.*

2.3.2 Physics-Based Degradation Model and Data Generation

This subsection builds on the approach introduced in Subsection 2.3.1 by defining the simplified, physics-based relations used to generate battery degradation data. These relations capture how specific flight characteristics influence ageing based on established degradation mechanisms.

The conceptual basis of this formulation follows McDonald [9], who argues that battery ageing arises from the combined effects of cycling and calendar mechanisms. In line with this view, the total degradation per cycle is modelled as the sum of a calendar component and a cycling component, each scaled by empirically informed modifiers that approximate their dominant behaviours under operational conditions. The two ageing mechanisms are outlined below as background for the degradation relations used in the model.

1. *Calendar ageing:* Refers to the time-dependent degradation occurring while the battery is idle, driven by processes such as Solid electrolyte interphase (SEI) layer growth, electrolyte decomposition, and electrode balancing shifts. Although often modelled as a simple function of storage time and state of charge, experimental studies show that the rate is strongly influenced by temperature, anode potential, and overall storage conditions, which together determine the extent of passive lithium loss and long-term capacity fade [23, 24].
2. *Cycling ageing:* Represents degradation caused by repeated charge discharge cycling, where electrochemical and mechanical stresses gradually reduce usable capacity. The dominant driver is the DoD, as deeper cycles induce stronger electrode strain and side reactions. During early life, degradation progresses relatively fast due to SEI formation, surface film growth, and structural adjustments within the electrode. As the SEI layer thickens, the rate stabilises throughout mid-life before accelerating again near the knee point, driven by cumulative mechanical fatigue and loss of active material [22]. The degradation rate at an instant, $\frac{d(\mathrm{SoH})}{dt}$, therefore depends on both the current SoH, which influences impedance and active-material loss [25], and the cumulative energy throughput (expressed as Equivalent Full Cycles, EFC), which reflects the total electrochemical and mechanical load history.

Both ageing modes are implemented using simplified, empirically inspired relations that approximate their dominant effects under operationally relevant conditions. Calendar ageing is modelled as a constant daily SoH decay equivalent to 2 % per year, representing the average degradation expected for thermally stable $LiFePO_4$ cells in controlled environments [24]. Cycling ageing, by contrast, exhibits more complex dependencies, as degradation per cycle varies with depth of discharge, current SoH, and EFC. Although the mechanisms are complex and interdependent, they can be approximated by empirical relations that describe their dominant dependencies under operational conditions. These are expressed through scaling relations that link the factors to the incremental capacity fade per cycle. The degradation relations are applied iteratively to update the SoH after each simulated cycle, by combining calendar and cycling contributions as in Equation 19.

$$\mathrm{SoH}_{t+1} = \mathrm{SoH}_t - \Delta\mathrm{SoH}_{\mathrm{cal}} - \Delta\mathrm{SoH}_{\mathrm{cyc}} \tag{19}$$

In Equation 20, k_{cal} defines the fixed calendar degradation rate, while Δt represents the fraction of a day allocated to each cycle within the simulation. This means that if several flights occur on the same day, the total daily calendar ageing is distributed evenly across those cycles. Thus each cycle contributes proportionally to the overall calendar degradation.

$$\Delta\mathrm{SoH}_{\mathrm{cal}} = k_{\mathrm{cal}}\,\Delta t \tag{20}$$

The cycling component defined in Equation 21 links operational use and degradation. The base rate k_{cyc} determines the nominal cycle damage and is varied to calibrate the degradation to the selected scenario's 90% SoH and target cycles. The underlying relations remain identical across scenarios, as only the calibrated magnitude of k_{cyc} differs, ensuring that batteries with slower degradation experience less capacity loss per cycle. The modifiers f_{DoD} and f_{EFC} adjust this rate for DoD and EFC to reflect how degradation evolves with usage and operational history.

$$\Delta\mathrm{SoH}_{\mathrm{cyc}} = k_{\mathrm{cyc}}\, f_{\mathrm{DoD}}(\mathrm{DoD})\, f_{\mathrm{EFC}}(\mathrm{EFC}) \tag{21}$$

The modifiers f_{DoD} and f_{EFC} are defined through empirical scaling relations that reproduce the observed degradation behaviour of general lithium-ion cells. The DoD relation in Equation 22 increases linearly for deeper cycles, modelled after experimental data that shows that a full 100 % discharge can reduce the cycle life to roughly half of that achieved at 60 % DoD under comparable 0.5 C conditions during flight [26]. Although the true DoD to

degradation relationship is exponential, a piecewise linear approximation is used to maintain interpretability.

$$f_{\mathrm{DoD}}(\mathrm{DoD}) = \begin{cases} 1 + 4(\mathrm{DoD} - 0.60), & \text{for DoD} \geq 0.60, \\ 1 - 2(0.60 - \mathrm{DoD}), & \text{for DoD} < 0.60. \end{cases} \tag{22}$$

The cumulative energy-throughput factor f_{EFC} captures the gradual reduction in incremental degradation over the cell's operational history, reflecting the slowdown typically observed during mid-life operation. This behaviour arises from diffusion-limited SEI growth, where further degradation slows as the layer thickens [22, 27, 28]. The decline is steepest early in life and gradually stabilises toward two-thirds of the target cycle life, after which the degradation rate levels off as the factor reaches its lower bound. Although the exact shape of this decay varies with chemistry and conditions, this formulation with an exponential decay term and a lower bound of 0.7 captures the general empirical trend observed across studies.

$$f_{\mathrm{EFC}}(\mathrm{EFC}) = \max\left(0.7 + 0.3\,\exp\left(-2.0\,\frac{\mathrm{EFC}}{(2/3)\,N_{\mathrm{target}}}\right),\, 0.7\right) \tag{23}$$

To reproduce the accelerated degradation observed near end of life, a knee-point modifier is incorporated into the data generation process, as shown in Equation 24. The knee point typically occurs around 80% for most lithium-ion cells [6]. For aviation, SoH levels below 85% are avoided for safety reasons. This factor is not included in the main degradation equation for clarity, because it only becomes active once the SoH drops below the operationally relevant range. However, the knee-point is used during data generation and its effect is visible as the downward bend in Figure 5 at around 82.5% SoH. The modifier gradually amplifies degradation once the SoH passes the knee threshold, reaching a maximum factor η_{knee} over the range $\Delta\mathrm{SoH}_{\mathrm{knee}}$.

$$f_{\mathrm{knee}}(\mathrm{SoH}) = \begin{cases} 1, & \mathrm{SoH} > \mathrm{SoH}_{\mathrm{knee}}, \\ 1 + (\eta_{\mathrm{knee}} - 1)\,\dfrac{\mathrm{SoH}_{\mathrm{knee}} - \mathrm{SoH}}{\Delta\mathrm{SoH}_{\mathrm{knee}}}, & \mathrm{SoH} \leq \mathrm{SoH}_{\mathrm{knee}}. \end{cases} \tag{24}$$

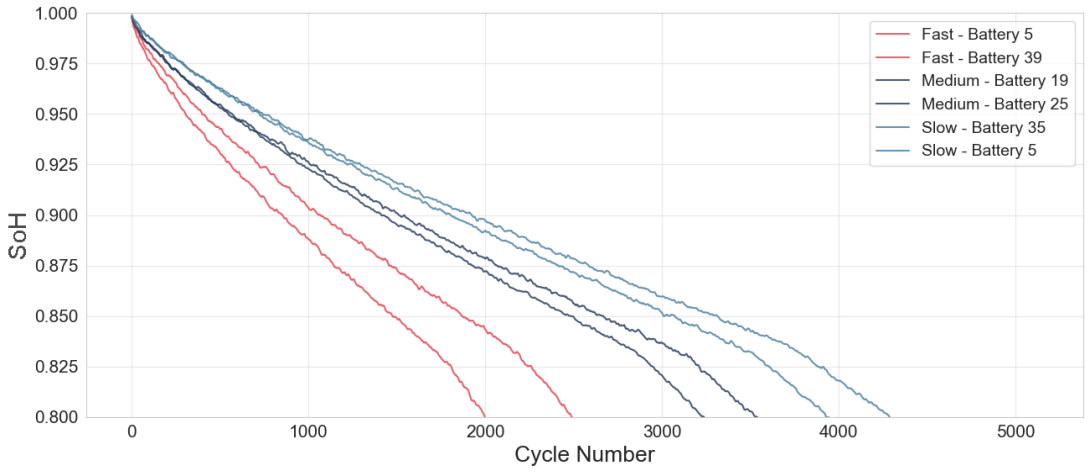

Figure 5: *Representative SoH trajectories with 2 batteries per degradation scenario, showing variation from sampled operational and degradation-rate differences.*

The cycling coefficient k_{cyc} is calibrated through an iterative procedure. For each scenario, operational cycles are first sampled from realistic distributions of DoD and daily cycle

counts representative of regional aircraft usage. To introduce realistic dispersion across batteries, fifty simulated cells are generated per scenario, each assigned a slightly different usage profile together with a small variation in degradation rate. Using these profiles, SoH trajectories are calculated according to the physics-based relations introduced earlier. The value of k_{cyc} is then adjusted and the trajectories regenerated until the simulated batteries reach the scenario's target cycle-life and usage characteristics. This process produces batteries with realistic dispersion in the trajectories, a subset of which is shown in Figure 5.

2.3.3 Model Development and Validation

Building on the physics-based dataset from Subsection 2.3.2, this subsection develops a predictive model that estimates the incremental degradation ΔSoH per flight.

Ridge regression is selected as the predictive method because it provides a stable and interpretable mapping of flight-level operating characteristics to incremental cycle damage. The underlying physics-based dataset does not contain complex relationships, meaning that more advanced machine learning models would provide little additional benefit while reducing interpretability. The formulation of Ridge regression, shown in Equation 25, extends the standard least-squares loss function with an additional L_2 penalty term $\lambda\|\boldsymbol{\beta}\|^2$. This regularisation stabilises coefficient estimates under correlated inputs such as EFC and SoH and reduces overfitting to the synthetic training distribution, which in turn improves generalisation when the model is applied to operational flight data whose feature distributions differ from those in the synthetic degradation trajectories.

$$L(\boldsymbol{\beta}) = \sum_{i=1}^{n}(y_i - \hat{y}_i)^2 + \lambda \sum_{j=1}^{p} \beta_j^2 \tag{25}$$

In this formulation, y_i and $\hat{y}_i$ denote the observed and predicted incremental degradation values, respectively, while β_j represents the model coefficients associated with the input features. The regularisation strength λ controls the balance between minimising prediction error and constraining coefficient magnitudes. By enforcing smoother and more stable coefficients, Ridge regression maintains interpretability and consistency across all degradation scenarios. The model uses three input features: the battery SoH and EFC at the start of the flight, and the DoD of the flight. Cumulative cycle count and battery age are excluded because their information is largely contained in the current feature set and would introduce collinearity.

Because Ridge regression penalises coefficient magnitudes directly, the EFC values are scaled to ensure a balanced regularisation across input features. The SoH and DoD features, already bounded between 0 and 1, do not require additional scaling. A custom scaling approach is applied to the EFC feature to prevent distortions caused by a few statistically extreme but physically valid batteries with unusually high cycle life resulting from low a DoD operation average and slow degradation coefficient. The standard min–max scaling would otherwise compress most of the data into a narrow range, reducing model sensitivity in the typical operating regime. To address this, EFC values are scaled using scenario-specific 95^{th} percentile caps from the training data and physics-informed upper bounds corresponding to the expected cycles until 82.5% SoH.

The dataset is split by battery to avoid information leakage across cycles, allocating 70% of batteries to training, 15% to validation, and 15% to testing. The Ridge regularisation strength λ is tuned using Optuna [29] with a Tree-structured Parzen Estimator sampler. For each trial, the model is fitted on the training set and evaluated on the validation set, minimising the Root Mean Squared Error (RMSE) under autoregressive roll-forward prediction. After selecting the best λ, the model is retrained on the combined training and validation sets and evaluated on the independent test set. Model accuracy is quantified using the RMSE

and the Mean Absolute Percentage Error at 85% SoH ($\text{MAPE}_{85\%}$). The RMSE captures the overall prediction accuracy of incremental degradation values, while $\text{MAPE}_{85\%}$ measures the relative deviation between predicted and actual SoH at the cycle where the *true* battery health first falls below 85%, thereby assessing the cumulative error from the initial 100% SoH. Their formulations are shown in Equation 26.

$$\text{RMSE} = \sqrt{\frac{1}{n}\sum_{i=1}^{n}(y_i - \hat{y}_i)^2} \qquad \text{MAPE}_{85\%} = \left|\frac{N_{\text{pred},85} - N_{\text{true},85}}{N_{\text{true},85}}\right| \times 100\% \tag{26}$$

Table 3: *Performance of Ridge regression model across degradation and DoD-shift scenarios.*

Scenario	**RMSE**	**$\text{MAPE}_{85\%}$ (%)**	**95% CI (%)**	**Max (%)**
Fast	0.0105	1.32	0.64–2.01	2.52
Medium	0.0109	1.30	0.45–2.15	3.02
Slow	0.0077	0.79	0.30–1.28	1.92
Fast (DoD-shift)	0.0094	0.97	0.73–1.21	3.77
Medium (DoD-shift)	0.0101	1.18	0.91–1.45	4.24
Slow (DoD-shift)	0.0093	0.98	0.74–1.23	4.19

The Ridge model demonstrates consistent predictive accuracy across the three regular degradation scenarios, as summarised in Table 3. Across all cases, the RMSE remains around 0.01, indicating smooth and stable prediction of the degradation over time. The average end-of-life $\text{MAPE}_{85\%}$ across these regular degradation scenarios is 1.14% compared to the full SoH. Interpreted in operational terms, this equates to a range deviation of about 12 km for the *Elysian E9X V2* (1020km max range). The 95% confidence intervals remain narrow, mostly within 2%. The maximum deviations across all batteries do not exceed 3% in the baseline scenarios, confirming that prediction errors remain operationally overseeable. In practice, a built-in range buffer is applied within the range calculations discussed in Section 2.4, and in the rare event that individual aircraft degrade much faster than expected, early maintenance or reassignment strategies can be used to mitigate potential disruptions, with a fuel-powered reserve propulsion system available in the *E9X*, providing additional operational margin.

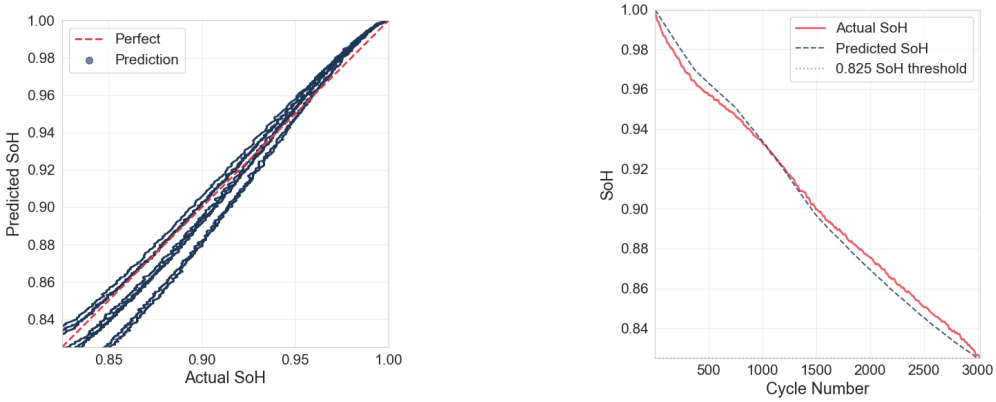

(a) *All test set batteries.*

(b) *Battery 3 with a shift in average DoD in the usage pattern.*

Figure 6: *Model validation comparing actual and predicted SoH for medium scenario.*

As shown in Figure 6a, the predicted and actual SoH values align closely along the 1:1 line. The slightly higher $\text{MAPE}_{85\%}$ observed in the *fast* and *medium* scenarios arises from a mild overprediction tendency relative to the *slow* scenario, which centres more tightly around the perfect prediction line.

To assess robustness under changing operational conditions, a supplementary validation was performed in which the average DoD of selected batteries was varied over extended cycle sequences. Across all DoD-shift scenarios, the model achieved an RMSE of 0.0096 and a $\text{MAPE}_{85\%}$ of 1.05% [95% CI: 0.90–1.19%], with a maximum deviation of 4.24%. As shown in Figure 6b, the Ridge predictor continues to track the degradation trajectory smoothly under these altered usage patterns. While the shifted regimes produce slightly higher maximum deviations than the regular scenarios, these effects remain limited and do not affect the suitability of the model.

With the model development and validation complete, the final implementation models are retrained on the full dataset with the training, validation, and test subsets combined using the optimal λ. This final version is then integrated into the BDAEFA framework to predict the individual degradation for the flights flown in the control period of the simulation horizon.

2.4 Electric Aircraft Range Estimation

This section introduces the methodology for calculating the cruise range of the electric aircraft using a modified version of the Breguet equation adapted for electric propulsion. The formulation follows the work of de Vries et al. [30], who adapted the conventional Breguet relation for electric and hybrid-electric aircraft by replacing fuel energy terms with the battery energy density and the according system efficiency parameters.

The formulation in Equation 27 is used to calculate the aircraft range both at full SoH and after degradation. After each planning horizon, the range is re-evaluated using the updated battery SoH predicted by the degradation module, and the maximum achievable cruise range R_{max} is obtained from this relation.

$$R_{\text{max}} = \eta_{\text{elec}} \eta_p \frac{e_{\text{bat}}}{g} \left(\frac{L}{D}\right)_{\text{max}} \left(\frac{EM}{MTOM}\right) \tag{27}$$

Here, η_{elec} and η_p denote the electric powertrain and propeller efficiencies, e_{bat} is the usable battery energy density, g is the gravitational acceleration, $(L/D)_{\text{max}}$ is the maximum lift-to-drag ratio, and $EM/MTOM$ is the ratio of battery mass to maximum takeoff mass. To incorporate battery degradation, the effective battery energy density is updated between each planning horizon according to the relation given in Equation 28, which links the usable energy density to the current battery SoH.

$$e_{\text{bat}} = \text{SoH} \cdot e_{\text{bat,init}} \tag{28}$$

The estimated maximum range R_{max} serves as a dynamic constraint in the EFAM, limiting the feasible legs each aircraft can operate.

2.5 Maintenance Decision Module

This section introduces the battery replacement maintenance strategies developed to ensure operational continuity of the electric fleet. In addition, this section also addresses the financial treatment of battery replacements through a depreciation fund system. To limit reliance on very high-SoH aircraft and reduce maintenance strain, the flight network in Figure 7a is filtered to include only routes below 970 km, keeping operations comfortably within the aircraft's maximum range.

2.5.1 Maintenance Triggers and Scheduling

When an aircraft is scheduled for maintenance, it is excluded from operations for one simulation horizon, during which its battery is replaced and its SoH is restored. During this period, routine inspections and minor system servicing are assumed to take place alongside the battery replacement. Since airlines typically plan their services on a weekly basis, the maintenance strategy was designed to preserve the ability to operate a stable weekly schedule.

To achieve this, two triggers are applied. The first is an operational requirements (or continuity) trigger, which monitors whether a sufficient number of healthy aircraft remain available to cover the most demanding routes in the first week's flight network. An aircraft is considered healthy when its degraded range is still adequate for all routes exceeding 900 km, while moderately degraded aircraft continue to serve shorter segments. This process is visualised in Figure 7b. The second battery replacement trigger is activated once the SoH advances below 85%, avoiding operation near the degradation knee point (Section 2.3). It is likely that in situations where the SoH-threshold trigger is used as sole maintenance trigger, that the full base schedule cannot be operated and certain flights will not be scheduled in weeks where the fleet health cannot accommodate it. Replacements are limited to one aircraft per week, and always assigned to the most degraded aircraft.

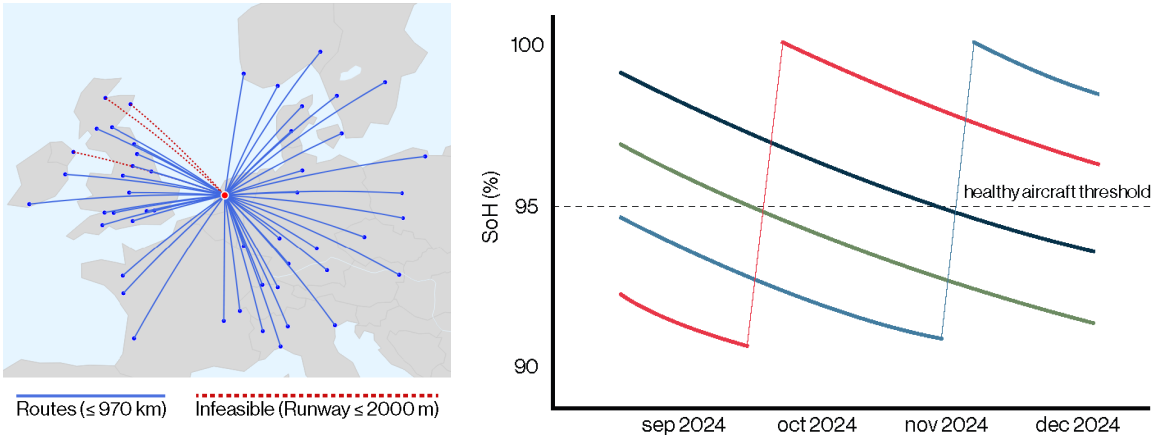

(a) KLM Cityhopper network adjusted for maintenance relief.

(b) Aircraft SoH evolution using the operational trigger.

Figure 7: *Maintenance strategy visualisation with the network route choice and operational continuity strategy.*

To analyse the effect of different replacement strategies, experiments are run that vary both the SoH threshold and the use of the operational requirements trigger. Two families of strategies are considered. Threshold-based strategies, denoted as *T85–T93*, replace the battery once the SoH falls below the specified threshold. Operational-continuity strategies, denoted as *B0–B3*, combine the operational trigger with increasing levels of aircraft buffer for operational continuity. The most balanced strategy between cost reduction and network utilisation will be used as the baseline configuration throughout the experiments.

2.5.2 Depreciation and Battery Replacement Cost Accounting

This subsection introduces the battery replacement cost accounting system, as these replacements are expensive and take up a substantial part of the total operational costs, calculated in Section 3.2 to be €1,250,000. The battery depreciation costs in in the objective function are designed to gradually offset the replacement expenses over time. In this system each

flight has a battery depreciation cost component that is proportional to its distance, which is funnelled into a depreciation fund for all aircraft combined. This per flight contribution spreads the cost of battery replacements over its operational lifetime rather than as single events, improving cost predictability and stability. The fund has a safety upper and lower bound for fluctuations in the fund, where it limits how far the balance is allowed to deviate from the expected depreciation. Required corrections are handled through additional costs or revenue. *Elysian Aircraft* plans to repurpose or resell the degraded battery-packs, most likely as power units at airports. To account for this residual value at different SoH levels, a linear resale function is applied. The function has a value of €175,000 at 87.5% SoH, with an upper bound of €250,000 for earlier retirements at 92.5% SoH, and decreasing to €100,000 for late retirements at 82.5% SoH.

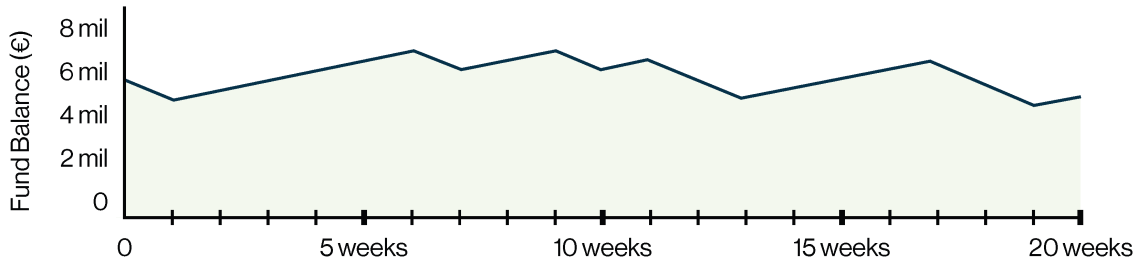

Figure 8: *Illustration of the depreciation fund balance over time*

The depreciation rate is recalculated after each simulation horizon, based on the observed SoH degradation and the total kilometers flown in the week. The rate is calibrated for the cumulative depreciation contribution to approximately break even with the expected replacement 87.5% SoH threshold.

To ensure consistent accounting and operational continuity, aircraft that are initialized with already partially degraded batteries have a proportionate amount of prior depreciation assigned to the fund.

3 Economic Formulation and Cost Accounting

This chapter defines and calibrates all monetary components used in the analysis of the BDAEFA framework. It first establishes the revenue and ticket pricing formulation, followed by the derivation of key cost parameters such as battery and electricity prices, including their sensitivity analyses. Afterwards, non-modelled airline costs such as overheads and broader maintenance considerations are discussed to clarify their exclusion and maintain transparency in the economic scope.

3.1 Revenue Modelling and Yield Calibration

This section defines how passenger revenues are represented in the model through a distance-based yield formulation and describes the calibration of its parameters. The yield–distance relationship from Equation 3 is calibrated using real-world fare data retrieved through the Amadeus Travel API [31] for all OD pairs in the *KLM Cityhopper* case study, as described in Chapter 4. The dataset includes both one-way and return flights across economy and business classes for multiple departure dates in January 2026 with detailed price breakdowns including the ticket base fare that excludes taxes paid by the customer and enables the retrieval of the average fare an airline would receive for a seat.

For the tuning of the model parameter weights 75% of fares in an aircraft are assumed to be booked with a return ticket and 25% as a one-way with 8 business class seats. The parameters (β, α, γ) of the yield are tuned by minimizing the Huber loss using Optuna, similar to the degradation model calibration. The Huber loss, defined in Equation 29, behaves quadratically for small residuals and linearly for large residuals, thereby reducing the influence of extreme fares caused by seasonal variations, irregular booking patterns, or last-seat price spikes.

$$L_\delta(r) = \begin{cases} \frac{1}{2}r^2 & \text{if } |r| \leq \delta, \\ \delta \cdot (|r| - \frac{1}{2}\delta) & \text{otherwise.} \end{cases} \tag{29}$$

Here r is the residual and δ is a tunable threshold parameter that determines where the loss function transitions from quadratic to linear. The threshold is selected through a sensitivity analysis in which candidate δ values between 1 and 250 are tested. A value of $\delta = 50$ is selected, representing a realistic transition point, as deviations of roughly €50 in short-haul fares are considered significant in airline pricing. Therefore the model avoids overfitting extreme fares while focusing on the more representative cluster of returns. Using this approach, the fitted values are obtained as $\beta = 4.430$, $\alpha = 0.442$, and $\gamma = 0.00$. The resulting curve lies relatively low in Figure 9, which is consistent with the dominance of return tickets in the calibration. At the same time, yields appear high for an airline overall, which can be explained by the focus on short-haul flights within the already limited *KLM Cityhopper* network. In this segment, yields are structurally higher because fixed costs are spread over shorter stage lengths and turnaround times are relatively long.

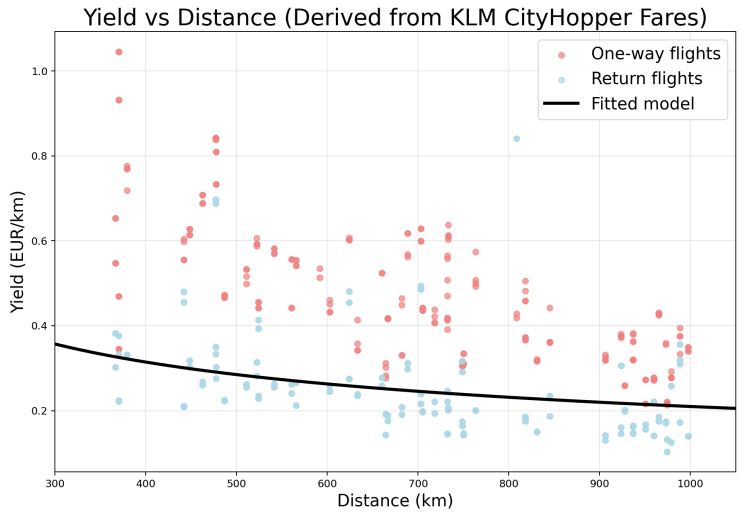

Figure 9: *Yield–distance relationship based on retrieved KLM Cityhopper fares.*

3.2 Operating Cost Optimizable Components

This section defines the cost parameters that are directly optimized within the MILP formulation of the BDAEFA framework. These parameters represent the operational and degradation-related expenses that are included in the objective function, as well as their associated sensitivity analyses, as summarized below. All other broader airline overhead and non-flight dependent costs are excluded from the optimization and discussed in Section 3.3. Where possible, cost values reflect forecasts for the expected entry-into-service period of the Elysian V2 (±2035) However, when reliable projections are unavailable or contain too much uncertainty, the most recent empirical values are used instead.

1. *Flight service and airport fees:* Costs include landing, take-off (LTO), parking, and passenger-related charges from the official Schiphol Airport Charges and Conditions [32]. For the *Elysian E9X*, the LTO charge is €2.34 per tonne of aircraft weight and the passenger-related charge is €18.33 per passenger. The aircraft falls under the quietest S7 noise category with reduced tariffs. Baggage handling fees are included at €300 per flight.
2. *Crew salaries and expenditures:* Crew costs are parameterized as per-block-hour expenses within the optimization model. Annual wage estimates are derived from Glassdoor averages for *KLM Royal Dutch Airlines*, assuming two cockpit and three cabin crew per aircraft. These salaries are converted to a total rate per block hour. Extra costs for employer taxes (30%) and additional expenditures (25%) are applied to reflect employment costs [33].
3. *Elysian E9X lease cost:* To calculate the lease cost of the *E9X* it is compared with the new *Embraer 175* with a purchase price of €45M [34]. The electric *E9X* will be cheaper to manufacture due to a simpler airframe and less complexity in the propulsion system [4, 5, 35]. Therefore, an aircraft value of €35M is adopted for the *E9X*. By applying a lease-rate factor of 0.75% [36] for a newer aircraft a monthly lease of €262,500, or roughly €240,000 per four-week period is calculated. However, battery replacements are assumed to be paid by the operator, reducing the effective lease burden. Therefore the rounded price of €200,000 is taken into account as the four-weekly lease cost.
4. *Electricity pricing:* The electricity price p_{elec} represents the average cost of charging energy supplied to the fleet. It is based on expert forecasts for Dutch industrial electricity tariffs in 2030–2035 and evaluated across the three levels €0.225, €0.30, and €0.375 / kWh, to capture potential market deviations beyond the predicted range [37].
5. *Battery pricing:* The battery pack price per kWh is a key driver of total replacement cost. BloombergNEF reports an average pack price of about €105/kWh in 2024, continuing a long-term decline [38], while academic projections indicate further reductions to €75–95/kWh by 2030 [39]. Based on these forecasts and discussions with Elysian Aircraft, the three cost levels *low* (€0.8 M), *medium* (€1.25 M), and *high* (€2.5 M) are defined per 11 MWh pack to reflect future uncertainty and the expected premium of aviation-grade battery pack systems, which involve higher performance and safety requirements.
6. *Emission factors:* Two emission parameters are used. (i) A grid-emission intensity of 0.202 kg CO_2/kWh is applied to electricity use [40], and (ii) a lithium-ion production emission factor of 17.63 kg CO_2/kg based on Clemente et al. [41]. This latter factor is only used for the CO_2 comparison of battery replacements in Section 5.5. Future emission intensities are expected to decline, but projections vary significantly, so current values are used here as a conservative assumption.
7. *Carbon allowance pricing:* Although current regulations exempt electric aircraft from paying EU ETS aviation charges, electric passenger aviation is not yet operational and therefore future regulation is uncertain. Thus the same carbon price is applied here to ensure a fair comparison. The carbon price is €200 /t CO_2, based on forecasted EU Emissions Trading System allowance levels for 2035 [42, 43]. Note that this is only for the operational energy use and battery replacement emissions are not included.

Together, these components form the full economic inputs of the optimization model and are presented as the operational costs in Chapter 5. The *Embraer 175* derivations used in Section 5.5 are listed in Appendix B.

3.3 Non-Modelled Airline Cost Components

This study focuses exclusively on direct operating costs. Broader airline-level overheads expenses, such as administration, ticketing and sales, are excluded. These costs scale with airline

size and business model rather than aircraft technology and cannot be meaningfully allocated to individual flights. Their omission does not affect the comparative results, which rely on normalised operational and revenue costs.

Maintenance costs may differ between electric and conventional aircraft due to the simpler electric powertrain architecture. While recent studies suggest that electric propulsion could reduce maintenance requirements [35], other work highlights that new infrastructure, certification, and training demands may offset these benefits [44]. Given this uncertainty, maintenance is not modelled explicitly. Battery replacement costs are treated separately to transparently capture their economic impact.

4 KLM Cityhopper Case Study

This chapter introduces the primary case study used to evaluate the operational behaviour of the BDAEFA framework. The study is based on the *KLM Cityhopper* network, a dense short-haul feeder system centred around Amsterdam Schiphol Airport. A second network, based on *American Eagle* operations in the North-East U.S., is presented separately in Appendix C and is used later to assess the transferability of the framework.

The *KLM Cityhopper* network case study was originally developed by Kruidenier [17], who reconstructed the network from FlightRadar24 data [45] with additional information tailored to electric aviation. His dataset was compiled from one representative week of *KLM Cityhopper* operations to and from Amsterdam Schiphol and filtered to include only flights operated by the airline. As a dedicated feeder network for *KLM's* long-haul operations, its structure follows a hub-and-spoke pattern with direct itineraries only and no demand between spokes.

For the operational framework developed in this research, the case study data is adapted to meet different modelling requirements. The original dataset supplied the route structure, airport information, and baseline passenger demand, while the scheduling logic, cost parameters, and final demand levels are independently developed and calibrated for this research.

To capture the system-wide effects of battery degradation on airline performance, it is necessary to simulate a full and realistically scaled network. As the actual *KLM Cityhopper* operation carries roughly 200,000 passengers per week with a fleet of 66 aircraft [46], the network demand is proportionally scaled down to represent a ten aircraft operation compatible with the computational scope of this study. Initial tests show that under fully saturated demand conditions, the ten aircraft setup can serve approximately 36,000 passengers a week. In practice, a system with exactly this demand would accommodate less, as not all potential demand can be captured within operational constraints. Therefore to reflect realistic operations, a 20% margin above this baseline is applied to achieve a slightly saturated but still reasonable demand level for the network. Given this downscaling, some low-frequency routes become infeasible under daily limits, so a weekly demand structure is implemented, complemented by daily caps in the constraints. An overview of the resulting network, including all potential routes and the subset of flights that are feasible within the fleet's range and runway constraints, is illustrated in Figure 7a.

The potential schedule used in this framework for the selection of flights is generated from the processed demand, routes and airport feasibility. Flights are distributed across the operational day using fixed 20-minute time intervals. In each interval, 25 feasible routes are activated and appear in the potential schedule. This design realistically reflects slot and operational constraints, as airlines cannot depart to all destinations simultaneously due to limited airport capacity and slot availability across the network. The result is a schedule representing a set of potential flights within the network, from which the EFAM subsequently selects those to be operated based on costs, constraints, and evolving aircraft conditions.

5 Results and Sensitivity Analysis

This chapter presents and interprets the outcomes of the experimental evaluation of the BDAEFA framework. The analyses assess whether the model behaves as intended under different operational, technical, and economic conditions and quantifies how battery degradation and its key drivers influence electric aircraft operations over time.

All experiments share a common simulation setup. The framework simulates a representative operational year composed of 52 consecutive weekly horizons. In the first horizon, the EFAM is optimized to generate a tactical base schedule, which serves as the reference plan for the remainder of the simulation. The model is deterministic, with variations across runs arising only from solver optimality gaps when the four hour time limit is reached for the first horizon. Because the solver may terminate at slightly different optimality gaps, it can return different base schedules across runs. Therefore, minor performance differences may arise even with identical models [47], leading to slightly different solutions across repeated runs. However, the resulting MIP gaps, overall performance, and the observed model trends remain consistent across experimental groups, ensuring fair comparison.

Unless stated otherwise, all simulations use the 90-seat *Elysian E9X V2* aircraft [4, 5], a load factor of 85%, and the *KLM Cityhopper* case study network. This model, with a design range of 1020km, is selected as it is more representative of the capabilities likely to be achieved beyond the first fully electric passenger aircraft. All experiments are evaluated under the three degradation scenarios *fast*, *medium*, and *slow*, corresponding to 1000, 1500, and 2000 cycles respectively. To evaluate economic performance, the analysis uses the standard airline metrics Cost per Available Seat-Kilometer (CASK) and Revenue per Available Seat-Kilometer (RASK), defined in Equation 30. These measures quantify the cost and revenue per unit of offered capacity and allow comparison across experiments.

$$\text{CASK} = \frac{\text{Total Operating Costs}}{\text{ASK}} \qquad \text{RASK} = \frac{\text{Total Operating Revenue}}{\text{ASK}} \tag{30}$$

CASK reflects the cost required to produce one seat-kilometer, while RASK represents the revenue earned per seat-kilometer. In this study, operational CASK includes energy, crew, carbon allowances, airport fees, battery depreciation and aircraft lease costs. The lease component is tracked separately and reported in Table 5, enabling the computation of CASK with or without lease depending on the preferred definition. The Operational Profit Margin (OPM), defined in Equation 31, expresses the share of revenue remaining after operational costs and indicates the room available for overhead, profit, and other excluded cost components.

$$\text{OPM} = \left(1 - \frac{\text{Operational CASK}}{\text{RASK}}\right) \times 100 \tag{31}$$

The following sections begin by identifying the preferred maintenance configuration and examining its behaviour as the baseline setup in Section 5.1 and Section 5.2, which serves as the reference for all subsequent experiments. Afterwards, through sensitivity analyses of parameters it is explored how the system responds to variations in battery pack and energy prices the in Section 5.3 and in the network demand and flight frequency in Section 5.4. Then, the *Elysian E9X* and its performance is compared with a version of itself without battery degradation effects and an *Embraer 175* in Section 5.5. Lastly, Section 5.6 assesses the framework's transferability using a second case study.

5.1 Baseline Configuration Selection

This section identifies the preferred, best-balanced maintenance strategy that is implemented and analysed in the subsequent experiments, while also providing initial validation that the framework behaves consistently across numerous simulations in the three degradation scenarios with different maintenance strategies. To determine this best-balanced strategy, the configurations are evaluated on the continuity of their operations, operational CASK and OPM. The resulting operational CASK values for all threshold strategies (*T85*-*T93*) and operational-buffer strategies (*B0*-*B3*) are shown in Figure 10, while Table 4 presents the corresponding OPM.

The RASK is effectively the same across all simulations, with all values rounding to 0.271 €/km in every degradation scenario and for every maintenance configuration. Within each scenario, all strategies produce identical RASK values in the unrounded results because the optimiser returns the same base schedule across strategies. For *T85*, the unrounded RASK differs slightly because a small number of flights may remain unassigned in some horizons, but the rounded value remains 0.271 €/km. Across scenarios, small differences arise from changed optimisation parameters due to differing depreciation rates, yet all scenarios still produce a rounded RASK of 0.271 €/km. The CASK progression follows a clear and logical trend across scenarios in Figure 10. The *fast* scenario is the most costly, followed by the *medium* and *slow* cases. Lower SoH replacement thresholds and smaller operational buffers yield lower CASK values, as batteries remain in service for more cycles before replacement, reducing depreciation per flight. Because the increase in cycle life from *medium* to *slow* is smaller than from *fast* to *medium*, the associated depreciation difference is also smaller, leading to more similar CASK values for the *medium* and *slow* scenarios.

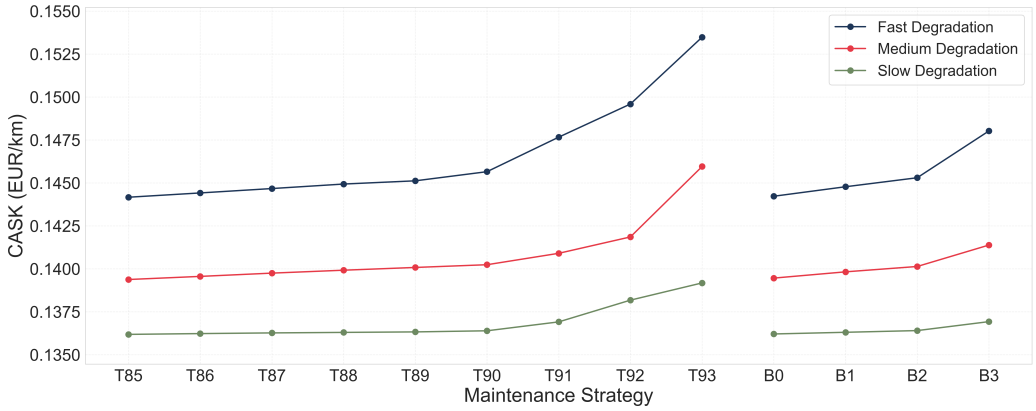

Figure 10: *Operational CASK across maintenance strategies and the degradation scenarios.*

Table 4: *Operational Profit Margin (%) by maintenance strategy and scenario.*

	T85	**T86**	**T87**	**T88**	**T89**	**T90**	**T91**	**T92**	**T93**	**B0**	**B1**	**B2**	**B3**
Fast	46.8	46.7	46.6	46.5	46.5	46.3	45.5	44.8	43.4	46.8	46.6	46.4	45.4
Med.	48.7	48.6	48.5	48.5	48.4	48.3	48.1	47.7	46.2	48.6	48.5	48.4	47.9
Slow	49.7	49.7	49.6	49.6	49.6	49.6	49.4	48.9	48.6	49.7	49.6	49.6	49.4

Across all degradation scenarios, profitability under the threshold strategies decreases gradually with higher replacement levels. The lowest threshold, *T85*, yields the highest operational profit margin, and its advantage over the next-best strategies is extremely small, averaging only about 0.02 percentage points above *B0* across the three scenarios. From *T86*

upward, the threshold strategies are able to maintain full network operability throughout the simulation, and all operational-buffer strategies do as well. Only *T85* occasionally leaves a small share of flights unassigned, which slightly reduces the total ASK. Even so, it still achieves the highest total profit across scenarios, averaging about €169.15 M compared with €169.08 M for *B0*, although the difference is almost negligible. This effect remains limited because the network includes only routes up to 970 km, allowing aircraft with lower SoH to still operate most flights. In networks with longer or more demanding routes, such missed flights would occur more frequently and therefore pose a more substantial operational challenge.

Among the fully robust strategies, *B0* achieves the highest OPM and is the second most profitable configuration overall, with margins nearly indistinguishable from *T85*. Unlike the threshold-based strategies, *B0* is explicitly designed to avoid dropped flights by ensuring that enough high-SoH aircraft remain available in every horizon. This combination of profitability very close to the best-performing strategy and guaranteed operability motivates the selection of *B0* as the preferred baseline used in the subsequent analyses.

5.2 Baseline System Overview

This section examines how degradation unfolds across the degradation scenarios within the baseline *B0*-configuration, and evaluates several battery and economic metrics that establish a benchmark for the remaining experiments.

The SoH evolution of the first four aircraft in the *medium* degradation scenario is shown in Figure 11. The trajectories display an almost linear decline with a slight convex curvature. This shape arises from the EFC-dependent slowdown in cycling degradation, which reduces incremental capacity loss as cumulative cycling increases. In the calibration trajectories shown in Figure 5, this convexity is more pronounced, as the usage profile remains broadly constant across cycles.

In operational conditions, however, the effective discharge depth gradually increases as the aircraft lose range over time. This shift toward deeper relative discharges strengthens the DoD-dependent degradation contribution, counteracting the EFC-driven curvature and resulting in the weaker convex shape observed in Figure 11. The optimizer evenly distributes route utilisation across the fleet, resulting in uniform degradation among aircraft. Small week-to-week deviations arise when certain aircraft operate slightly longer or shorter legs, but these do not affect the overall trend.

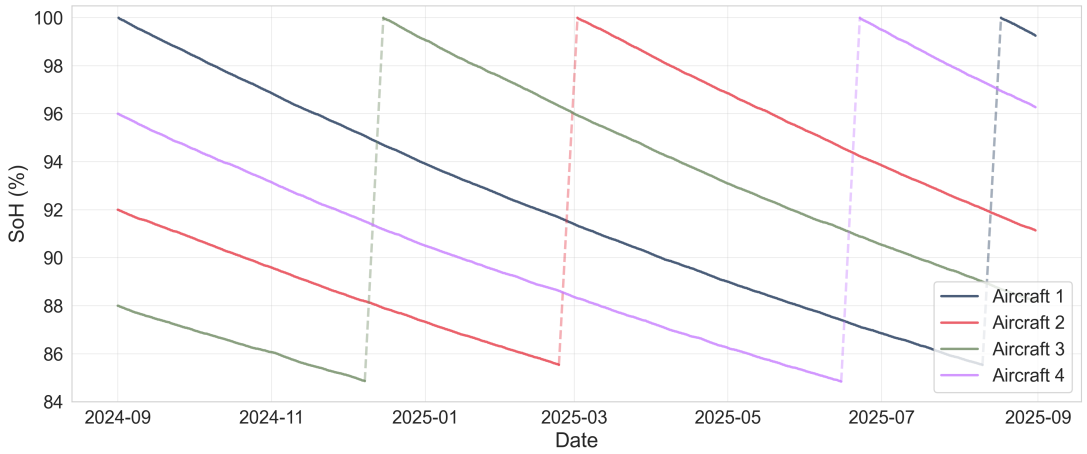

Figure 11: *Evolution of SoH for four aircraft using B0 for medium degradation. Dotted lines indicate maintenance events restoring aircraft to full SoH.*

The behaviour of the battery degradation module is further illustrated by the metrics in Table 5. Across the three scenarios, the model converges very closely to the intended degradation lifetimes, reaching 90% SoH after 998, 1468, and 2077 cycles in the *fast*, *medium*, and *slow* scenarios, respectively. A notable operational insight is that the simulated schedules consistently produce a deep-discharge share of around 35%, slightly higher than the 30% assumed during calibration. This increase arises naturally as aircraft lose range over time, causing the same missions to become deeper relative discharges.

Because deeper cycles accelerate the DoD-dependent component of degradation, a modest reduction in lifetime relative to the targets is expected. However, DoD is only one of several factors influencing degradation in the model. Other dependencies, such as the EFC-related slowdown that emerges during mid-life cycling, counteract part of the additional DoD-related ageing. The specific network and sequence of flights flown also contribute to these small differences. Overall, the simulated lifetimes remain close to the calibrated targets, with the *fast* scenario matching almost exactly, the *medium* scenario about 2% lower, and the *slow* scenario about 4% higher.

Table 5: *Battery degradation and operational metrics under the baseline configuration (B0).*

Metric	**Fast**	**Medium**	**Slow**
Operational performance			
Total flights	24,870	24,866	24,863
Demand fulfilment (%)	81	81	81
RASK (€/km)	0.271	0.271	0.271
Total revenue (M€)	349	349	351
Economic and cost metrics			
Operational CASK (€/km)	0.1442	0.1395	0.1362
Energy cost CASK (€/km)	0.0191	0.0191	0.0190
Battery depr. CASK (€/km)	0.0151	0.0102	0.0076
Lease CASK (€/km)	0.0202	0.0202	0.0200
Energy share of operating cost (%)	15.3	15.9	16.3
Battery depr. share of operating cost (%)	13.7	9.3	7.0
Battery degradation characteristics			
Avg. cycles at 90% SoH	998	1468	2077
Avg. replacement SoH (%)	85.3	85.7	85.7
Battery replacements	14	10	7
Deep-discharge share (%)	35.9	34.6	34.8
Battery depr. rate (€/km)	1.35	0.91	0.68
Battery cost per block hour (€/h)	529	357	267

The number of battery replacements reflects the different degradation rates across scenarios, with the *fast* scenario requiring 14 replacements, the *medium* scenario 10, and the *slow* scenario 7. This ordering aligns with the expected cycle lifetimes, as faster degradation naturally triggers maintenance more frequently. During testing of the model, the optimiser occasionally produced network patterns in which several long flights had to be operated at the same time, requiring aircraft with sufficiently high SoH. This may be feasible in the first week, but as aircraft degrade it creates more operational strain than a network with fewer simultaneous long flights and can lead to earlier maintenance triggers. The optimiser almost always converges for the *KLM Cityhopper* network to a configuration where three healthy aircraft are sufficient to cover the long-range flights, keeping the maintenance pattern and depreciation fund stable. In rare cases it required four, which increased replacement frequency and caused

the depreciation fund to drift slightly downward over time; in one of the *fast* scenario test runs this pattern occurred, and over a horizon of one to two years it would require replenishing the fund, adding roughly €0.10 per kilometre to battery depreciation costs. This behaviour did not occur in any of the experiments used in the results chapter. Future research could integrate maintenance planning directly within the scheduling optimisation to dynamically prevent such situations, optimize battery strategies and further improve long-term robustness of the model.

The RASK values in Table 5 of 0.271 €/km appear high compared with typical airline operations, which follows directly from the network structure. Because the electric aircraft can only operate the shortest routes in the *KLM Cityhopper* network, the schedule consists of many short legs with frequent turnarounds, which limits the distance flown and reduces the total seat-kilometres produced. At the same time, each leg carries fixed service and operational elements that must be recovered through revenue on every flight, regardless of distance. When these fixed components are spread over very short sectors, the revenue required per kilometer becomes larger.

Looking at the cost composition, the relative behaviour of the energy- and battery-related components remains consistent across scenarios. Energy expenditures constitute roughly 15–16% of total operating costs in all cases, while battery depreciation accounts for 13.7%, 9.3%, and 7.0% in the fast, medium, and slow degradation scenarios, respectively.

5.3 Battery and Energy Cost Sensitivity

This section assesses how different battery and electricity price levels affect the share of revenue allocated to energy and battery depreciation, as well as the overall profitability of operations. Simulations use the cost parameters defined in Section 3.2: battery pack prices of €0.8 million, €1.25 million, and €2.5 million, and electricity costs of €0.225, €0.30, and €0.375 per kWh. Comparing results in terms of percentage-point deviations from each scenario's baseline provides a consistent, scale-independent measure of cost sensitivity.

The deviations in Table 6 therefore indicate how far the combined energy and battery-depreciation share moves away from the baseline levels of roughly 12.6%, 10.8%, and 9.9% in the *fast*, *medium*, and *slow* scenarios. Each percentage-point change directly translates into an equivalent change in operational profit margin, highlighting the importance of understanding the impact of underlying battery and electricity prices.

Table 6: *Deviation in combined energy and battery cost share of total revenue from scenario baseline (pp) under B0.*

	Fast			**Medium**			**Slow**		
Elec. (€/kWh)	0.225	0.300	0.375	0.225	0.300	0.375	0.225	0.300	0.375
Bat. €0.80M	-3.9	-2.3	-0.5	-3.3	-1.5	0.3	-2.9	-1.1	0.6
Bat. €1.25M	-1.6	0.0	1.8	-1.7	0.0	1.8	-1.7	0.0	1.7
Bat. €2.50M	5.0	6.3	8.1	2.5	4.3	6.0	1.5	3.2	4.9

Each percentage-point deviation shown in Table 6 directly translates into an equivalent change in the operational profit margin. This sensitivity is substantial given the sector's thin average net margin of about 3.7% in 2025 [48]. Nevertheless, stated-preference studies suggest that passengers are often willing to pay more for low- or zero-emission flights, although this willingness varies across income groups and travel purposes [49, 50].

Overall, the results show that battery and energy prices introduce notable variability in operating economics and can strengthen or erode profitability significantly across scenarios.

5.4 Impact of Demand and Flight Frequency

This section analyses how variations in passenger demand influence aircraft utilisation and subsequently battery degradation. Demand levels are scaled from –30% to +30% around the baseline defined in Chapter 4 to simulate lighter and more intensive operations. The resulting contrast in flight frequency, SoH loss, and battery depreciation cost provides operational benchmarks linking utilisation to degradation.

Higher demand raises the number of flights per day, partly because the revenue model is calibrated using *KLM Cityhopper* fares from the faster *Embraer 175* (≈830 km/h true airspeed at FL350). When applied to the slower *Elysian E9X* (≈640 km/h), longer routes generate less revenue per unit time, making shorter flights more attractive. As demand increases, the optimiser shifts toward shorter flights, increasing daily flight counts and battery cycling.

Figure 12 shows the resulting trends in average daily flights, annual SoH loss, and battery depreciation cost across the three degradation scenarios. Higher demand increases flight frequency and, with it, annual SoH loss per aircraft, particularly in the fast-degradation case. SoH loss is reported excluding replacements to isolate the underlying degradation dynamics. Despite the increase in total utilisation, battery depreciation cost per kilometre remains nearly constant.

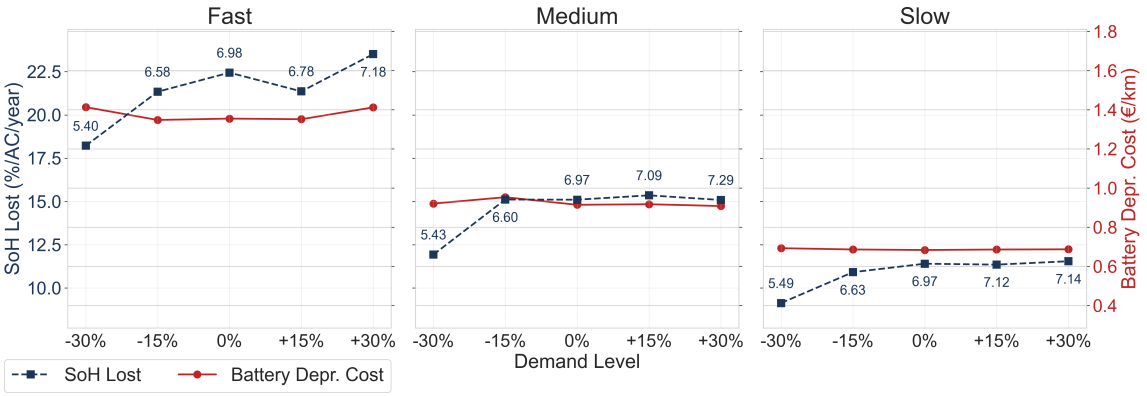

Figure 12: *Battery degradation and depreciation across demand scenarios. Dashed blue lines show annual SoH loss per aircraft (left y-axis), solid red lines show battery depreciation cost per kilometer (right y-axis). Labels indicate average number of flights per day per aircraft.*

Overall, the results show that the relationship between demand and degradation is not perfectly proportional, as changes in demand also influence which routes are flown and how often. At higher demand levels, the optimiser shifts toward shorter routes, which reduces cycling depth per flight and slightly moderates additional degradation, contributing to the flattening of the SoH-loss curve. Although total utilisation and annual wear increase, the SoH loss per kilometre remains nearly constant, keeping the battery depreciation cost per kilometer effectively unchanged.

5.5 Electric vs Conventional Aircraft Benchmark

This section benchmarks the electric *E9X* in the medium degradation scenario against a no-degradation variant and the conventional *Embraer 175* on the same *KLM Cityhopper* network. The comparison evaluates how battery ageing affects operations, costs, and emissions over a representative year. The three panels in Figure 13 summarise the differences in OPM, CASK composition, and CO_2 emissions, which are discussed in the following paragraphs.

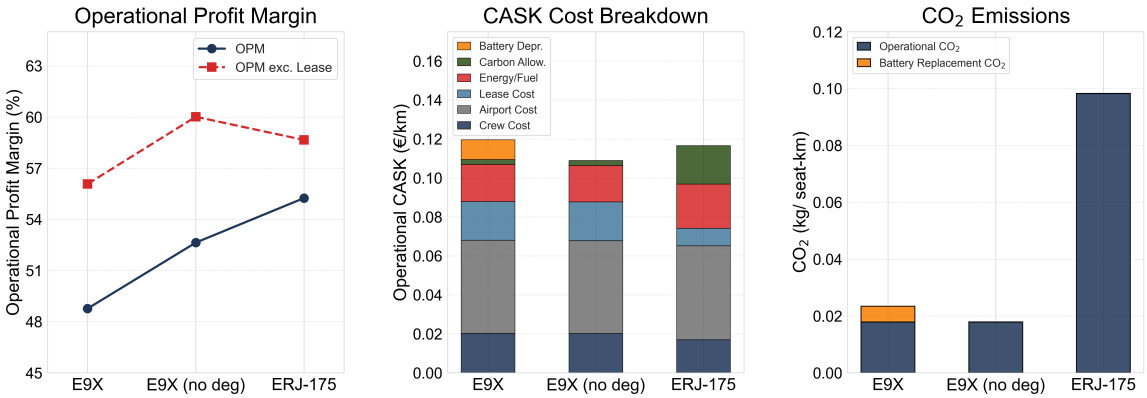

Figure 13: *Comparison of operational profit margin, CO_2 emissions and CASK compositions for the electric E9X (with and without degradation) and the conventional Embraer 175.*

The left panel in Figure 13 shows the operational profit margin. The *E9X* with degradation performs the worst, with an OPM of 48.6%. The no-degradation *E9X* achieves a higher margin of 52.6% because it retains full network access throughout the year and avoids battery depreciation costs. When lease costs are included, the *Embraer 175* achieves the highest OPM due to its lower capital cost. When lease is excluded, it becomes less profitable than the no-degradation *E9X* because fuel and carbon allowance expenses dominate its cost structure. The middle panel shows how battery depreciation drives most of the cost gap between the degradation and non-degradation *E9X* variants, while the remaining CASK components are broadly similar across both aircraft.

Compared with the no-degradation *E9X*, range losses restrict the flights the *E9X* with degradation can operate, which reduces its total ASK by 0.96%. This reduction in available ASKs leads to 0.76% lower revenue. Battery ageing then further raises total costs through replacement requirements, resulting in a 9.1% higher operating cost. A comparison between the *Embraer 175* and the *E9X* with degradation highlights the broader performance differences between the electric and conventional aircraft, as the jet generates 6.6% more revenue. This is primarily because its higher cruise speed allows it to operate more flights and produce 9.4% more ASKs, and partly because it retains full network access throughout the year. Its total operating cost is 6.53% higher, driven by fuel and carbon allowance expenses, although it avoids the battery depreciation costs incurred by the electric aircraft.

The right panel in Figure 13 compares operational CO_2 emissions per seat-kilometer. Both *E9X* variants emit far less than the *Embraer 175* because electric aircraft avoid combustion emissions and only reflect upstream electricity emissions. Battery replacements add a small emissions component. Converting the results to passenger-kilometres using a load factor of 0.85 yields emissions roughly 25% below the 0.04 kg CO_2/pax-km reported by Delft [51] for the *E9X (V1)*. This is a notable outcome because CE Delft uses a lower electricity emission factor, which should result in lower values on their side. A possible explanation is that the BDAEFA framework assumes fully electric operations, while Elysian has indicated that the *E9X* is expected to use the fuel-powered reserve energy system on a share of the flights, which would raise emissions in practice. CE Delft does not state whether this reserve system is included in their modelling. The *Embraer 175* value is similar to the 0.117 kg/seat-km reported by Bernardo and Fageda [52], with minor deviations expected due to simplified fuel-burn assumptions in the BDAEFA input.

Together, these results show that ignoring battery degradation leads to overly optimistic economic outcomes for electric aircraft and masks the operational and financial disadvantages

that emerge once battery ageing is accounted for, which can determine whether electric aircraft are more or less profitable than conventional aircraft. Nevertheless, the electric variants maintain a clear CO_2 benefit over the *Embraer 175*.

5.6 American Eagle North-East U.S. Regional Case Study

This section applies the BDAEFA framework to a second case study on a North-East U.S. regional network based on *American Eagle*, the regional affiliate brand of *American Airlines* operated by several carriers [53]. Although *American Eagle* is a nationwide operator, its North-East sub-network is characterised by short flight lengths and a dense hub–and–spoke structure with additional spoke-to-spoke flights, operated by a considerable amount of *Embraer 175*. These characteristics enable the evaluation of the transferability of the BDAEFA framework. The analysis focusses on the *medium* degradation scenario and compares the outcomes of the simulation with those obtained in the *KLM Cityhopper* network of the previous sections. The construction of the case study network is described in Appendix C.

The *American Eagle* network, visualised in Figure 14 in Appendix C, differs from the *KLM Cityhopper* case in several ways. The network includes spoke-to-spoke routes, the route distances in the case study are about 40 km shorter on average, and demand is served by a smaller set of airports. As shown in Table 7, utilisation is slightly lower in the North-East U.S. case (6.5 flights per day) than in the *KLM Cityhopper* network (6.8). This counterintuitive result is likely explained by the much higher optimality gap in the U.S. case (23.5% versus 3.65%), since spoke-to-spoke connectivity and the shorter legs create far more feasible aircraft routing combinations for the solver to evaluate, even when the total number of flights is similar.

Table 7: *Network and degradation comparison between the KLM Cityhopper and American Eagle North-East U.S. case studies for the medium-degradation scenario.*

Metric	**KLM Cityhopper**	**NE U.S.**
Avg. flight length flown (km)	563	544
Flights per day per aircraft	6.8	6.5
Demand fulfilment (%)	81.0	80.9
Annual SoH loss (%/year)	14.8	13.7
Deep-discharge share (%)	34.6	35.7
Battery replacements	10	9
Battery depr. rate (€/km)	0.91	0.92

Overall, the degradation behaviour in the North-East U.S. network is very similar to that in the *KLM Cityhopper* case study. The shorter route distances and slightly lower utilisation both act to reduce annual SoH loss, while the marginally higher deep-discharge share has a small counteracting effect. The resulting degradation metrics and replacement requirements remain almost the same, aside from a modest reduction in SoH loss and one fewer battery replacement over the simulation period. The similarity in outcomes across these two structurally different networks shows that the framework responds logically to changing operational patterns and is transferable to other regional settings.

6 Conclusion

This research developed the Battery Degradation-Aware Electric Fleet Assignment (BDAEFA) framework to address an important gap in current electric airline operations modelling, in which battery degradation is currently omitted despite its significant influence on operational and economic viability. Ignoring battery degradation for electric aircraft can lead to physically infeasible schedules, as cumulative range loss may prevent several aircraft from operating longer sectors simultaneously. The primary research goal was to enable the systematic integration of battery ageing into a tactical electric airline planning framework. The secondary goal was to quantify how battery degradation shapes the long-term operational and economic performance of electric regional aviation.

To achieve these goals, the framework combines a rolling-horizon electric fleet assignment model with a battery degradation module that updates each aircraft's health between planning horizons based on the missions it has flown. The resulting battery state determines the aircraft's operational capability in the successive horizons, enabling the scheduling to adapt as the fleet's condition evolves. Multiple maintenance strategies were designed to govern when batteries are replaced and how fleet health is prioritized throughout operations. The framework was applied to a full-year simulation of the *KLM Cityhopper* network using the *Elysian E9X* to evaluate its behaviour under realistic operating conditions.

The BDAEFA framework showed realistic and coherent behaviour, with degradation patterns aligning with trends reported in the literature on battery ageing in electric passenger aircraft. The maintenance analysis showed that the most profitable option was not always the one maintaining full network coverage, and that the best balanced strategy preserved fleet health, avoided premature maintenance, and still delivered profitability close to the optimum, with only a negligible difference.

The degradation effects also proved to be economically significant. Battery depreciation amounted to roughly 0.91 €/km flown, equivalent to an added CASK of about 0.010 €/km, making it a meaningful contributor to operating costs. Comparing the *E9X* with and without battery degradation showed clear operational consequences: range loss reduced the ASK by 0.96%, which lowered revenue by 0.76%, while degradation increased total operating costs by 9.1% due to replacement requirements. The sensitivity analyses further demonstrated that the future degradation speed, battery and electricity price levels decisively influence economic viability, with outcomes shifting significantly across these conditions. The results showed that degradation reduces revenue by limiting range and increases operating costs due to battery wear, and studies that omit ageing therefore overstate the profitability of electric aircraft.

Together, these findings show that the inclusion of battery degradation is essential in the modelling of realistic electric airline operations. By integrating battery degradation into a tactical electric fleet assignment problem, this work addresses a key research gap, and the quantified degradation effects provide insights on how to approximate the impact without requiring a complex degradation-aware modelling framework.

While the BDAEFA framework advances the modelling of electric airline operations, certain limitations are acknowledged. Maintenance is applied through a rule-based system between simulation horizons rather than within the optimization framework, limiting the model's ability to evaluate maintenance-related network strain and planning choices. The degradation module captures expected ageing behaviour informed by current research, but necessarily remains high-level given the significant uncertainty surrounding future electric aircraft batteries. Finally, the revenue model is calibrated using *KLM Cityhopper* ticket data from the faster *Embraer 175*, creating a slight bias toward shorter routes that may influence degradation outcomes. Future work should address these limitations to further refine the framework and deepen the understanding of how degradation shapes electric airline operations.

Appendices

A Optional Fleet Activation Extension

This appendix outlines how the model can be extended to cases where aircraft activation becomes a decision rather than a fixed assumption. In the main model the fleet remains fully active, making lease costs constant. When activation decisions matter, for example in fleet sizing, the model can include a binary activation variable u_t for each aircraft $t \in T$, with consistency enforced through Equation 32.

$$\sum_{f \in F} y_{ft} \leq |F| \cdot u_t \qquad \forall t \in T \tag{32}$$

In a model where aircraft activation is explicitly decided, lease expenses appear as a decision-dependent term in the objective function. This is expressed in Equation 33.

$$\sum_{t \in T} c^{\text{lease}} u_t \tag{33}$$

This formulation allows the optimiser to determine the number of active aircraft based on profitability and operational need. Block-time feasibility similarly applies only to active aircraft, as shown in Equation 34.

$$\sum_{f \in F} \text{dur}_f \, y_{ft} \leq BT^{\max} \, u_t \qquad \forall t \in T \tag{34}$$

These adjustments allow the EFAM to jointly determine fleet utilisation and scheduling. They are omitted in the main formulation because the case study assumes a fixed active fleet and would otherwise be redundant in the formulation.

B Embraer 175 Parameters

This appendix summarizes the technical and economic parameters of the *Embraer 175* used for the experiments presented in Section 5.5.

1. *Flight service and airport fees:* Costs include landing, take-off, parking, and passenger-related charges from the official Schiphol Airport Charges and Conditions [32]. For the *Embraer 175*, the LTO charge is €7.01 per tonne of aircraft weight and the passenger-related charge is €18.33 per passenger. The aircraft falls under the S4 noise category with higher tariffs. Baggage handling fees are included at €300 per flight.
2. *Embraer 175 4-weekly lease cost:* In 2024 *American Airlines* purchased 133 *Embraer 175* for €45M per aircraft [34]. The *KLM Cityhopper* average fleet age is around 9 years [54]. Using the aircraft value depreciation rate of 5% by International Air Transport Association [55], the aircraft is calculated to be priced at around 50% of its original price in 2035, resulting in a residual value of €22.5M. Using a slightly conservative lease rate of 0.5% per month for the older aircraft results in a four-weekly lease cost of €100.000 [36].
3. *Embraer 175 fuel burn rate:* The fuel consumption is modelled at 2.5 kg/km. This is derived from an average 800 km flight burning approximately 2000 kg of mission fuel, with additional fuel carried as reserve, keeping in mind the E175 has a fuel capacity of 9,000 kg

and a range of 3,300 km [56]. The estimate is close to the 2.92 kg/km reported for aircraft from before 2024 fleet in [57], with this slightly lower value reflecting a newer 2030-2035 variant.

4. *Embraer 175 fuel cost:* A blended fuel price is applied following a 90% Jet A-1 and 10% SAF mix according to [58], with respective prices of €0.80/kg including additional airport charges and €2.00/kg for 2030-2035 [59, 60]. This results in an average fuel cost of €0.92/kg.
5. *Embraer 175 emission factor:* The well-to-wake emission factor of the blended fuel is derived from 90% Jet A-1 (3.15 kg CO_2/kg) and 10% SAF with a 65% lifecycle reduction [58, 61], leading to an emission factor of 3.42 kg CO_2/kg of fuel.
6. *Cruise speed:* The *Embraer 175* operates at a cruise true airspeed of ≈830 km/h at FL350 [56].

C Case Study Design - American Eagle North-East U.S.

This appendix discusses the creation of the North-East U.S. case study used in Section 5.6. The objective is to create a realistic regional airline network by using real commercial aviation data from Bureau of Transportation Statistics [62]. The network and its corresponding schedule is tailored to the operational range and specifics of the *Elysian E9X*. The case study is based on routes flown by *American Eagle*, the regional brand of *American Airlines* affiliated with several partner carriers operating short-haul and feeder services the hubs.

To construct a representative network for the degradation-aware electric airline planning framework from these operations, the T–100 Domestic Segment (All Carriers) dataset was transformed. This dataset reports every domestic flight segment, with accompanying operational and traffic metadata. The dataset was merged with airport geolocation information to form the initial network representation. Preprocessing steps removed invalid or incomplete records and filtered the dataset to keep only routes operating between airports within a selected group of North-Eastern U.S. states. The air-traffic across the *American Eagle* carriers was aggregated by airport pair to create demand profiles. Also, estimated block times for the *E9X* were computed using great-circle distances with the *E9X* cruise speed, adjusted by a factor of 1.08 to account for routing inefficiencies and a factor of 0.85 to reflect reduced average speeds during climb and descent and an additional 40 minute turnaround time.

LaGuardia Airport (LGA) is chosen for the network hub of the case study, as it is one of the primary *American Eagle* hubs. For the selection of included routes and airports the top 14 routes linking LGA to airports within the selected states are selected, filtered to those below the 970 km network range limit of the *E9X*. Minor route-specific adjustments were applied to outliers and form a balanced network.

Additional spoke-to-spoke routes were added for routes already containing both airports in the LGA hub-to-spoke network, selected again by the 970 km range limit and prioritised by weekly passenger volume. Resulting in a final network of 15 airports and 56 directional routes being used in this case study, as depicted in Figure 14. To match the demand of the *KLM Cityhopper* network the total weekly demand was uniformly scaled to 43,000 passengers.

A full weekly schedule of potential flights was generated in a similar manner to the *KLM Cityhopper* case study in Chapter 4. However, as there are high fluctuations in demand per OD pair flights for routes are generated proportionally to their demand with high demand OD pairs receiving 40% more options than the lowest demand, ensuring that higher-demand connections received more frequent service. Subsequently, each flight was annotated with the economic formulation.

The final case study includes a cleaned airport set, passenger demand matrix, distance

matrix, and a schedule with weekly flight options.

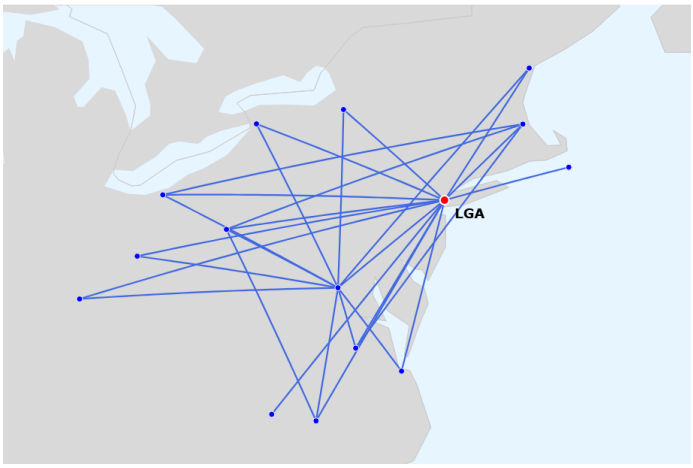

Figure 14: *Depiction of the available routes in the North-East U.S. Case Study with La-Guardia Airport (LGA) as hub.*

References

[1] Dev, Astha, Faizan, Sneha, Vaibhavi, and Prasanna Raut. The economic impact of aviation. *International Journal of Research Publication and Reviews*, 4(12):4193–4198, December 2023.

[2] International Energy Agency (IEA). Aviation. `https://www.iea.org/energy-system/transport/aviation`, 2025.

[3] Air Transport Action Group (ATAG). Fact sheet 4: Aviation 2050 goal and the paris agreement. `https://aviationbenefits.org/media/167476/fact-sheet_4_aviation-2050-and-paris-agreement2.pdf`, October 2021.

[4] R. de Vries, R. E. Wolleswinkel, M. F. M. Hoogreef, and R. Vos. A new perspective on battery-electric aviation, part ii: Conceptual design of a 90-seater. In *Proceedings of the AIAA SciTech 2024 Forum*, Orlando, Florida, United States, 2024. American Institute of Aeronautics and Astronautics (AIAA). doi: 10.2514/6.2024-1490. Article AIAA 2024-1490.

[5] Rob E. Wolleswinkel, Reynard De Vries, Maurice Hoogreef, and Roelof Vos. A New Perspective on Battery-Electric Aviation, Part I: Reassessment of achievable range. *AIAA SCITECH 2022 Forum*, 1 2024. doi: 10.2514/6.2024-1489. URL `https://doi.org/10.2514/6.2024-1489`.

[6] J. Zhang et al. Cycle life studies of lithium-ion power batteries for electric vehicles in recent years: A systematic overview. *eTransportation*, 22:100748, 2024. doi: 10.1016/j.etran.2024.100748.

[7] Jean-Marc Tarascon. The li-ion battery: 25 years of exciting and enriching experiences. *Interface*, 25(3):79–83, 2016. doi: 10.1149/2.F08163if.

[8] Jacqueline S. Edge, Simon O'Kane, Ryan Prosser, Niall D. Kirkaldy, Anisha N. Patel, Alastair Hales, Abir Ghosh, Weilong Ai, Jingyi Chen, Jiang Yang, Shen Li, Mei-Chin

Pang, Laura Bravo Diaz, Anna Tomaszewska, M. Waseem Marzook, Karthik N. Radhakrishnan, Huizhi Wang, Yatish Patel, Billy Wu, and Gregory J. Offer. Lithium-ion battery degradation: what you need to know. *Physical Chemistry Chemical Physics*, 23 (13):8200–8221, 2021. doi: 10.1039/D1CP00359C.

[9] Rob Alan McDonald. Batteries are not fuel. *EngRxiv (Preprint)*, 2023. doi: 10.31224/2803. Preprint. Originally posted Jan. 30 2023.

[10] Laxman Timilsina, Payam R. Badr, Phuong H. Hoang, Gokhan Ozkan, Behnaz Papari, and Christopher S. Edrington. Battery degradation in electric and hybrid electric vehicles: A survey study. *IEEE Access*, 11:42431–42465, 2023. doi: 10.1109/ACCESS.2023.3271287.

[11] Luca Biggio, Tommaso Bendinelli, Chetan Kulkarni, and Olga Fink. Dynaformer: A deep learning model for ageing-aware battery discharge prediction. *arXiv preprint*, arXiv:2206.02555, 2022. URL `https://arxiv.org/abs/2206.02555`.

[12] Friedrich von Bülow and Tobias Meisen. A review on methods for state of health forecasting of lithium-ion batteries applicable in real-world operational conditions. *Journal of Energy Storage*, 57:105978, 2023. ISSN 2352-152X. doi: 10.1016/j.est.2022.105978.

[13] Ming-Feng Ge, Yiben Liu, Xingxing Jiang, and Jie Liu. A review on state of health estimations and remaining useful life prognostics of lithium-ion batteries. *Energy Conversion and Management*, 245:114528, 2021. doi: 10.1016/j.enconman.2021.114528.

[14] Daniel J. Caetano and Nicolau Dionísio Fares Gualda. A flight schedule and fleet assignment model. In *12th World Conference on Transport Research (WCTR)*, Lisbon, Portugal, July 11–15 2010.

[15] H. D. Sherali, E. K. Bish, and X. Zhu. Airline fleet assignment concepts, models, and algorithms. *European Journal of Operational Research*, 172(1):1–30, 2006. doi: 10.1016/j.ejor.2005.01.056.

[16] M. F. M. Hoogreef, N. R. Zuijderwijk, E. Scheers, P.-J. Proesmans, and B. F. Santos. Coupled hybrid & electric aircraft design and strategic airline planning. In *AIAA AVIATION 2023 Forum*. American Institute of Aeronautics and Astronautics (AIAA), 2023. doi: 10.2514/6.2023-3869. AIAA 2023-3869.

[17] Wessel L. Kruidenier. Integrated flight scheduling and routing of hybrid and electric aircraft: Enhancing network performance through partial recharging. Master's thesis, Delft University of Technology, 6 2025. URL `https://resolver.tudelft.nl/uuid:3a8b116a-8650-47f0-b83f-7ec2bfce87d4`. Master's thesis, Faculty of Aerospace Engineering, TU Delft. Available at: `https://resolver.tudelft.nl/uuid:3a8b116a-8650-47f0-b83f-7ec2bfce87d4`.

[18] Todd A. Spierling, Alexander Lynch, and Thomas H. Bradley. Battery optimization for sustainable aviation: A comprehensive analysis for battery electric aircraft. *Journal of Aircraft*, May 2025. doi: 10.2514/1.C038197.

[19] Elysian Aircraft. Electric aircraft — e9x concept and company overview. `https://www.elysianaircraft.com/`, 2025.

[20] Finn Jørgensen and John Preston. The relationship between fare and travel distance. *Journal of Transport Economics and Policy*, 41:451–468, 09 2007.

[21] Leevi Lignell, Minh Tran, and Tomi Roinila. Impedance measurement of lithium-ion batteries using optimized pulse patterns. *Journal of Energy Storage*, 137:118590, 2025. ISSN 2352-152X. doi: https://doi.org/10.1016/j.est.2025.118590. URL https://www.sciencedirect.com/science/article/pii/S2352152X25033031.

[22] Jacqueline S. Edge, Simon O'Kane, Ryan Prosser, Niall D. Kirkaldy, Anisha N. Patel, Alastair Hales, Abir Ghosh, Weilong Ai, Jingyi Chen, Jiang Yang, Shen Li, Mei-Chin Pang, Laura Bravo Diaz, Anna Tomaszewska, M. Waseem Marzook, Karthik N. Radhakrishnan, Huizhi Wang, Yatish Patel, Billy Wu, and Gregory J. Offer. Lithium ion battery degradation: what you need to know. *Physical Chemistry Chemical Physics*, 23(14):8200–8221, 2021. doi: 10.1039/D1CP00359C. URL https://doi.org/10.1039/D1CP00359C.

[23] Peter Keil, Simon F. Schuster, Jörn Wilhelm, Julian Travi, Andreas Hauser, Ralph C. Karl, and Andreas Jossen. Calendar aging of lithium-ion batteries: I. impact of the graphite anode on capacity fade. *Journal of The Electrochemical Society*, 163(9):A1872–A1880, 2016. doi: 10.1149/2.0411609jes. Open Access (CC BY 4.0).

[24] Gülşah Yarimca and Erdal Cetkin. Review of cell level battery (calendar and cycling) aging models: Electric vehicles. *Batteries*, 10(11):374, 2024. doi: 10.3390/batteries10110374. URL https://www.mdpi.com/2313-0105/10/11/374. Open access review article.

[25] Trishna Raj, Andrew A. Wang, Charles W. Monroe, and David A. Howey. Investigation of path-dependent degradation in lithium-ion batteries. *Batteries & Supercaps*, 3(12):1377–1385, 2020. doi: 10.1002/batt.202000160. URL https://doi.org/10.1002/batt.202000160.

[26] T. Yüksek and A. Alkaya. Effect of the depth of discharge and c-rate on battery degradation and cycle life. In *Proceedings of the 15th International Conference on Electrical and Electronics Engineering (ELECO 2023)*, pages 212–217. Bursa Technical University, 2023. URL https://www.eleco.org.tr/ELECO2023/eleco2023-papers/212.pdf.

[27] Matthew B. Pinson and Martin Z. Bazant. Theory of SEI formation in rechargeable batteries. *Journal of The Electrochemical Society*, 160(2):A243–A250, 2013. doi: 10.1149/2.044302jes. URL https://doi.org/10.1149/2.044302jes.

[28] Dominik Werner, Fabian Walther, Adnan Nuhic, Thomas Waldmann, Marc Kasper, and Michael A. Danzer. How to model aging processes of lithium-ion batteries—a comprehensive overview and comparison of aging models. *Batteries*, 7(2):28, 2021. doi: 10.3390/batteries7020028. URL https://www.mdpi.com/2313-0105/7/2/28.

[29] Takuya Akiba, Shotaro Sano, Toshihiko Yanase, Takeru Ohta, and Masanori Koyama. Optuna: A next-generation hyperparameter optimization framework. In *Proceedings of the 25th ACM SIGKDD International Conference on Knowledge Discovery and Data Mining*, 2019.

[30] Reynard de Vries, Maurice F. M. Hoogreef, and Roelof Vos. Range equation for hybrid-electric aircraft with constant power split. *Journal of Aircraft*, 57(3):552–557, 2020. doi: 10.2514/1.C035734. Engineering Notes.

[31] Amadeus IT Group. Amadeus for developers: Connect to amadeus travel apis, n.d. URL https://developers.amadeus.com/.

[32] Royal Schiphol Group N.V. Amsterdam airport schiphol charges and conditions 2025–2027. https://www.schiphol.nl/nl/aviation-partnerships/ams-airport-charges-levies-slots-and-conditions/, June 2025. URL https://www.schiphol.nl/nl/aviation-partnerships/ams-airport-charges-levies-slots-and-conditions/. Final setting following ACM decision, effective April 1, 2025.

[33] Glassdoor LLC. Werken bij klm – overzicht. https://www.glassdoor.nl/Overzicht/Werken-bij-KLM-EI_IE3486.11,14.htm, 2025.

[34] Embraer S.A. American airlines places order for up to 133 embraer aircraft. https://www.embraer.com/media-center/en/?detail=13847-American-Airlines-Places-Order-for-up-to-133-Embraer-Aircraft, 2024.

[35] Reynard de Vries, Rob E. Wolleswinkel, Joaquin Exalto, Pieter van den Berg, Roelof Vos, and Maurice F. M. Hoogreef. Conceptual redesign of a 90-seater battery-electric aircraft. In *AIAA Aviation Forum*, 2025. doi: 10.2514/6.2025-3153. Available at https://doi.org/10.2514/6.2025-3153.

[36] Shane Matthews, Darren Naughton, and David Griffin. Push and pull factors on aircraft lease rates 2025. White paper, SMBC Aviation Capital, 2025. URL https://www.smbc.aero/sites/smbc.aero/files/2025-03/SMBC_AC_PushPull_Whitepaper_AW.pdf.

[37] Rob Geldhof, Rutger Bianchi, and Jort Wolda. De energierekening in 2035 – vooruitblik naar beleidseffecten en tariefontwikkeling. Technical report, Berenschot, Jan 2024. URL https://www.berenschot.nl/media/yyhip2qv/240124_essent_betaalbaarheid_energierekening_rapportage_deela.pdf. Report commissioned by Essent on energy bills in 2035.

[38] BloombergNEF. Lithium-ion battery pack prices see largest drop since 2017 – falling to us$115/kwh. article on BloombergNEF website, 2024.

[39] Alessandra Zanoletti, Eleonora Carena, Chiara Ferrara, and Elza Bontempi. A review of lithium-ion battery recycling: Technologies, sustainability, and open issues. *Batteries*, 10(1):38, 2024. doi: 10.3390/batteries10010038.

[40] Co_2-uitstoot per kwh elektriciteit nederland. https://dashboardklimaatbeleid.nl/mosaic/mosaic/elektriciteit, 2024.

[41] Maurizio Clemente, Prapti Maharjan, Mauro Salazar, and Theo Hofman. Meta-analysis of life cycle assessments for li-ion batteries production emissions. Technical report, arXiv.org, June 2025. URL https://arxiv.org/abs/2506.05531. Preprint.

[42] Esg economist — scenarios shaping eu ets prices. https://www.abnamro.com/research/en/our-research/esg-economist-scenarios-shaping-eu-ets-prices, 2025.

[43] Eu emissions trading system (eu ets). https://climate.ec.europa.eu/eu-action/carbon-markets/eu-emissions-trading-system-eu-ets_en, 2025.

[44] Anmol Jain, Alberto Martinetti, and Lex van Dongen. Mapping the needs of design for maintenance in electric aviation. In *Proceedings of the International Conference on Through-life Engineering Services (TES)*. University of Twente, 2021. URL https://ris.utwente.nl/ws/portalfiles/portal/275123722/TESConf_2021_paper_18_34_39final.pdf.

[45] Flightradar24. Live flight tracker – real-time flight tracker map. https://www.flightradar24.com/, 2025.

[46] Air France–KLM Group. Fleet – klm at december 31, 2024 (66 long-haul aircraft) and other fleet data. https://www.airfranceklm.com/en/group/fleet, 2024.

[47] Gwyneth Butera. Is gurobi deterministic? Gurobi Help Center article, Oct 2025. https://support.gurobi.com/hc/en-us/articles/360031636051-Is-Gurobi-deterministic?

[48] International Air Transport Association (IATA). Industry set to deliver sustainable profitability in 2025. https://www.iata.org/en/pressroom/2025-releases/2025-06-02-01/, June 2025.

[49] Knut Veisten, Paal Brevik Wangsness, Eivind Farstad, and Inga Margrete Ydersbond. Will people prefer future travel with battery-powered airplanes? *Transportation Research Part D: Transport and Environment*, 126:104013, 2024. doi: 10.1016/j.trd.2023.104013. URL https://doi.org/10.1016/j.trd.2023.104013.

[50] Nicole Wendt, Gorm Kipperberg, and Henrik Lindhjem. Consumer willingness to pay for emission reduction in air travel: A meta-analysis. *Transportation Research Part D: Transport and Environment*, 134:104347, 2024. doi: 10.1016/j.trd.2024.104347. URL https://doi.org/10.1016/j.trd.2024.104347.

[51] CE Delft. Climate change impact analysis of electric aviation. Technical Report 240152, CE Delft, January 2025. URL https://ce.nl/wp-content/uploads/2025/02/CE_Delft_240152_Climate_Change_Impact_Analysis_of_Electric_Aviation_Def_.pdf. Report prepared for CE Delft.

[52] Valeria Bernardo and Xavier Fageda. The impact of new aircraft on carbon emissions. *Transportation Research Part D: Transport and Environment*, 147:104949, 2025. doi: 10.1016/j.trd.2025.104949. URL https://www.sciencedirect.com/science/article/pii/S1361920925003591.

[53] AeroTime Editorial. Piedmont, envoy, psa: Aa's 'american eagle' regional subsidiaries explained, January 30 2025. URL https://www.aerotime.aero/articles/american-airlines-regional-subsidiaries-explained.

[54] Planespotters.net. Klm cityhopper fleet and age statistics. https://www.planespotters.net/airline/KLM-Cityhopper, n.d.

[55] Industry Accounting Working Group International Air Transport Association (IATA). Airline disclosure guide: Aircraft acquisition cost and depreciation. https://www.iata.org/contentassets/4a4b100c43794398baf73dcea6b5ad42/airline-disclosure-guide-aircraft-acquisition.pdf, 2024.

[56] KLM Royal Dutch Airlines. Embraer 175 — aircraft types. https://www.klm.nl/en/information/travel-class-extra-options/aircraft-types/embraer-175?showredirectnotice=1, 2025.

[57] Esteban García, Dan Rutherford, Xinyi Zheng, and Shiyuan Shao. Committed emissions from existing aircraft fleets: 2024 status update. Technical report, International Council on Clean Transportation (ICCT), July 2024. URL https://theicct.org/wp-content/uploads/2024/07/ID-188-%E2%80%93-Committed-emissions_wp_final.pdf.

[58] KLM Royal Dutch Airlines. Saf: alternative aviation fuel. https://www.klm.nl/en/information/sustainability/saf, 2025.

[59] International Air Transport Association. Jet fuel price monitor. https://www.iata.org/en/publications/economics/fuel-monitor/, 2025.

[60] World Economic Forum, Delta Air Lines, Breakthrough Energy, and International Air Transport Association. Clean skies for tomorrow: Sustainable aviation fuels as a pathway to net-zero aviation. Technical report, World Economic Forum, October 2020. URL https://www3.weforum.org/docs/WEF_Clean_Skies_Tomorrow_SAF_Analytics_2020.pdf.

[61] Greenhouse Gas Management Institute and Stockholm Environment Institute. Using carbon credits for air travel. https://offsetguide.org/using-carbon-credits-for-air-travel/, 2025.

[62] Bureau of Transportation Statistics. Data bank 28ds - t-100 domestic segment data (world area code). U.S. Department of Transportation, Bureau of Transportation Statistics, 2025. URL https://www.bts.gov/browse-statistical-products-and-data/bts-publications/data-bank-28ds-t-100-domestic-segment-data.

4

Literature Study

Research Proposal

Battery Degradation and Ageing-Aware Electric Airline Optimization Planning

MSc Thesis

Duncan van Woerkom

Delft University of Technology

TU Delft

Research Proposal

Battery Degradation and Ageing-Aware Electric Airline Optimization Planning

by

Duncan van Woerkom

Supervisor I:	Dr. I.I. (Ingeborg) de Pater
Supervisor II:	P. (Pieter-Jan) Proesmans
Project Duration:	Feb 2025 - Jan 2026
Faculty:	Faculty of Aerospace Engineering, Delft

Cover: Elysian Aircraft E9X Render [1]

TU Delft

Summary

In response to the growing urgency of climate change, the aviation industry is under significant pressure to reduce its environmental impact. International climate accords such as the Paris Agreement and the Advisory Council for Aviation Research and Innovation in Europe have made ambitious goals to enable climate neutral air travel. Where the target is to have net-zero CO_2 emissions by the year 2050. To reach these targets, a huge transformation in in propulsion technologies and technological development is necessary. Here, battery-electric aircraft emerge as a potential pathway for decarbonizing regional air transport.

However, to realize the full potential of electric aircraft more than just innovative aircraft design is necessary. The traditional airline planning models and tools assume fixed aircraft performance, which is not applicable for electric aircraft as their battery systems degrade over time. This key difference renders them insufficient for managing the operational and economic challenges that come due to battery ageing and degradation.

This thesis addresses that gap by focusing on the operational challenges of managing battery-electric aircraft as they age. In particular, it identifies the need for a fleet planning framework that can dynamically incorporate battery degradation effects into realistic strategic airline operations.

A literature review was conducted to evaluate the future battery-electric aircraft design, degradation modeling, and airline operations. This has revealed that while much work has been done in aircraft conceptual design and battery performance characterization, there is a lack of integrated approaches that incorporate battery health into fleet-level operational planning. These insights highlighted the need for research in the development of suitable planning frameworks. Based on these insights the research question that this thesis seeks to address is:

> *"How can battery degradation and ageing be systematically incorporated into an electric fleet assignment model to optimize realistic operational and economic performance over time?"*

To achieve this objective, the literature research has a structured methodology consisting of four key components: (i) a data-driven machine learning battery degradation model, (ii) a range model linking battery health to electric aircraft range using a modified version of the Breguet equation, (iii) a mixed-integer linear programming setup for the electric fleet assignment problem, and (iv) a rolling horizon simulation framework that enables the continuous adaptation of the updated battery states. This modular architecture enables forward-looking decision-making in electric airline planning.

By linking battery performance to operational outcomes, this methodology lays the foundation for electric airline planning that goes beyond static models. It enables the evaluation of long-term strategies for aircraft assignment and battery replacement, with the goal of ensuring both realistic operational outcomes and economic viability. On this basis, the objective of this thesis is:

> *"To develop a rolling horizon fleet assignment model for battery-electric aircraft that integrates battery degradation and ageing. The model aims to support optimal and realistic operational planning and battery replacement strategies, with a focus on maintaining aircraft performance and minimizing long-term costs."*

The model will be tested according to two case studies. The first uses fictional data from a regional Italian network to benchmark model behavior and identify areas for refinement. The second case study will use real schedule data to evaluate the model's transferability and sensitivity analyses will explore the impact of parameter variation, such as battery technology scenarios and degradation speed uncertainty.

This research will contribute a modular framework designed for degradation-aware electric fleet planning. The findings will offer operational insights into battery replacement strategies and realistic planning, where the modelled aircraft is the Elysian E9X, currently in development by Elysian Aircraft.

Contents

Nomenclature

Abbreviations

Abbreviation	Definition
ADP	Approximate Dynamic Programming
AI	Artificial Intelligence
ASK	Available Seat Kilometer
BART	Bayesian Additive Regression Trees
BMS	Battery Management Systems
BNN	Bayesian Neural Network
CI	Confidence Interval
DDP	Deterministic Dynamic Programming
DoD	Depth of Discharge
DP	Dynamic Programming
EIS	Electrochemical Impedance Spectroscopy
ECM	Equivalent Circuit Model
e-SAF	Electrofuels-based Sustainable Aviation Fuel
EM	Electrochemical model
EV	Electric Vehicle
FAM	Fleet Assignment Model
GPR	Gaussian Process Regression
ISU - ILCC	Iowa State University - Iowa Lake Community Collage
KPI	Key Performance Indicator
KTAS	Knots True AirSpeed
Li-ion	Lithium-ion
LSTM	Long Short Term Memory
MAE	Mean Absolute Error
MC	Monte Carlo
MCMC	Markov Chain Monte Carlo
MILP	Mixed-Integer Linear Programming
MSE	Mean Squared Error
NASA	The National Aeronautics and Space Administration
NCA	Nickel Cobalt Aluminum
NMC	Nickel Manganese Cobalt
NN	Neural Network
PV	Photovoltaic
RL	Reinforcement Learning
RMSE	Root Mean Square Error
RFR	Random Forest Regression
RNN	Recurrent Neural Network
RUL	Remaining Useful Life
SAF	Sustainable Aviation Fuel
SEI	Solid Electrolyte Interphase
SoC	State of Charge
SoH	State of Health
SVR	Support Vector Regression
XGBOOST	eXtreme Gradient Boosting
bioSAF	Bio-based Sustainable Aviation Fuel

Symbols

Symbol	Definition	Unit
AC_k	Number of aircraft in the fleet of type k	[units]
C	C-rate (charge/discharge rate multiplier relative to nominal capacity)	[1/h]
C	Context length (sequence length input to encoder)	[samples]
C_f	Capacity fade or loss relative to nominal capacity	[%]
C_{ret}	Capacity retention	[%]
C_t	Cell state at time step t	[–]
$CASK$	Cost per Available Seat Kilometer	[€/ASK]
$\text{CI}_{95\%}$	95% confidence interval for prediction	[same as y]
D	Drag force	[N]
d_i	Distance of flight i	[km]
d_k	Dimensionality of key vectors	[–]
E_d	Energy density (gravimetric or volumetric)	[Wh/kg], [Wh/L]
e_{bat}	Usable battery energy density	[Wh/kg]
EM	Total usable battery energy (mass-equivalent)	[kg]
EoL	End-of-Life threshold	[% SoH]
F	Set of flights	[–]
f_t	Forget gate activation at time step t	[–]
f_i^k	Binary variable: 1 if flight arc i is assigned to aircraft type k, 0 otherwise	[–]
G_k	Set of ground arcs for aircraft type k	[–]
g	Gravitational constant	[m/s^2]
$g(x; T_j, M_j)$	Regression tree function with structure T_j and parameters M_j	[–]
h	Hidden dimension size in projection layers	[–]
h_t	Hidden state at time step t	[–]
H_p	Optimal prediction horizon	[flight hours] or [cycles]
H_p	Prediction horizon	[cycles], [flight hours]
i_t	Input gate activation at time step t	[–]
$I(k, n)$	Flight arcs terminating at node n in fleet k	[–]
K	Key matrix in attention mechanism	$\mathbb{R}^{T \times d_k}$
K	Set of aircraft types	[–]
L	Lift force	[N]
L	Original input sequence length	[samples]
LCC/FH	Lifecycle Cost per Flight Hour	[€/h]
m	Total number of regression trees in the model	[–]
M_j	Terminal node parameters of the j-th tree	[–]
$MTOM$	Maximum Take-Off Mass	[kg]
n	Token length (number of points per token)	[samples]
n^+	Ground arcs originating at node n	[–]
n^-	Ground arcs terminating at node n	[–]
N	Set of airports	[–]
N_{cycle}	Cycle life (number of charge-discharge cycles)	[cycles]
N_G^*	Set of flight and ground arcs intersecting the time cut	[–]
$O(k, n)$	Flight arcs originating at node n in fleet k	[–]
oc_i^k	Unit operating cost for aircraft type k on flight i	[/ASK]
o_t	Output gate activation at time step t	[–]
P_d	Power density	[W/kg]
$p(w\|\mathcal{D})$	Posterior distribution over weights given data	[–]
$p(y^*\|x^*, \mathcal{D})$	Posterior predictive distribution	[–]

Symbol	Definition	Unit
$p(y^*\|x^*, w)$	Likelihood of output given input and weights	[–]
q_i	Traffic demand for flight i	[passengers]
q_{max}	Maximum charge capacity of the battery	[Ah]
Q	Query matrix in attention mechanism	$\mathbb{R}^{T \times d_k}$
R_0	Internal resistance of the battery	[Ω]
R_k	Range of aircraft type k	[km]
R_{max}	Maximum achievable still-air cruise range	[m] or [km]
$RASK$	Revenue per Available Seat Kilometer	[€/ASK]
rev	Revenue per Revenue Passenger Kilometer (RPK) flown	[/RPK]
s	Number of seats per aircraft	[seats]
s_i	Sub-sequence token i in the input sequence	$\mathbb{R}^n$
σ	Standard deviation of prediction error	[%]
σ	Sigmoid activation function	[–]
σ^2	Prediction variance (uncertainty estimate)	[same as y^2]
σ^2	Variance of the error term	[same as Y^2]
$\tilde{C}_t$	Candidate cell state at time step t	[–]
$\tanh$	Hyperbolic tangent activation function	[–]
T	Calendar life	[years]
T	Number of stochastic forward passes	[–]
T	Number of tokens in sequence, $T = L/n$	[–]
T_j	Structure of the j-th regression tree	[–]
V	Value matrix in attention mechanism	$\mathbb{R}^{T \times d_v}$
V	Velocity	[m/s]
W	Neural network weights	[–]
W_f, W_i, W_C, W_o	Weight matrices for forget, input, candidate, and output gates	[–]
W_t	Dropout-sampled weights during forward pass t	[–]
x	Input feature vector	[–]
x	Input features (e.g., voltage, current, temperature)	[varies]
x_t	Input feature vector at time step t	[–]
x^*	New input sample	[varies]
y	Target output (e.g., capacity or RUL)	[varies]
y^*	Predicted output corresponding to x^*	[varies]
y_a^k	Number of aircraft of type k on ground arc a	[–]
Y	Predicted output variable	[varies]
$\hat{y}_t$	Prediction from forward pass t	[varies]
μ	Mean of predictions across T forward passes	[same as y]
b_f, b_i, b_C, b_o	Bias vectors for forget, input, candidate, and output gates	[–]
w	Neural network weights (random variable)	[–]
$\mathcal{D}$	Training dataset	[–]
η_{elec}	Electric powertrain efficiency	[–]
η_p	Propeller efficiency	[–]
$(L/D)_{\text{max}}$	Maximum lift-to-drag ratio	[–]

Materials and Compounds

Material/Compound	Description
Li	Lithium
Si	Silicon
Ni	Nickel
Co	Cobalt
Mo	Molybdenum
Li-S	Lithium-Sulfur
H_2	Hydrogen
CO_2	Carbon Dioxide
$Li[Ni_{0.95}Co_{0.04}Mo_{0.01}]O_2$	Molybdenum-doped nickel-rich cathode material
$LiCoO_2$	Lithium Cobalt Oxide
$LiNiMnCoO_2$ (NMC)	Lithium Nickel Manganese Cobalt Oxide
$LiFePO_4$	Lithium Iron Phosphate
$LiNiCoAlO_2$ (NCA)	Lithium Nickel Cobalt Aluminum Oxide
$LiPF_6$	Lithium Hexafluorophosphate

List of Figures

List of Tables

1

Introduction

The aviation industry plays a vital role in global connectivity. However, it is also a major contributor to global warming and one of the fastest growing contributors to climate change. The sector is responsible for approximately 2-3% of global CO_2 emissions [2]. Maybe even more concerning is aviation's non-CO_2 impact, which includes nitrogen oxides (NO_X), water vapor, and contrail-induced cloud formation, all of which contribute significantly to global warming [3]. These factors bring the need to urgently reduce greenhouse gas emissions and contrail formation, and hereby adhering to international climate targets such as the Paris Agreement [4].

To address these environmental pressures, the aviation sector is exploring alternative technologies [5] with electric aircraft emerging as one of the promising pathways [6]. The electric aircraft will have more efficient and quieter propulsion, making them attractive for both environmental and operational reasons. However, there are still numerous obstacles to overcome, most notably the limitations of battery technology [6, 7].

Modern lithium-ion batteries currently offer around 250-300 Wh/kg [8], while A-1 jet fuel provides approximately 12,000 Wh/kg of energy. This stark contrast in energy density results in reduced range and payload capacity, limiting the potential of electric aircraft. In addition to this limitation, batteries deteriorate over time, causing their performance and maximum battery capacity to decrease [9], having significant financial and logistical implications [7] for the aircraft.

Despite these challenges, the advancements technology offer promising solutions for integrating electric aircraft into commercial operations [6, 7, 10]. Current airline planning models do not account for the dynamic nature of electric aircraft, they treat batteries as static energy sources rather than components that degrade over time. This key literature gap highlights the need for a more thought through approach to airline optimization that accounts for the degradation effects.

This thesis aims to address this key research gap by developing a degradation-aware optimization framework for electric airline planning. By integrating battery degradation models into airline scheduling, this research seeks to improve the operational viability of electric aviation and the understanding of the operational differences. This literature study focuses on relevant factors such as battery cycle life, battery state of health predictions, and electric airline planning to develop a robust planning framework.

This paper consists of ten chapters in total. Chapter 2 explores various pathways to decarbonizing aviation. Chapter 3 gives background on electric aviation. Chapters 4, 5, and 6 delve into the key technical domains relevant to this research. chapter 7 presents the research proposal. The paper concludes with the project planning in chapter 8 and the final conclusions in Chapter 9.

2

Decarbonizing Aviation: Pathways Toward Sustainable Flight

Building on growing climate urgency, several technological pathways are being explored to decarbonize aviation, each of these with unique trade-offs in feasibility, scalability, and readiness. The pathways are sustainable aviation fuels (SAFs), hydrogen propulsion, hybrid-electric systems, and full battery-electric propulsion.

2.1. The Environmental Imperative

International policy frameworks and goals such as the European Commission's Green Deal [11] and the Advisory Council for Aviation Research and Innovation in Europe goals [12] have established the goal of a net-zero aviation sector by the year 2050. Accomplishing this target requires significant development in every layer of aircraft design and the airline planning operations.

As aircraft were initially developed, fuel sources similar to jet fuel enabled the range and flexibility needed for global air transport. This fuel had a high energy density. However, it was carbon-intensive and not developed with emissions in mind. Even the most efficient turbofan engines emit substantial CO_2 and non-CO_2 pollutants [13]. Incremental improvements in aerodynamics and engine efficiency are no longer sufficient to meet climate goals. A shift in the focus of research is required to investigate better pathways.

2.2. Pathways to Decarbonization

Research in the aviation sector is pursuing several technological pathways toward decarbonization. Each of these offer different benefits and limitations:

Sustainable Aviation Fuels: These replacements for kerosene have been thoroughly developed over the last few years and can be used in existing aircraft with minimal modifications. SAFs can be created through multiple manners, from biomass (bio-SAF) or synthesized from captured CO_2 and renewable hydrogen (eSAF) [14, 15]. They offer significant CO_2 emission and lifecycle reductions but face constraints in availability, land use, and production costs. These SAFs also do not eliminate non-CO_2 emissions and contrails [5].

Hydrogen Propulsion: Hydrogen can be combusted or used in fuel cells. During flight, it produces zero CO_2 emissions and the hydrogen can be created with renewable electricity. However, its storage is complex due to low volumetric energy density and has infrastructure and aircraft integration challenges [16]. In its most dense form it occupies around four times more volume than conventional jet fuel, while it must be stored at temperatures below –253°C. When stored as a gas, hydrogen is a lot less dense and needs to be stored in high-pressure tanks that are heavy and bulky. For these reasons, hydrogen-powered aircraft are not yet seen as feasible replacements for conventional jets due to these limitations [17], but they hold the potential in the future to do so.

Electric and Hybrid-Electric Propulsion: Electric and hybrid-electric aircraft can substantially reduce pollution. The majority of the technologies necessary for electric aviation already exist in some form. Hybrid-electric aircraft combine engines with electric motors, using this dual propulsion they can optimize power distribution and even improve fuel efficiency. Whilst the fully-electric aircraft are in development, hybrid aircraft are seen as a transitional solution [18]. Fully electric aircraft eliminate in-flight emissions entirely with a higher efficiency in their propulsion. Recent innovations suggest that electric aircraft could be viable for larger regional markets [6].

2.3. Conclusion on Decarbonizing Aviation

Every one of the pathways toward sustainable aviation faces distinct hurdles. The contribution of SAF and hydrogen technologies offer important contributions, but both face significant challenges that must still be addressed. At the same time, electric aviation stands out as an opportunity, especially for short-haul and regional flights. However, the success depends on overcoming key technical challenges.

Therefore, future investments and innovations are essential to make regional electric transport viable, and also to reduce the reliance on scarce renewable fuels, while diversifying the aviation sector's decarbonization strategy. In the end, there is no single solution for all problems. A wide variety of technologies will be necessary to achieve a desired net-zero future.

3

Background on Aircraft Electrification

This chapter elaborates on the history of the electrification of aircraft. It begins with a review of the origins of electric aviation and how it has evolved over time, discussing important milestones that have shaped the field. The following sections go deeper into the technical challenges faces by electric aviation and their potential solutions, mostly focusing on battery technology. Lastly, several concept aircraft currently under development are discussed. A focus is set on the Elysian E9X, as the research is done in collaboration with Elysian Aircraft.

3.1. Historical Development of Electric Aircraft

This section contains an overview of the historical developments of Electric Aircraft throughout history and the foundations that brought the Electric Aviation concepts to where they are now.

Electric Aviation has been around longer than usually is thought. The first concepts for electric aviation emerged in the late 19th-century, at the same time as the development of early aviation [19]. These early aircraft concepts and developments faced significant technological limitations. The battery technology at the time was too primitive for practical flight, despite this hefty limitation these engineers considered electric motors as potential power sources for the flight.

The first manned flight took place in 1973, when Fred Militky, a pioneering engineer for the model aircraft company Graupner, converted a Brditschka HB-3 motor glider into the MB-E1, the world's first person-carrying electric aircraft [20, 21]. The historic flight, piloted by Heino Brditschka, lasted approximately around 10 minutes and the aircraft reached an altitude of 360 meters. During this breakthrough Militky used a Bosch 13hp electric motor powered by nickel-cadmium batteries. The original two-seater aircraft was modified to accommodate a battery storage behind the pilot. This achievement represented the culmination of Militky's decades of work in electric flight, which began with his experiments in the 1940s and included the development of successful electric model aircraft like the "Silentius" in the early 1960s.

In 1981 Electric Aviation took a step further through Paul MacCready's work. His "Solar Challenger" project was the first solar-powered aircraft designed to fly long distances at significant altitudes without battery assistance [22]. With 16,128 photovoltaic cells covering its flat-wings and tail surfaces, the aircraft could generate approximately 3,800 watts of power under optimal sunlight conditions. On July 7, 1981, Paul MacCready made aviation history by flying the Solar Challenger upon a 163-mile flight from Paris, France to Canterbury, England, hereby trying to demonstrate the viability of pure solar and electric flight across significant distances, an image of this flight is displayed in Figure 3.1. This achievement built upon earlier work with the Gossamer Penguin, which had achieved the first sustained solar-powered flight in 1980 piloted by Janice Brown [23].

The real advancements in electric aviation came with the development of lithium-ion battery technology. These improvements were developed mostly in the 1990s-2000s and their capabilities are advancing to this day [24] with these developments largely increasing the specific energy. This was demonstrated in 2005, where Alan Cocconi's SoLong UAV demonstrated the potential of this technology by completing

Figure 3.1: Paul MacCready's Solar Challenger in flight over the canal.

a remarkable 48-hour continuous solar-electric flight [25], proving that electric propulsion could support extended operations with the right energy storage. These newly developed lithium-ion batteries led to the next developments in the industry, with the Pipistrel Taurus Electro becoming the world's first commercially available electric aircraft in 2007 [26]. These early electric aircraft were crucial in demonstrating that electric propulsion systems are able to transition from experimental concepts to practical, certified aircraft that pilots could use in a commercial setting and and operate in real-world conditions.

Despite the progression that has been made over the years, current electric aviation technology still faces limitations. Battery technology with its specific energy has significantly improved. However, it remains insufficient for large scale commercial passenger aviation in the medium/long haul. For this reason, the manufacturers are focusing on hybrid electric designs and short range electric aircraft [18]. Some of these companies, like Elysian, are focusing on fully electric aircraft design and even though these aircraft are designed to fly fully electric, they have fuel reserves to save weight on batteries to comply with additional range requirements for aircraft [7, 6]. In conclusion, the industry consensus sees full electrification of large passenger aircraft as a long-term goal, with some companies directly developing fully electric aircraft and others focusing on hybrids serving as an important step towards more sustainable and fully electric air transportation.

3.2. Technical Limitations and Challenges

This section covers the technical limitations and challenges electric passenger aircraft face and that must be overcome to achieve large scale operations. The most fundamental constraint is the battery energy density and the challenges it brings along.

3.2.1. Overview of Technical Challenges

Several recent studies provide comprehensive analyses of the technical challenges facing electric aviation. Papers by *Wolleswinkel et al. (2024)* [6], *De Vries et al. (2024)* [7], *Adu-Gyamfi and Good (2022)* [8], and *Chen (2023)* [27] collectively examine the limitations and potential solutions in battery technology, propulsion systems, aircraft design, and operational requirements. An overview of the technical limitations has been constructed from these papers and they presented in Table 3.1.

The table captures the most significant challenges that must be addressed for viable commercial electric aircraft, although there are also more challenges identified in the literature that are not included in the table due to their secondary nature and/or lesser importance to the overall research. These additional limitations include bur are not limited to: certification and regulatory frameworks, battery-pack development and integration, thermal management, and economic viability considerations. They represent broader industry and policy challenges rather than core technical limitations of the aircraft systems to be analyzed in the scope of this research themselves.

Table 3.1: Overview of primary technical limitations of electric aircraft

Parameter	Definition and Application	Units
Energy Density	The quantity of energy stored per unit of mass in batteries (250–300) compared to jet fuel ($\sim 12{,}000$); determines range and payload capacity	Wh/kg
Charging Time	Duration required to restore battery capacity, affecting ground time and operational efficiency of aircraft	min
Cycle Life	Number of charge-discharge cycles before degradation to 80% of original capacity (typically 500–1500 cycles)	cycles
Battery-Structure Integration	Design challenges in integrating batteries into wings for optimal weight distribution and structural integrity	N/A
Airport Infrastructure	Airports are not yet fully adapted to support electric aircraft's broader wingspans and charging requirements, necessitating facility modifications and new operational protocols	N/A

3.2.2. Pathways to Implementation

The technical limitations outlined in Table 3.1 shows the hurdles that need to be overcome for widespread electric commercial aviation and the ongoing research and development across the domains are showing promising solutions. The timeline of these solutions can vary significantly from each other and this section examines the potential solutions and if available provides a temporal analysis of when these technologies might be usable for commercial application.

Solutions to Technical Limitations

For Energy Density Improvements several pathways are being pursued to address the fundamental energy density limitations of current battery technologies. These are listed below.

- **Advanced Lithium-ion Chemistries:** The combination of Silicon-dominant anodes, high-nickel cathodes, and improved electrolytes could potentially achieve 350–400 Wh/kg at the cell level by 2026–2028 [28]. Recent research has demonstrated that Mo-doped Ni-rich cathodes ($Li[Ni_{0.95}Co_{0.04}Mo_{0.01}]O_2$) can achieve energy densities of up to 895 Wh/kg [29].
- **Solid-State Batteries:** These batteries seek to replace the liquid electrolytes with solid conductors. This would result in energy densities of 400–500 Wh/kg with improved safety. Companies like QuantumScape, Solid Power, and Toyota are making significant progress in this area [30, 31]. If these batteries become available with aviation grade quality, they are expected to be a key candidate for aviation applications.
- **Lithium-Sulfur Batteries:** This new battery composition with lithium as anode and sulfur as cathode have theoretical energy densities of up to 2,600 Wh/kg. Li-S technology could create a breakthrough, though significant challenges in cycle life and sulfur utilization efficiency remain [28]. Due to this no timeline is available for the development progression.
- **Hybrid Solutions:** It could be a solution to combining batteries with hydrogen fuel cells or even sustainable aviation fuels in hybrid configuration. In such a manner a transitional solution can be designed while battery technology matures for fully electric aircraft.

For the development of charging time reduction technologies:

- **High-Power Charging Infrastructure:** Recent studies highlight the importance of the development of reliable airport charging systems designed to enable the simultaneous charging of multiple electric aircraft at moments of peak demand [32]. Such systems are currently being researched, but will require large investments.
- **Battery Swapping:** Recent analysis suggests that battery swapping in aircraft designs that allow it, is more cost-effective for electric aviation in most cases, while plug-in charging becomes more viable when electric aviation penetration exceeds certain discharge thresholds [33].

- **Cell Design Optimization:** New electrode materials and designs that facilitate faster ion transport without compromising safety or cycle life. Recent studies have demonstrated that Mo-doped Ni-rich cathodes maintain 90% capacity retention even at 5C charge rates, enabling full charging in as little as 12 minutes. However, the battery choice for electric aircraft will most likely be prioritized by the capacity in comparison to charging speed. This would mean that charging speed would be a secondary characteristic of batteries in aviation [29].
- **Solid-State Electrolytes for Fast Charging:** The high-throughput critical current density testing method has enabled the identification of solid electrolytes that can sustain high current densities without failure [31]. This would be interesting for battery developments, as these solid-state batteries have a high specific energy with a favorable charging speed.

For the improvement of battery cycle life and durability for aviation applications:

- **Advanced Battery Management Systems:** AI-driven systems that optimize charging and other flight patterns could extend battery life through precise monitoring and flight decision-making.
- **Self-Healing Materials:** Some batteries could have self-healing properties that can autonomously repair microdamages in electrodes and electrolytes due to wear and tear of the batteries. These properties are inspired by biological systems. Techniques that are expected to have potential include self-healing polymers, microcapsules with healing agents, and bio-inspired materials. This would extend durability significantly [34].
- **Temperature Management:** To combat battery degradation from thermal stress, more efficient cooling systems should be designed that maintain optimal battery operating temperatures [29].

For Structural Battery Integration innovative approaches are:

- **Reserve Energy System Considerations:** The use of a fuel-powered reserve energy system (RES) instead of batteries for flights would drastically save weight. While allowing aircraft to fly further without having to deploy the RES in regular flights [6].
- **Battery Wing Placement:** Strategic placement of batteries inside the wings helps optimize weight distribution due to reduced moment on the airframe. This placement also reduces aerodynamic penalties [7].

Solutions for airport infrastructure adaptation:

- **Standardized Charging Protocols:** Industry-wide standards for electric aircraft charging to ensure usability across manufacturers and airports.
- **Smart Grid Integration:** Systems that manage charging loads and potentially use aircraft batteries for grid stabilization during ground time. Optimized charging systems incorporating smart grid management and dynamic power allocation strategies have been proposed to balance demand and minimize operational disruptions [32].
- **Modular Airport Design:** Flexible infrastructure that can accommodate both conventional and electric aircraft during the transition period.
- **Renewable Energy Integration:** Airport-based solar systems can supplement electric aviation charging demand and reduce dependence on external grid power [33].

3.3. Current Electric Aircraft Projects and Elysian

This section discusses several promising (concept) aircraft designs of different leading companies in the electric passenger plane development, followed by a more in-depth analysis of the Elysian E9X.

3.3.1. Heart Aerospace

Heart Aerospace is a Swedish company developing the in Figure 3.2 portrayed ES-30, a hybrid-electric regional aircraft designed for 30 passengers [35]. The aim is to have the aircraft enter service by 2028. The company is based around Säve Airport, Sweden. Major investors such as United Airlines, Air Canada, and Saab back the aircraft and some have even made orders. This positions the ES-30 is as a future hybrid alternative for short-haul regional flights.

Figure 3.2: The Heart Aerospace ES-30 concept portrayed in flight.

Design and Propulsion

The ES-30 is designed with a high-wing, T-tail for improved stability and ground clearance. The aircraft's interior has a 2-1 seating layout to optimize aerodynamic efficiency. Also, it has fixed landing gear to reduce weight and simplify maintenance. The aircraft is powered by four electric motors and will use a lithium-ion battery system, with the ability to allow for future upgrades when technology progresses. It claims to have a fully electric range of 200 km, which can be extended to 400 km using a reserve-hybrid system powered by SAF to meet certification and safety requirements without reducing range, and with a reduced passenger load, the ES-30 can achieve a range of up to 800 km. With the with low noise and emissions, the ES-30 is ideal for regional airports, offering a flexible and sustainable solution for very short-haul air travel.

3.3.2. Maeve Aerospace

Maeve Aerospace is a Dutch company developing the M80, a hybrid-electric regional aircraft designed for 80 passengers [36] that is to enter service somewhere in the coming years. This design would offer airlines a cost-efficient and sustainable alternative for regional operations as it has an increased range in comparison to the ES-30. The aircraft is designed to outperform turboprops while delivering the performance of a regional jet.

Figure 3.3: The Maeve M80 aircraft portrayed in flight.

Design and Propulsion

The M80 features a high wing to reduce drag. Its hybrid-electric propulsion system is optimized to have a high efficiency at cruise altitude, providing a balance between operational performance and sustainability between conventional and fully electric aircraft. The aircraft is powered by two hybrid-electric engines, reducing fuel consumption by over 40% compared to conventional regional jets. Maeve claims an operational range of just under 1500 km while carrying 84 passengers, allowing the M80 to operate a variety of short/medium haul routes. Its advanced hybrid-electric system lowers operating costs, with a 25% lower trip cost than regional jets and a 20% lower seat-km cost than turboprops.

3.3.3. Elysian Aircraft

Elysian Aerospace is a Dutch company pioneering battery-electric commercial passenger aviation with the development of the Elysian E9X, a 90-passenger fully electric aircraft with a RES to cover required range reserves for flights [7]. The E9X aims to achieve a zero in flight emission range of 800 km on a single charge for the first version, with the second version extending this to 1000 km. This positions the E9X as a viable replacement for 50% of scheduled flights when considering a 1 stop flight for charging, contributing to a potential 20% reduction in global aviation CO_2 emissions. The aircraft is expected to enter service by 2033 according to Elysian.

Design and Propulsion

The E9X, seen in Figure 3.4, features a low-wing configuration with distributed electric propulsion and wing mounted landing gear, which replaces traditional twin-propeller designs. The aircraft incorporates large, high-aspect-ratio wings to enhance aerodynamic efficiency that reduces energy consumption without relying on having to develop new advanced propulsion technologies. The battery system is housed within the wings, reducing the structural weight necessary for the aircraft, while placing the energy storage system directly where the lift is generated. The E9X also features folding wingtips that allow the aircraft to fit within standard airport gate constraints.

The aircraft has a fuel-based RES is supply additional range to the aircraft during diversion and loitering scenarios. With a battery-based reserve energy system this would cannibalize the range. The E9X also features folding wingtips, which optimize aerodynamic performance and allow the aircraft to fit within standard airport gate constraints.

Figure 3.4: The Elysian Aircraft concept with its 8 propellors distributed propulsion system.

Operational Performance and Efficiency

The E9X is designed to rival regional jets and turboprops by offering comparable range and passenger capacity while drastically reducing operating costs. A key advantage of its battery-electric propulsion system is its energy efficiency, with 82% of renewable energy converted into usable flight power, battery-electric propulsion far surpasses hydrogen fuel cells (35%), hydrogen turbines (24%), and e-SAF (19%) in energy efficiency [6, 1]. Also, the E9X offers other cost benefits. Direct grid-to-battery energy conversion results in lower fuel costs than hydrogen or e-SAF alternatives and electric motors have significantly fewer moving parts than gas turbines, reducing maintenance costs. These factors contribute to competitive per-trip and seat-mile costs.

3.4. Conclusion on the Background on Aircraft Electrification

The literature presented in this chapter on aircraft electrification highlights the growing potential for aviation. In only around 50 years humankind has gone from early experimental 10 minute flights with a single passenger, to large-scale passenger aircraft concepts projected to enter production in the coming 10 years. Still, large hurdles remain, but the overall development shows a promising trajectory.

4

Battery Degradation & Ageing

This chapter explores the degradation of lithium-ion batteries and begins by outlining the fundamentals of lithium-ion batteries, afterwards the key metrics relevant to batteries in aviation and degradation mechanisms are discussed and an overview of three major battery health datasets is given. Building on this theoretical foundation, the chapter researches a wide range of predictive approaches for battery degradation and methods for uncertainty quantification.

4.1. Lithium-Ion Battery Fundamentals

Since the development of the first lithium-ion batteries around 1990, they have become the dominant energy storage technology for electric transportation systems due to a favorable combination of characteristics; a high energy density, relatively long cycle life, and increasingly competitive cost structure.

4.1.1. Operating Principles and Chemistry

The operating principles and chemistry of lithium-ion batteries are well known, this specific section is derived from *Finkelstein et al. (2024)* [37]. In Figure 4.1 a typical lithium-ion cell is displayed and it has four main components: the anode, cathode, electrolyte, and a separator. When the battery delivers power during a discharge cycle, electrons flow through an external circuit from the anode to the cathode, while lithium ions migrate from the anode through the electrolyte and separator to the cathode. This produces an electrical current that can be used by the external circuit. During charging, this process reverses, with lithium ions returning to the anode.

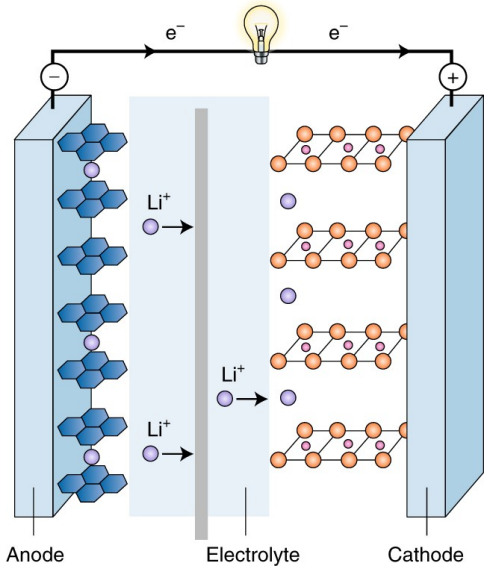

Figure 4.1: Illustration of Lithium-ion cell [38]

Graphene is often used for the anode, as it can accommodate lithium ions between its layers. For the cathode, a wide range of lithium metal oxides can be used such as: lithium cobalt oxide ($LiCoO_2$), lithium nickel manganese cobalt oxide (NMC), lithium iron phosphate ($LiFePO_4$), and lithium nickel cobalt aluminum oxide (NCA). Each cathode chemistry has different trade-offs between energy density, power capability, cycle life, thermal stability, and cost.

The electrolyte typically is a lithium salt (such as $LiPF_2$) dissolved in organic solvents that enables ion transport. It does this while the separator, a micro-porous polymer membrane, prevents direct contact between electrodes while allowing lithium ions to pass through.

4.1.2. Performance Metrics and Characteristics

To be able to assess the performance of batteries, Key Performance Indicators (KPI's) are set up with the help of *Hasa et al. (2023)* [39] for lithium-ion batteries. In Table 4.1 the overview can be found. As there are many different aspects and manners that battery performance can be measured, only a number of these KPI's is listed in the table, chosen on relevance for the research.

Table 4.1: Key Performance Indicators for Lithium-Ion Batteries in Electric Aircraft

Parameter (Symbol)	Definition and Application	Units
Energy Density (E_d)	The quantity of energy stored per unit of mass (gravimetric) or volume (volumetric); directly impacts aircraft range and payload capacity	Wh/kg or Wh/L
Power Density (P_d)	Maximum power output per unit of mass; determines aircraft acceleration and climb performance capabilities	W/kg
Cycle Life (N_{cycle})	Number of charge-discharge cycles before capacity degradation to 80% of initial value; affects operational economics and battery replacement intervals	cycles
Calendar Life (T_{calendar})	Maximum lifespan regardless of usage; crucial for long-term aircraft operation planning and maintenance schedules	years
Capacity Retention (C_{ret})	Measure of how well a battery maintains its original capacity over time and cycles; key performance metric for reliability in aviation applications	%
State of Health (SoH)	Indicator of battery condition relative to a new battery (100%); critical for operational decision-making and safety management	%
C-Rate Capability (C)	Measure of charge/discharge current relative to capacity; affects fast-charging ability and power delivery during demanding flight phases	C

Other relevant KPI's relevant for the prediction of battery capacity in aviation is quantified through several measures in Table 4.2.

Table 4.2: Capacity Prediction Performance Metrics for Aviation Battery Management

Parameter (Symbol)	Definition and Application	Units
Prediction Accuracy (RMSE, MAE)	Root Mean Square Error (RMSE) or Mean Absolute Error (MAE) between predicted and actual capacity; critical for flight planning reliability	% or Ah
Remaining Useful Life (RUL)	Estimated time or cycles until battery reaches end-of-life criteria; essential for maintenance scheduling and replacement planning	cycles or flight hours
Prediction Horizon (H_p)	How far into the future capacity can be accurately predicted; longer horizons enable better long-term operational planning	cycles or flight hours
Uncertainty Quantification (σ, CI)	Statistical confidence bounds on capacity predictions; crucial for risk assessment and safety margin determination	%
Model Adaptability	Ability of prediction models to adjust to varying operational conditions and battery aging patterns; essential for reliable long-term performance	N/A

4.1.3. Battery Degradation Mechanisms

This section discusses battery degradation and its mechanisms. Understanding degradation is important for optimizing battery durability and safety. The knowledge of this section is derived from the papers *Han, Lu, Zheng et al. (2019)* [40] and *Rahman and Alharbi (2024)* [41] and the Battery University

Website [42].

Electrochemical and Chemical Degradation

This subsection discusses electrochemical and chemical degradation mechanisms affecting mostly the anode, cathode and electrolye. One of the foremost contributors to degradation is the formation of the Solid Electrolyte Interphase (SEI) on the anode, visualized in Figure 4.2. This layer forms in the first cycles due to electrolyte decomposition and is a necessary component for the battery. While a stable SEI layer protects the anode and allows for reversible lithium intercalation, it has a continued growth over the cycles and it irreversibly consumes lithium ions. This decreases the lithium available and thus leads to capacity loss. Additionally, excessive SEI thickening increases internal resistance.

Another significant degradation effect on the anode is lithium plating, which occurs when lithium-ions react to become metallic lithium on the anode surface instead of intercalating into the layers of the graphite structure. This phenomenon occurs more under high charging rates or low-temperature conditions. This plated lithium can form into dendrites that penetrate the separator, creating internal short circuits and thermal runaway.

Besides degradation on the anode, degradation at the cathode also occurs. Changes in the structure of the cathode caused during charge-discharge cycles hinder lithium-ion mobility. This effect is highly dependent on the chosen cathode material and is often a trade-off with other battery qualities. Transition metal ions also dissolve from the cathode into the electrolyte and migrate to the anode, which destabilizes the SEI layer.

The electrolyte itself is subject to degradation mostly through oxidative and reductive decomposition at the surfaces of the electrodes. High temperatures and overcharging accelerate the degradation and breakdown of the electrolyte, producing byproducts such as CO_2, H_2, and hydrocarbons. This reduces the conductivity, increases internal pressure, and can even lead to hazardous cell swelling and venting.

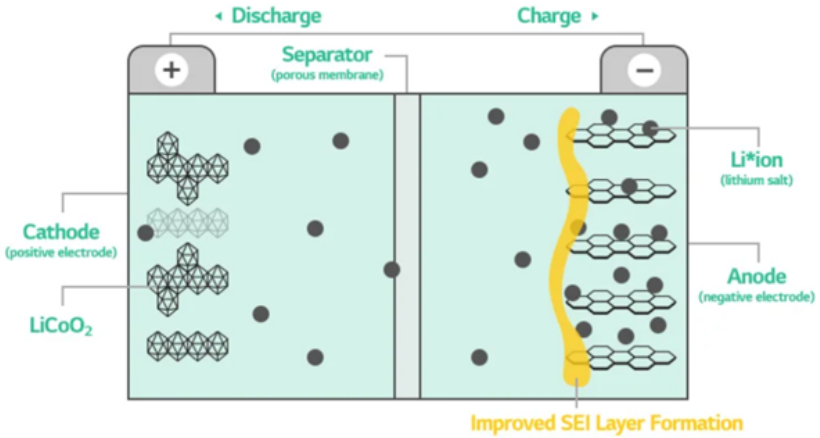

Figure 4.2: Visualization of SEI layer of lithium-ion batteries

Mechanical and Thermal Degradation

Mechanical and thermal degradation mechanisms impact battery degradation by increasing internal resistance and causing capacity loss. In every charge-discharge cycle the repeated expansion and contraction of electrode materials generate mechanical stress, this leads to cracking and loss of electrical contact due to the reduction of effective surface for intercalation. For most high capacity electrode materials, this issue is particularly pronounced (silicon anodes and nickel-rich cathodes).

Another critical degradation factor that occurs throughout the battery lifetime is the loss of active lithium due to SEI growth, lithium plating, and various side reactions. Since lithium ions are essential for charge storage, their gradual loss diminishes overall capacity.

Thermal effects further accelerate degradation mechanisms, as elevated temperatures accelerate SEI growth, electrolyte decomposition, and structural instability in the cathode. If this degradation becomes excessive and causes temperatures over 80 degrees Celsius thermal runaway can occur. Here,

exothermic reactions propagate uncontrollably. Resulting in cell venting, fire, or even explosion, making thermal management a crucial aspect of lithium-ion battery design for aviation applications. This thermal runaway is very difficult to distinguish, as it contains all necessary ingredients for its reactions to continue, posing a problem for future aircraft batteries.

4.1.4. Impact of Degradation on Aviation Applications

Battery degradation in electric aviation is an important challenge to overcome due to strict performance and safety requirements. Battery degradation effects reduce aircraft range and payload capabilities, while increased internal resistance limits the maximum power output and even the voltage stability during takeoff and climb. However, the reduction in maximum power due to the battery degradation will not compromise the overall usability of the aircraft and the battery design and maintenance scheduling will be designed to incorporate this aspect for safety precautions. Elysian Aircraft is even planning to only allow flights from airport with runways longer than 2000m, this reduces the maximum power necessary for takeoff to take advantage of optimal battery usage, and while doing so also reduces the effect of this power degradation. This effect would otherwise most likely not play a role without the runway constraint, as the power required for takeoff is well below the limit, unlike VTOL aircraft where peak power demand is a lot higher.

The degraded batteries will require frequent replacements and checks [7], impacting operational costs and maintenance schedules. Studies show that high discharge rates significantly accelerate battery degradation [43, 44]. Therefore, these effects are particularly relevant during cruise at higher speeds, take-off and landing and special maneuvers, where the C-rates are elevated for long periods of time. To mitigate these effects, advanced Battery Management Systems (BMS) monitor degradation indicators and can help guide the degradation within limits [45].

4.2. Battery Health Datasets

Accurate modeling of battery degradation requires high-quality datasets with many measurements and batteries for most methods. In this section, first two widely used battery health datasets will be discussed. The NASA - Li-ion Battery Aging Dataset [46] and the ISU-ILCC Battery Aging Dataset [47]. Afterwards, the more recent and less-used battery health dataset is discussed proposed in a paper by *He et al. (2022)* [48].

4.2.1. NASA Battery Health Dataset

This section discusses the NASA Battery Health Dataset, provided by the Prognostics Center of Excellence at NASA Ames Research Center. This dataset covers degradation data for Li-ion 18650 rechargeable batteries, that are subjected to different operational profiles throughout testing. The dataset covers charge-discharge cycles and Electrochemical Impedance Spectroscopy (EIS) measurements. Where the temperatures and load conditions vary across batteries. The batteries were cycled until they reached an end-of-life criterion of 70% SoH (from 2 Ah to 1.4 Ah). The dataset was gathered using a custom-built battery prognostics testbed consisting with an data acquisition rate of approximately 10 Hz.

The dataset includes:

- Charge and discharge cycle data with voltage, current, temperature, and capacity measurements.
- Impedance spectroscopy data, including electrolyte resistance and charge transfer resistance.
- Varied depth-of-discharge (DoD) levels and operational conditions to simulate real-world battery degradation.

This dataset is one of the most widely used for battery RUL prediction and battery capacity prediction. Many SoH prediction methods developed over the years have been tested on this dataset. This particular battery type is used in many high-end products such as certain Tesla EV models, making it a suitable benchmark for new methodologies [49].

4.2.2. ISU-ILCC Battery Aging Dataset

The ISU-ILCC Battery Aging Dataset [47] was created through a collaboration between the System Reliability and Safety Laboratory at Iowa State University (ISU) and Iowa Lakes Community College (ILCC). This dataset is specifically designed to analyze the effects of three key stress factors on battery capacity fade; charge rate, discharge rate, and depth of discharge (DoD).

The dataset contains cycle aging data from 251 lithium-ion polymer cells, which were subjected to 63 unique operational conditions. The data includes 238 cells, with the remaining 12 cells still undergoing testing and will be added once finished.

The dataset was acquired through a controlled consistent and reliable experimental setup. The differing conditions allow researchers to investigate the influence of different cycling parameters on battery degradation with the goal to enable the development of predictive models that estimate battery lifespan under varying operational conditions.

The dataset includes:

- Charge and discharge cycle data with voltage, current, temperature, and capacity measurements.
- A wide range of stress factors, including variations in charge rate, discharge rate, and depth of discharge.

This dataset is relevant for prognostics development, especially in predicting battery RUL. Differing from the NASA dataset, the ISU-ILCC dataset specifically tests lithium-ion polymer cells under a wider variety of cycling conditions.

4.2.3. EVBattery Dataset

This section discusses the EVBattery Dataset, introduced by He et al. (2022) [48]. This is a large-scale dataset derived from real-world data for battery health and capacity estimation in EVs. Unlike traditional laboratory-based or synthetically generated datasets, the EVBattery dataset contains extensive charging records collected from actual cars.

The dataset contains over 1.2 million charging datapoints from 464 EVs manufactured by three different companies. Each datapoint consists of time-series data recorded over the charging process in combination with other meta-information relevant to battery condition. The data is collected from charging stations, making it perfect for analysing battery degradation according to charging patterns

The dataset includes:

- Voltage and current measurements during charging.
- Temperature variations across cells.
- State of Charge estimates.
- Battery health and capacity labels.

The dataset has two uses according to the paper, anomaly detection in EV Batteries and for capacity/-SoH estimation. This dataset could be very valuable for creating insights for electric aircraft. However, for this research the focus will most likely be on discharging patterns.. The most important differences between the EVBattery dataset and the first two datasets is its size and its real-world nature that helps bridge the gap between controlled lab testing and actual operations, making it a potential resource for future battery degradation studies.

4.3. Predicting the Capacity of Batteries

This section discusses different methodologies for the prediction of battery degradation. As the application of the battery fade prediction is on electric aviation, correct predictions are crucial for ensuring the safety of meeting the range requirements for flights. These prognostics models often differ slightly from actual values. Therefore research is done into investigating the prediction of the lower bound of the confidence interval of where the actual value may lie. This lower bound is essential for maintaining proper safety margins, where battery failure is not an option.

4.3.1. Non-Data-Driven Approaches

The section discusses non-data-driven approaches for battery degradation prediction. These are based on physical and mathematical models that try to describe the underlying mechanisms of battery aging. This section is based on the physical and mathematical approaches in the papers of *Ge et al. (2021)* [50] and *Li et al. (2018)* [51].

Electrochemical Models

Electrochemical models describe the internal chemical and physical processes in lithium-ion batteries. These models use Partial Differential Equations to represent reactions within the battery. One of the most widely used electrochemical models is the Pseudo-Two-Dimensional model. This tries to capture the complex physicochemical properties of battery degradation, but comes at a computational cost and has led to the development of simplified variants, such as the Single Particle Model. To further improve efficiency, other reduced-order electrochemical models that integrate side reactions and interfacial degradation mechanisms have been developed.

Equivalent Circuit Models

Equivalent Circuit Models (ECM) simplify the dynamics of batteries by representing the electrical behaviours using an electronic circuit. The most common ECMs are the Thevenin model, the RC network model, and the nonlinear ECM and they estimate the battery SoH by tracking changes in circuit parameters. Despite their computational efficiency and ease of implementation in BMS, they struggle with accuracy and complex degradation behaviour.

Mathematical Models

Mathematical models use statistics to predict battery degradation without having to model the underlying electrochemical processes. One popular approach is Incremental Capacity Analysis, which functions by monitoring changes in the differential capacity curve to assess capacity fade. The probabilistic models are used to provide uncertainty quantification for RUL or battery degradation estimation. These mathematical models offer flexibility, as they are sometimes compatible across different battery chemistries, but require sufficient historical data for parameter calibration and their reliance on statistical assumptions and simplifications can cause errors.

Comparison and Considerations

The discussed Non-data-driven capacity/SoH estimation approaches provide valuable insights into battery degradation mechanisms. These are particularly useful when data is scarce, but the composition of the battery is known and researched. However, their applicability depends on the trade-offs between battery characteristics.

4.3.2. Regression Machine Learning Methods

This section discusses regression based machine learning methods. These methods model the relationship between historical battery performance metrics and capacity degradation trends and are often explainable and effective.

Linear Regression

Linear regression is one of the simplest machine learning methods. it assumes a linear relationship between input features and data and can be optimized through multiple functions such as ordinary least-squares. It works well in finding trends and their magnitude and it is often used as a baseline model [52]. However, due to the highly nonlinear nature of battery degradation, linear regression struggles to capture complex degradation patterns. *Abdillah et al.* (2025) [53] found that linear regression had the highest prediction error among tested methods in its test repertoire for estimating battery RUL with several approaches. While it may be useful when degradation has a near-linear trend, its use in real applications is limited.

Support Vector Regression

Support Vector Regression (SVR) addresses some of these limitations by mapping input features into a higher-dimensional space, which enables nonlinear trends to be found [54]. It works by optimizing a loss function that allows for a certain margin of error *Abdillah et al.* (2025) [53] demonstrated that SVR

outperformed linear regression in his tests. However, its performance heavily depends on the selection of the kernel function. SVR is can work for moderately complex datasets, it struggles with computation for large-scale applications, limiting its applications [54].

Gaussian Process Regression

Gaussian Process Regression (GPR) is regression method that that provides both predictions and their uncertainty quantification. It works by modeling degradation as a stochastic process, allowing it to handle noise in datasets well. *Naresh and Thangavelu* (2024) [55] applied GPR to predict battery health in over-discharged Li-NMC systems and found that it provided reliable uncertainty estimates alongside accurate predictions. However, just like SVR, GPR's computational complexity rises quickly with dataset size, limiting its real world applications.

Suitability of Regression Methods

The suitability of these regression methods for battery degradation depends on the application and the amount and complexity of the data available. While these methods may not often achieve similar quality in predictions of ensemble techniques. They offer advantages in interpretability, low computational efficiency, and the enabling of uncertainty quantification, which makes them viable when these factors are prioritized [56].

4.3.3. Ensemble Regression Methods

This section discusses ensemble machine learning methods methods. These combine multiple models to achieve higher performance than individual models and have gained significant popularity in battery degradation prediction as they are able to capture complex nonlinear relationships.

Random Forest Regression

Random Forest Regression (RFR) is an ensemble learning method that works by building numerous decision trees during training and finds the average prediction of the individual trees. The trees in the model are trained on different subsets of data and features, that allow it to focus on many different parts of the variance in the data [57]. used RFR to predict the RUL of lithium-ion batteries by extracting aging features based on the incremental capacity curve and achieved a mean error of estimated SoH of 1.81% on the dataset, more specifically he was able to predict the RUL within 32 cycles, outperforming several common non-ensemble methods. The study focused on the ability of RFR to handle many features without requiring advanced feature selection.

RFR has an inherent feature importance ranking mechanism that gives valuable insights into the factors driving capacity fade. This is useful as it can determine the most important features to focus on in the predictions, as demonstrated in the work by Wang et al. (2023) [58], where the model's learning and generalization ability was enhanced through Bayesian optimization of hyperparameters to better understand battery aging processes. Ng et al. (2020) [59] also showed that random forest can consistently outperform linear models, SVR, and even neural networks in many cases. There is a limit to RFR's prediction accuracy though, it plateaus with increased tree depth and quantity, risking that the model will overfit with too many trees and depth. RFR is a powerful and simple to implement model that can still be interpreted, making it an attractive option for both predicting battery degradation.

Gradient Boosting and XGBoost

Gradient Boosting methods represent another powerful group of ensemble techniques, where they do not only combine multiple models, but also how these individual models interact with each other and the data. RFR builds trees in parallel, while Gradient Boosting constructs trees sequentially, allowing it to correct errors in previous trees and build stronger trees. While training it also in most Gradient Boosting methods will assign different weights to each tree, with newer trees focusing specifically on the residual errors of the ensemble. This allows it to capture a wide range of variance and degradation patterns [60]. In Figure 4.3 the two tree building algorithms of Random Forest and Gradient Boosting are visualized.

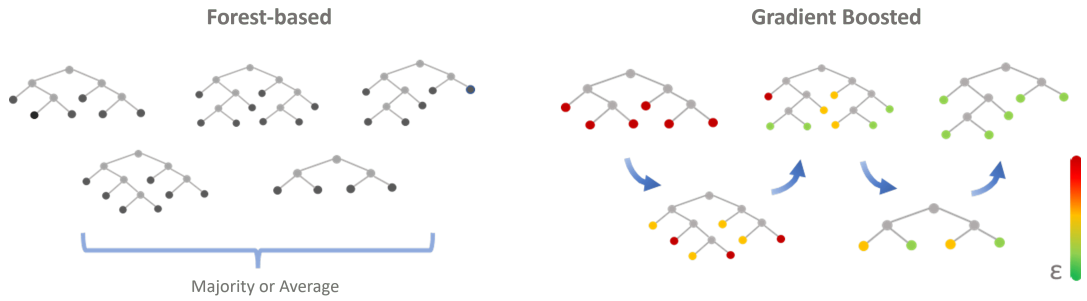

Figure 4.3: Random Forest Parallel Tree Building vs Sequential Gradient Boosting Tree Building [61]

The Gradient Boosting method that is most often seen as the most powerful is XGBoost. It is seen as one of the most effective machine learning methods predictive performance and efficiency. In a research done in battery capacity prediction by *He et al. (2022)* [48] where he used a newly developed dataset that is discussed in subsection 4.2.3. XGBOOSt outperformed other ML models such as RFR and the neural network based Multi-Layer Perceptron. Certain deep learning approaches were able to outperform XGBoost slightly, but XGBoost performed best in 1 of the 2 datasets, and on the other it came very close to the best predictor. XGBoost is able to do this while handling missing values or outliers, it prevent overfitting through regularization, and efficiently process data. Its interpretability, compared deep learning, also provides valuable insights into feature importance and allows for xAI methods like SHAP and LIME to create understanding of key factors influencing battery health.

4.3.4. Uncertainty Quantification in Regression Battery Degradation Prediction

This section discusses uncertainty quantification in regression. It is important to make accurate predictions of when predicting battery degradation, but it is also of importance to quantify prediction uncertainty, particularly when the predictions are made in safety-critical applications like electric aviation.

Ensemble-Based Uncertainty Quantification

Many ensemble methods are able to provide uncertainty estimation through the variance of predictions across individual or groups of the ensemble members. A common used version is Quantile regression, introduced in *Koenker et al. (1978)* [62]. It estimates relationships between variables at different points of the conditional distribution rather than just using the mean of the ensemble as prediction by minimizing the weighted sum of absolute residuals instead of squared residuals used in traditional regression methods.

Quantile regression can estimate prediction intervals in Gradient Boosting methods by targeting specific quantiles (e.g., 10th, 50th, and 90th percentiles) of battery capacity and it has great robustness to outliers and has the ability to capture tail behaviors of distributions, and effectiveness in handling heteroscedasticity [63].

Bayesian Methods for Uncertainty Quantification

Bayesian approaches offer a principled framework for prediction with integrated uncertainty quantification by modeling parameters as probability distributions rather than point estimates. .

BART is its own regression method, offering a Bayesian nonparametric approach to flexible regression with built-in uncertainty quantification [64]. BART creates a regression function by summing the contributions of many small decision trees, the equation is displayed in Equation 4.1.

$$Y = \sum_{j=1}^{m} g(x; T_j, M_j) + \varepsilon, \quad \varepsilon \sim N(0, \sigma^2) \tag{4.1}$$

Where each $g(x; T_j, M_j)$ represents a regression tree with its own structure T_j and terminal node parameters M_j. The word Additive in BART is used because these tree models are combined through addition. BART has be designed to be inherently different from other ensemble methods with the inclusion of its Bayesian framework [65]. BART uses a regularization during training and tree building

that constrains each individual tree to be a weak learner, meaning that they contribute only a small part to the overall prediction. This effectively shrinks the size of the tree and its branches and reduces tree effects toward zero and keeps the trees very generalizable , preventing overfitting but still keeping performance near some ensemble methods.

BART is a Bayesian method and it provides full posterior predictive distributions rather than just point predictions. For any input x BART gives both an expected value and its confidence intervals that naturally widen in areas of sparse knowledge or high variability and therefore this uncertainty quantification can be used for making decisions based on security of knowledge. The Bayesian backfitting Markov Chain Monte Carlo (MCMC) algorithm used by BART efficiently samples from the posterior distribution, making it computationally feasible even for moderately large datasets [66].

BART offers several methodological advantages:

- It automatically handles nonlinear relationships and complex interactions between features.
- The model provides reliable uncertainty bounds that quantify both aleatoric (inherent randomness in data) and epistemic (lack of knowledge due to limited data) uncertainty components.
- BART can identify important predictors through variable selection metrics, enhancing model interpretability.
- It is relatively robust to noisy data and requires minimal hyperparameter tuning compared to some machine learning methods.

Practical Considerations for Uncertainty-Aware Battery Management

Uncertainty estimation for battery management can be of high value. The acceptable width and confidence of prediction intervals depend heavily on the application, where some consumer devices would have broader acceptable intervals, whereas safety-critical domains like aviation or medical systems need more reliable estimates. The incorporation of such measures into BMS allow for more informed decisions and should be implemented depending on the usage.

4.3.5. Neural Network Architectures for Battery Degradation Prediction

This section discusses the use of Neural Networks (NN) for battery degradation and goes over the two most prevalent neural network architectures used for battery degradation prediction.

Recurrent Neural Networks and LSTM for Temporal Battery Degradation

This subsection discusses certain NN architectures that are commonly used for battery degradation prediction. These are Recurrent Neural Networks (RNNs), particularly Long Short-Term Memory (LSTM) networks because they can learn temporal patterns in data [67]. Regular RNNs have vanishing gradients that prevent them from capturing behaviour in the long term. However, LSTM architectures avoid this with their special cells that control which information is important enough to be stored, while discarding unnecessary data [67].

The mathematical formulation of an LSTM cell is given by:

$$f_t = \sigma(W_f \cdot [h_{t-1}, x_t] + b_f) \tag{4.2}$$
$$i_t = \sigma(W_i \cdot [h_{t-1}, x_t] + b_i) \tag{4.3}$$
$$\tilde{C}_t = \tanh(W_C \cdot [h_{t-1}, x_t] + b_C) \tag{4.4}$$
$$C_t = f_t * C_{t-1} + i_t * \tilde{C}_t \tag{4.5}$$
$$o_t = \sigma(W_o \cdot [h_{t-1}, x_t] + b_o) \tag{4.6}$$
$$h_t = o_t * \tanh(C_t) \tag{4.7}$$

where x_t represents input features (e.g., voltage, current, temperature), and h_t, C_t, f_t, i_t, o_t correspond to the hidden state, cell state, and gate activations.

A typical LSTM architecture for battery degradation has the following parts:

- An input layer that processes battery signals
- One or more LSTM layers that capture temporal dependencies

- Dropout layers to mitigate overfitting [68]
- A dense output layer that maps learned representations to capacity or RUL

Research has shows the potential of LSTM models for battery degradation prediction and trends. Xu and Lu showed that LSTMs can already find certain cycle life trends while using only the early discharge capacity data. This reduces the amount of data necessary to make meaningful predictions [68].

The key advantages of LSTMs for battery degradation prediction include:

- The ability to capture long-term degradation patterns crucial for predictive maintenance
- Flexibility in handling variable-length input sequences from different operational conditions
- Robustness against noise and irregular sampling
- The capability to integrate multiple sensor inputs and learn complex temporal relationships

LSTMs also have disadvantages as they require careful hyperparameter tuning, data availability, and they have a complex model design.

Transformer-based Models: The Dynaformer Architecture

This subsection discusses Transformer-based models for battery predictio and are alternative options to RNN architectures. Among these, the Dynaformer architecture, introduced by ***Biggio et al. (2022)***, represents a state-of-the-art approach battery degradation-aware discharge prediction [69].

The Dynaformer's architecture has two main components, an encoder used to extract battery's degradation state information and a decoder used to predict the voltage discharge curve for specific current profile. The encoder is able to process only a small context window of observations, usually the first minutes of discharge, to discover the aging state. Then the decoder uses this information to predict the complete voltage trajectory until end-of-discharge. This architecture could most likely be adjusted for the prediction of battery SoH prediction.

The encoder is a standard Transformer encoder comprising 6 layers with hidden dimension h equal to 128 and 8 self-attention heads. It takes as input a $C \times 3$ tensor representing voltage, current, and time, where C is the context length (typically 200 points, corresponding to 400s). The voltage and current values are projected into an h-dimensional space using a linear layer, while the time dimension is embedded using a standard positional encoding. The encoder output, a $C \times h$ tensor, effectively captures degradation features that influence battery aging.

The decoder is a Transformer decoder with the same 6-layer, 128-dimension, 8-head structure. To handle long sequences efficiently, the decoder does not process the entire current profile directly. Instead, the input sequence is divided into $T = L/n$ tokens, each of length $n = 64$, which are projected into an h-dimensional space before being passed into the Transformer layers. The decoder performs both self-attention on its input tokens and cross-attention on the encoded degradation representation, ultimately generating a predicted voltage discharge curve.

While the original Dynaformer framework is designed for voltage discharge prediction, it could potentially be modified to directly estimate the remaining battery capacity ($q_{\max}$). Instead of producing a full time-series voltage trajectory, the decoder can be adapted for a single scalar regression task by using the encoder's learned degradation state as input to a dense output layer predicting $q_{\max}$. Since prior research has shown that the latent representations of the encoder correlate strongly with physical degradation parameters such as internal resistance and maximum charge capacity, this approach provides a direct and efficient way to estimate battery health.

The mathematical foundation of Dynaformer uses the attention mechanism that allows focus on the most relevant parts of the input sequence:

$$\text{Attention}(Q, K, V) = \text{softmax}\left(\frac{QK^T}{\sqrt{d_k}}\right)V \tag{4.8}$$

where Q, K, and V represent the query, key, and value matrices, and d_k is the dimensionality of the key vectors.

To efficiently handle long time series data, Dynaformer incorporates an approach similar to Vision Transformers, dividing the input sequence into smaller sub-sequences, each treated as a single token:

$$\text{Input sequence} \rightarrow \{s_1, s_2, \ldots, s_T\} \tag{4.9}$$

where each sub-sequence $s_i \in \mathbb{R}^n$. The original sequence of length L is divided into $T = L/n$ tokens, each of length n.

The key advantages of the Dynaformer architecture include:

- **Aging inference and discharge prediction:** The Dynaformer can simultaneously predict ageing and discharge curves, which usually requires two models.
- **Efficient processing of long time series:** By dividing input sequences into tokens, Dynaformer reduces the complexity from $O(L^2)$ to $O(L^2/n^2)$.
- **Interpretable latent space:** Analysis shows that the first two principal components of the encoder's latent representation strongly correlate with physical degradation parameters, giving insights into its SoH.
- **Robust generalization:** Dynaformer exhibits strong performance and robust performance across varying scenarios and current profiles, even on unseen data complexities.
- **Transfer learning capabilities:** The model can be pre-trained on simulated data and fine-tuned with limited real battery data.

Experimental validation has shown that Dynaformer outperforms competing NN architectures [69]. The architecture could valuable for aviation as Dynaformer's ability to handle complex current profiles makes it suitable for modeling real-world usage patterns in aircraft systems and its transfer learning can be used for adaptation to specific battery types with minimal additional data collection.

4.3.6. Monte Carlo Dropout for Uncertainty Estimation

This subsection examines Monte Carlo (MC) Dropout, which provides an approach to approximate Bayesian inference in neural networks for various applications. This method uses dropout, which is mostly used as a regularization technique, to estimate prediction uncertainty by simulating the sampling from a posterior distribution over network weights [70].

Dropout is a technique for preventing overfitting in NN. While applicable to any neural network architecture, several studies in battery degradation have demonstrated its effectiveness in recurrent networks. Both *Xu et al. (2205)* [68] as well as *Dal Ronco et al. (2024)* [67] used dropout in their LSTM architectures to improve generalization as well as *Biggio et al. (2024)* [69] in the Dynaformer architecture.

The mathematical framework of MC Dropout interprets dropout as a variational approximation to the posterior in a Bayesian neural network. For a neural network with weights W, input x (such as battery voltage, current, and temperature measurements), and target y (battery capacity or RUL), the predictive distribution is approximated by:

$$p(y|x, \mathcal{D}) \approx \frac{1}{T} \sum_{t=1}^{T} p(y|x, W_t) \tag{4.10}$$

Where $\mathcal{D}$ represents the training data, and W_t denotes the weights with randomly applied dropout during each of the T forward passes, Figure 4.4 this dropout is illustrated in NN.

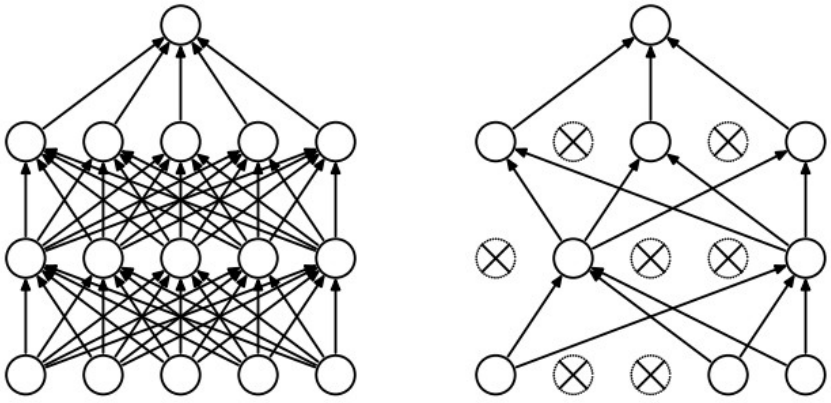

Figure 4.4: Standard Neural Network vs dropout Neural Network [71]

Implementation of MC Dropout for neural network prediction involves:

1. Training a neural network with dropout layers
2. Keeping dropout active during inference (contrary to standard practice)
3. Performing multiple forward passes
4. Computing statistics of the resulting predictions:
    - Mean prediction: $\mu = \frac{1}{T}\sum_{t=1}^{T}\hat{y}_t$
    - Prediction variance: $\sigma^2 = \frac{1}{T}\sum_{t=1}^{T}(\hat{y}_t - \mu)^2$

The variance σ^2 serves as an estimate of prediction uncertainty, which can be used to construct confidence intervals. For prediction these intervals typically take the form:

$$\text{CI}_{95\%} = \mu \pm 1.96 \cdot \sigma \tag{4.11}$$

MC Dropout is compatible with any neural network architecture, but it works naturally with networks like LSTMs since dropout layers are already often incorporated for regularization purposes. This dual functionality of dropout for training regularization and uncertainty estimation makes it an all-rounded approach for BMS.

However, MC Dropout has limitations as well, which include:

- Potential underestimation of uncertainty in regions far from training data [68]
- Sensitivity to dropout rate selection
- Cannot distinguish between aleatoric and epistemic uncertainty
- Challenges in generalizing to domains with significantly different patterns than those in the training data [68]

4.4. Transfer Learning for Electric Aviation Applications

This section discussed transfer learning that can be used to finetune Battery degradation models. This is important as models are often trained using data collected from controlled test environments (section 4.2) and they do capture all degradation effects specific to certain batteries/applications. As a result, predictive models trained solely on this ”artificial” data will often underperform in use.

Transfer learning offers a powerful solution to this challenge [72, 73]. It refers to the process, visualized in Figure 4.5, of reusing models trained for certain tasks for another task with limited data availability. For aviation, a model can be trained on a conventional battery dataset to learn general degradation behaviour. Once new becomes available, the model can be fine-tuned to incorporate application-specific characteristics.

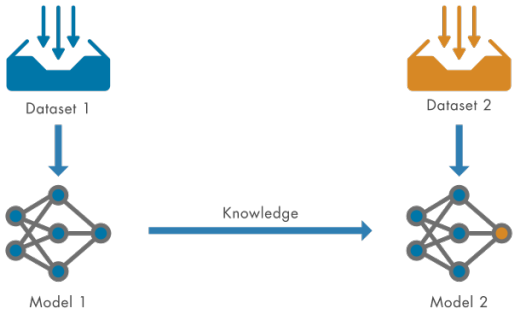

Figure 4.5: Visualization of the transfer learning process.

This approach is mostly used for NN architecture. During transfer learning, only the later layers need to be retrained or updated, which can be done with a small amount of new data.

Ensemble models are also able to have transfer learning, however it is less straightforward due to their non-parametric structure where they do not have explicit feature hierarchies that can be selectively retrained. Several approaches have been proposed in literature for this transferability, however they are not widely used in practice [74, 75].

4.5. Conclusion on Battery Degradation & Ageing

This chapter reviewed the fundamentals of battery ageing, relevant datasets, and the main modelling approaches used for predicting degradation in electric aviation. Physics-based and circuit models allow the derivatin of battery degradation without data but they struggle with scalability and accuracy under real-world applications. This makes data-driven methods more suitable for operational use.

Tree-based ensemble methods offer strong predictive accuracy, robustness, and useful uncertainty quantification. Neural networks can also reach great predictive strength, but can decrease explainability and be too advanced for some implementations.

Transfer learning can play an important role in adapting models trained on laboratory collected data to real world data. Overall, data-driven methods, and in particular ensemble techniques„ appear most promising for reliable battery health prediction in electric aviation.

5

Airline Planning Operations

This chapter explores electric airline planning. In contrary to traditional airline planning, future electric aircraft bring new challenges to the table that require updated models and strategies. First the key planning objectives and time horizons are outlined of airline planning operations, then conventional and electric aircraft requirements are compared. The Fleet Assignment Model (FAM) is introduced and how it can be adapted to account for battery health and operational limits. Finally, solution methods are discussed to solve the updated planning problem efficiently.

5.1. Optimizing Airline Operations: Balancing Sustainability and Profitability

Aviation operates at the intersection where ambitious climate impact reduction goals must be balanced with economic competitiveness, as airlines operate with thin profit margins. [76]. In Table 5.1 the objectives of airline planning optimization are outlined.

Table 5.1: Key Objectives of Airline Planning Optimization

Objective	Definition and Application
Cost Minimization	Reducing operational costs through efficient resource allocation, including aircraft, crew, fuel, and maintenance resources.
Revenue Maximization	Strategically deploying capacity to match demand patterns and maximize yield.
Resource Utilization	Ensuring high utilization rates of expensive assets while maintaining operational flexibility.
Regulatory Compliance	Meeting safety requirements, labor regulations, and environmental standards.
Passenger Experience	Creating schedules that provide convenient connections and travel times for passengers and fitting flight service.
Operational Robustness	Building schedules that can withstand disruptions with minimal impact on operations.
Environmental Sustainability	Reducing emissions and environmental impact through efficient operations.

Most research and development in goes to improvements in aircraft or airline technology that only makes incremental and modest contributions to reducing emissions. Electrifying aviation can make a much larger difference by more than halfing the climate impact, surpassing the environmental gains

possible through current optimization methods by far [3, 8].

5.2. Strategic Planning Horizons and Future Scenarios

This section gives and outline of strategic planning horizons in airline planning and is based on the *Airline Planning and Optimisation* course by *Dr.ir. dos Santos* [77]. The full picture of Airline Planning spans decades and the addition of electric aircraft to current fleets would require massive change in current plans and airlines would need to adapt their strategies to new technologies and regulatory changes.

In the long term of 10+ years, airlines need to make strategic decision for their fleet composition, infrastructure investments, and when and if to adopt electric aircraft. For the Medium-term planning of 1-10 years the focus is on fleet updates, network development, and evaluating the addition of hybrid-electric aircraft. In the short term of 1 month to 1 year, airlines optimize flight schedules, fleet assignments, and maintenance.

Many different strategies are possible in the adaptation of electric aircraft in aviation. Airline that decide to transition parts of their fleet to electric aircraft will need to invest in electric aircraft and infrastructure, gaining a competitive edge but facing high initial costs. It would also be possible to use a hybrid strategy where gradually integrating such aircraft for short-haul flights would be possible while relying on conventional aircraft for longer flights. Followers will wait for the technologies to mature and market conditions to stabilize. Each approach carries its own planning challenges,

5.3. Evolving Modeling Needs: From Conventional to Electric Airline Planning

This section outlines the change of modeling needs of traditional airline planning to the inclusion of electric airline planning and how certain aspects will need to change to incorporate electric aircraft. The research of this section is based around the work of *Zhou et al. (2020)* [78], *Lohatepanont et al. (2009)* [79] and *Hoogreef et al. (2023)* [80].

Table 5.2: From Traditional to Electric: Evolving Requirements in Airline Planning Models

Modeling Area	Conventional Aircraft	Electric Aircraft
Demand Forecasting	Based on historical passenger flows, pricing elasticity, and seasonality.	Pricing might differ for electric aircraft and therefore demand might differ.
Network and Schedule Design	Optimizes connectivity, passenger flow, and aircraft utilization.	Must include charging downtime and infrastructure constraints, limiting turnarounds and flexibility.
Fleet Assignment and Routing	Assigns aircraft to flights based on cost, capacity, and range.	Requires dynamic range tracking as planning progresses due to battery degradation and variable energy usage per route.
Maintenance and Crew Scheduling	Includes regular maintenance intervals and legal rest times.	Adds battery health monitoring and scheduled recharging, which affect crew and aircraft availability.
Operational Robustness	Uses slack time and recovery strategies to handle disruptions.	Needs additional buffers for charging delays and more buffers for unexpected battery degradation in aircraft

As shown in Table 5.2, numerous changes need to be made to the operations of airlines. In the following sections, we focus on adapting the FAM to account for these new constraints. In particular the focus

on incorporating battery degradation.

5.4. Fleet Assignment Model

The section discusses the Fleet Assignment Model (FAM), an important part of airline operations that has the goal to assign aircraft types and tails to scheduled flights. Traditionally, the FAM has focused on factors like aircraft operating costs, available fleet size, turnaround time, and connectivity within the flight network. For fuel-powered aircraft, these factors are stay fixed over time. However, the integration of electric aircraft introduces new challenges that significantly alter the operational landscape, mainly the battery degradation that throughout time that gradually limits the feasible routes aircraft can operate, making the FAM more dynamic and complex than before. Still, the objective of the model remains approximately the same: to determine the optimal aircraft-to-flight assignment plan.

5.4.1. Mathematical Formulation of the Basic FAM

Table 5.3 summarizes the key notation of sets, decision variables and parameters used in the FAM according to the Airline *Planning and Optimisation* course by *Dr.ir. dos Santos (2022-2023)* [77] and *Sherali et al. (2005)* [81].

Table 5.3: Notation for the Fleet Assignment Model (FAM)

Category	Definition
Sets	
N	Set of airports
F	Set of flights
K	Set of aircraft types
G^k	Set of ground arcs
NG^*	Set of flight and ground arcs intersecting the time cut
$O(k,n)$	Flight arcs originating at node n in fleet k
$I(k,n)$	Flight arcs terminating at node n in fleet k
n^+	Ground arcs originating at any node n
n^-	Ground arcs terminating at any node n
Decision Variables	
f_i^k	Binary variable: 1 if flight arc i is assigned to aircraft type k, 0 otherwise
y_a^k	Integer variable: number of aircraft of type k on ground arc a
Parameters	
d_i	Distance of flight i
s	Number of seats per aircraft
rev	Revenue per RPK flown (average yield)
q_i	Traffic demand in flight i
AC^k	Number of aircraft in the fleet of type k
R^k	Range of aircraft type k
oc_i^k	Unit operation cost (/ASK) for aircraft type k on flight i

The mathematical formulation of the Fleet Assignment Model is given as follows:

$$\text{Minimize} \quad \sum_{i \in F} \sum_{k \in K} oc_i^k \cdot s^k \cdot d_i \cdot f_i^k + \sum_{a \in G^k} \sum_{k \in K} gc_a^k \cdot y_a^k \tag{OF}$$

$$\text{s.t.} \quad \sum_{k \in K} f_i^k = 1, \qquad \forall i \in F \tag{C1}$$

$$y_{n^+}^k + \sum_{i \in O(k,n)} f_i^k - y_{n^-}^k - \sum_{i \in I(k,n)} f_i^k = 0, \qquad \forall n \in N^k,\ k \in K \tag{C2}$$

$$\sum_{a \in NG^k} y_a^k + f_{\bar{a}}^k \leq AC^k, \qquad \forall k \in K \tag{C3}$$

The objective function Equation OF minimizes the total operating cost, which consists of two components: the flight assignment cost and the ground arc cost. The first term represents the cost of assigning aircraft of type k to flight i, considering the operating cost per ASK, the aircraft seating capacity, and the flight distance. The second term accounts for the cost associated with ground arcs, such as waiting time or repositioning on the ground.

Equation C1 ensures that each flight is assigned to exactly one aircraft type, enforcing complete coverage of the flight schedule.

Equation C2 enforces aircraft flow balance at each node in the time-space network. This means that for every aircraft type k, the number of aircraft entering a node through ground arcs or flight arcs must equal the number of aircraft leaving it.

Equation C3 restricts the total number of aircraft used across the network for each fleet type to the available fleet size AC^k. It ensures that the number of aircraft active on the network (either in the air or on the ground) does not exceed operational capacity.

The final two constraints define the nature of the decision variables: f_i^k is binary, indicating flight assignment, while y_a^k is non-negative, representing the number of aircraft on ground arcs.

5.4.2. Additions to the Fleet Assignment Model

This section discusses several extensions to the FAM are necessary or potentially beneficial for the inclusion of electric aircraft.

Battery Degradation and Charging

Once batteries degrade, the maximum achievable energy capacity of each aircraft decreases and their range decreases. Reducing the set of feasible flight assignments for each individual aircraft.

In the FAM, battery degradation is tracked at the level of individual aircraft through its SoH that indicates the aircraft's maximum charge compared to its undegraded maximum charge. This approach eliminates the need to explicitly model remaining range [82]. Aircraft can only be assigned to flights if they have sufficient charge to complete the flight. Let $SoC_t^k(a)$ denote the SoH of aircraft a of type k at time t. Then:

$$f_{i,a}^k = 0 \quad \text{if} \quad \Delta SoC_{i,a}^k > SoC_t^k(a) \quad \forall i \in F,\ k \in K,\ a \in A^k \tag{5.1}$$

Here, $\Delta SoC_{i,a}^k$ denotes the estimated state-of-charge consumption for flight i by aircraft a of type k. This value can be calculated using a simplified version of the Breguet equation (see section 6.2) or, alternatively, approximated linearly based on flight distance as a proportion of the aircraft's current maximum achievable range.

Justification for this linear approximation stems from findings in the conceptual design study by *de Vries et al. (2024)* [7], which shows that take-off and landing phases contribute minimally to the total energy consumption of a flight. Hence, a proportional estimate is used:

$$\Delta SoC_{i,a}^{k} \approx \frac{d_i}{d_{\mathsf{max}}^{k}(a)}$$

Where d_i is the flight distance and $d_{\mathsf{max}}^{k}(a)$ is the current maximum achievable range of aircraft a of type k, adjusted for battery degradation.

After flight execution, the SoC is updated to reflect energy usage:

$$SoC_{t+1}^{k}(a) = SoC_{t}^{k}(a) - \Delta SoC_{i,a}^{k} \tag{5.2}$$

Charging operations restore SoC, subject to infrastructure constraints. The SoC after a charging period is:

$$SoC_{t+1}^{k}(a) = SoC_{t}^{k}(a) + \Delta SoC(a) \tag{5.3}$$

Where $\Delta SoC(a)$ is the charge gained during a charging cycle, depending on available power, duration, and charging efficiency. Optimal charging schedules are determined based on aircraft operational needs, time windows, and charging station availability.

Battery degradation is modeled through a reduction in the aircraft's maximum usable energy over time, impacting both flight feasibility and charge restoration rates. The full model can be implemented using a rolling horizon framework, in which the SoC, location, and availability of each aircraft are updated iteratively across planning windows. Further details on this approach are provided in section 6.3.

Optional Extensions for Electric Aviation

In addition to battery degradation and charging, the following optional model extensions could be integrated to better reflect electric aircraft operations:

Maintenance Scheduling [77]: Electric aircraft require periodic maintenance, not only for airworthiness but also for battery diagnostics and thermal management system checks for thermal runaway prevention. Maintenance periods can be scheduled every fixed number of planning periods (e.g., every 6 months) or around certain battery SoH during which the aircraft is unavailable. These intervals can also serve as reset points for battery performance.

Environmental Performance [83]: The model can be extended to include sustainability objectives. For instance, an environmental cost function can be incorporated, either as a separate objective or as a penalty term, based on lifecycle emissions of batteries and the emissions generated to produce the electricity they fly with.

5.5. Solution Approaches for the Electric Airline Planning Problem

This section discusses optimization approaches for the Fleet Assignment Model with the additional constraints imposed by the electric aircraft. Mixed-Integer Linear Programming and Dynamic Programming are discussed as solution methods, followed by potential heuristic techniques for computational efficiency.

5.5.1. Mixed-Integer Linear Programming

MILP is a one of the most common optimization approaches used for solving fleet assignment problems. The objective in the MILP can be to minimize operational costs or maximize revenue with additional terms for battery powered aircraft such as battery depreciation according to the set of constraints specified. MILP guarantees that the solution found is optimal, under the assumption that sufficient computational resources are available. In this formulation the decision variables are flight assignments and aircraft on ground arcs.

Optimizers such as Gurobi [84] are often used to solve MILP formulations of FAM [77]. These solvers utilize branch-and-bound or branch-and-cut algorithms to explore the solution space. For FAM problems

MILP is often the most appropriate choice. This is because it provides optimal solutions with detailed constraint sets and with reasonable scalability. However, there is a limit to the problem size that can reach optimality in an achievable time. When the problem grows, particularly with the introduction of electric aircraft related constraints like battery degradation, range limitations or new dimensions like maintenance and charging the computational effort required to solve the MILP problem increases significantly. In such cases, applying heuristics could be considered to achieve a solution in a reasonable timeframe.

5.5.2. Dynamic Programming

Dynamic Programming provides a powerful alternative to MILP. As it can integrate the solving of multi-stage decision problems with a time-dependent structure [85, 86]. For this research this could be used for integration of battery degradation with evolving parameters as the simulation progresses .

DP is well suited for problems where the system evolves over discrete time steps and the state of each component must be tracked explicitly, which could be the battery SoH. This is similar to rolling horizon frameworks, where each stage represents a specific planning window, where decisions are made based on the current state of the system in that window. DP's recursive structure allows for the efficient construction of solutions that account for sequential dependencies. However, the primary limitation of DP is the dimensionality, as the state and action spaces grow exponentially with problem complexity and therefore often additional methods are necessary to mitigate this issue for large-scale problems.

5.5.3. Heuristic and Approximate Solution Methods

This subsection discusses approaches that can be used once MILP and DP formulations become too computationally intensive. These heuristic and approximate methods offer a scalable alternative and they build on the structure of MILP or DP but trade off exact optimality for faster runtimes. The following subsections highlight key methods from both families.

MILP-Based Heuristics

MILP-based heuristics are grounded in the linear formulation of the Fleet Assignment Model but use tailored strategies to reduce problem complexity or solution time.

Column Generation [87] is an approach that tackles large MILP problems by separating it into multiple parts. The master problem and subproblem. Instead of directly optimizing with the whole variable set, it iteratively introduces only the most promising variables (columns) into the model. This is particularly useful when dealing with many aircraft types, itineraries or routing options and is commonly used in airline operations.

Genetic Algorithms [77] work by simulating natural selection by evolving a population of solutions over time. Each generation in the optimization applies operations such as selection, crossover, and mutation to gradually improve solution quality. However, Genetic algorithms do not guarantee optimality, but they can produce high-quality solutions within limited time.

Simulated Annealing [88] is a solution meta-heuristic that applies a probabilistic search, where at each iteration the algorithm proposes a small modification to the current solution. When the solution improves the objective it is accepted and when it could still be used to escape local optimization minima/maxima.

Dynamic Programming and Approximate Methods

DP problems can also use heuristics when they suffer from the curse of dimensionality. Approximate approaches discussed in *Wang et al.(2024)* [89] can address this:

Deterministic Dynamic Programming (DDP) breaks down the problem into multiple stages, where it recursively solves the optimal doecision by applying Bellman's principle of optimality. It is exact but only feasible for small state and action spaces.

Approximate Dynamic Programming (ADP) uses function approximators or lookup tables to estimate value functions instead of computing them exactly to save computational necessities.

5.6. Conclusion on Electric Airline Planning Operations

The addition of electric aircraft to airline planning operations introduces new challenges that require extensions or adaptations to traditional models. The FAM must especially be modified to incorporate time-dependent performance to remain realistic with evolving aircraft states. New constraints and formulations need to be applied to capture the nature of electric aircraft.

MILP is the preferred method for solving such optimization problems due to its ability to handle complex constraints and guarantee optimality. DP also offers its benefits, mostly in the modelling of the sequential nature of the battery degradation effects. This offers a highly interesting potential research direction to model battery degradation using both frameworks and compare results across approaches.

6

Integration of Disciplines

This chapter presents the integration of battery degradation modeling into electric airline planning. The chapter begins by introducing the technical and operational characteristics of the Elysian E9X electric aircraft, followed by the use of battery degradation forecasts to calculate range decrease using a modified version of the Breguet equation. It then outlines a rolling horizon methodology for the continuous operation modelling. Finally, the chapter introduces two potential case studies.

6.1. Aircraft Model: Elysian Electric Aircraft

The aircraft to be modelled in the research is currently under development by Elysian Aircraft [1], with whom the research is done in collaboration. Using the extensive research on electric aviation and electric aircraft design for the E9X Aircract in the *Wolleswinkel et al. (2024)* [6] and *de Vries et al. (2024)* [7] a framework for the important design parameters and assumptions are given for the model and summarized in Table 6.1.

Table 6.1: Elysian Aircraft Technical Parameters

Parameter	Description
Energy Specifications	Battery cell energy densities: 300 Wh/kg (conservative), 450 Wh/kg (baseline), 550 Wh/kg (future-oriented). Initial assumptions: 90% max depth of discharge (DoD), 90% end-of-life (EoL) capacity. Parameters to be varied in subsequent sensitivity analyses.
Operational Parameters	Standard commercial runway length (2000 m), cruise Mach number (0.6), cruise altitude (>7000 m), aligned with typical narrow-body operations.
Reserve Energy System	Hybrid (fuel-based reserve) scenario primarily adopted due to practical operational advantages (reduced battery mass, enhanced flexibility, minor emissions only during emergency usage).
Aerodynamics and Propulsion	Lift-to-drag ratio (L/D): 23, propeller efficiency: 0.87.
Mass Distribution	Operating empty mass: approximately 42%, Battery mass: approximately 46%, Payload fraction: 12%

Elysian currently is considering three battery energy density scenarios that may occur to evaluate potential aircraft ranges. Each of these three scenarios impacts the operational ability of the aircraft. The conservative scenario represents current battery technology, and the baseline and future-oriented scenarios reflect anticipated advancements. Table 6.2 highlights the impact of these scenarios.

Table 6.2: Battery Cell Energy Density Scenarios and Corresponding Aircraft Range

Scenario	Cell Energy Density (Wh/kg)	Useful Range (km)
Conservative	300	500
Baseline (1st Gen)	450	800
Future (2nd Gen)	550	1000

The Aircraft also has a Fuel-based reserve system to support the electric propulsion. This approach is designed to meet regulatory safety requirements, without excessive range ”cannibalization” due to additional reserve battery requirements that would increase aircraft weight significantly. For modeling the hybrid approach will be relevant, however it remains an option to test and do a sensitivity analysis with the battery reserve system possibility.

The E9X will operate at Mach 0.6 for high aero-propulsive efficiency to maximize range. Elysian has taken battery degradation into account in their calculations. They discuss optimized DoD strategies and with their battery performance they expect to achieve around 1500 cycles before reaching 90% SoH. With these flights the expected percentage of flights with flights crossing the 70% DoD is 30%. They do not explicitly account for the effects of the discharge rates that would be necessary at different cruise conditions, making it difficult to model degradation impacts for certain cruise speeds. Thus, the focus could rely more on spreading DoD planning for improved battery health and potentially adding constraints to the MILP problem for this if the results deem it necessary.

6.2. Breguet Equation for Electric Aircraft Range Calculation

This section discusses the calculation of the initial range of the electric aircraft and after the aircraft battery is degraded. A modified version of the Breguet equation discussed in *Wolleswinkel et al. (2024)* [6] can be used to predict aircraft range. The original Breguet equation is designed for fuel-based propulsion systems and can be adjusted to account for electric-specific parameters. With the provided framework, this research uses a modified form of the Electric Breguet Range equation.

The maximum achievable still-air cruise range of a battery-electric aircraft is described by the following equation:

$$R_{max} = \eta_{elec}\eta_p \frac{e_{bat}}{g} \left(\frac{L}{D}\right)_{max} \left(\frac{EM}{MTOM}\right) \tag{6.1}$$

where η_{elec} and η_p represent the electric powertrain efficiency and propeller efficiency, respectively. The term e_{bat} denotes the usable battery energy density (in Wh/kg), adjusted to account for degradation as expressed through battery State-of-Health (SoH), g is the gravitational constant, and $(L/D)_{max}$ is the aircraft's maximum lift-to-drag ratio. Crucially, the $EM/MTOM$ term—the ratio of the energy mass to maximum take-off mass—is dependent upon the available energy stored in the battery, and thus directly impacted by battery degradation. This degradation will be taken into account by multiplying the Battery SoH (percentage battery capacity left) predictions with the initial battery capacity.

6.3. Rolling Horizon Methodology

This section discusses the rolling horizon methodology, that can be used to dynamically account for battery degradation in operational planning. This enables the adjustment of parameters throughout the MILP optimization [90, 91]. Using this methodology periodic re-optimization of fleet assignment can be done and maintenance actions can be planned based on updated battery health information and performance constraints derived from the electric Breguet equation. This process is visualized in Figure 6.1 and consists of the following steps:

1. **Prediction Horizon:** At each stage t, the system evaluates a prediction horizon composed of a control period and a look-ahead period. Within this horizon, battery degradation forecasts are generated using recent flight data, such as DoD and Battery age. These predictions inform potential

future constraints on aircraft performance via the electric Breguet equation.

2. **Control Period:** This is the immediate timeframe over which the optimized fleet assignment and maintenance actions are actually realized. Fleet routing is adapted accordingly, with optimization ensuring that range feasibility is preserved.
3. **Look-ahead Period:** Beyond the control period, a longer-term plan is established to anticipate degradation trends and schedule future battery interventions. The MILP model incorporates expected capacity decline and recalculates projected range using the Breguet-based performance model to avoid infeasible missions in future stages.
4. **Stage Advancement and Iteration:** At the end of each control period, actual operational and maintenance data are collected. This data updates the degradation models and inform the subsequent prediction horizon in stage $t+1$, maintaining an ongoing feedback loop for ageing-aware fleet management.

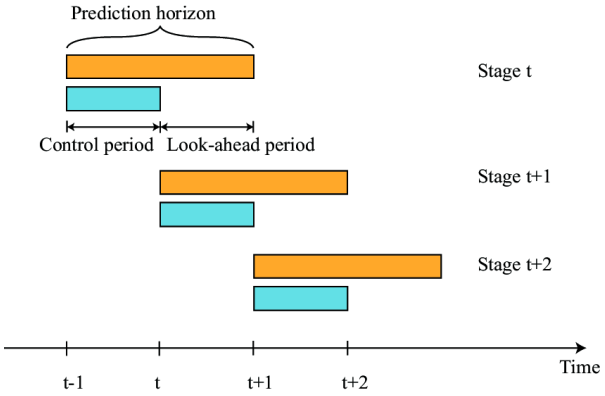

Figure 6.1: Visualization of the Rolling Horizon Methodology [92]

6.4. Simulation and Case Studies

To validate the research on integration of battery degradation forecasts with operational planning, case studies will be conducted to demonstrate the viability of the impacts of battery degradation in electric aviation operations. The first case study is a modified version of an assignment of the*Airline Planning and Optimisation* course by *Dr.ir. dos Santos* [77], where regional flight network is setup throughout Italy. The scale of this problem perfectly matches the scale for the first generations of electric aviation, posing a great initial testing environment of the model. The second case study will be a more complex problem, where real flight data will be scraped from the Flightradar24 website [93] according to the necessities of the outcome of the first case study. The focus will be on answering and analyzing the research questions and Key Performance Indicators discussed in section 7.2.

6.5. Conclusion on Integration of Disciplines

This chapter demonstrated how battery degradation modeling can be effectively integrated into airline planning to create a more realistic framework for electric aviation. Starting from the technical assumptions of the Elysian E9X aircraft, the chapter connected cell-level battery health forecasts with mission-level range limitations using a modified Electric Breguet equation.

To translate these insights into actionable fleet management strategies, a rolling horizon methodology was proposed. This allows battery degradation to be updated throughout iterative optimization. The final case studies bridge theory and practice, enabling evaluation in both simplified and real-world scenarios.

In conclusion, this chapter provides the missing link between predictive battery modeling and airline operations—enabling ageing-aware electric fleet planning that is not only efficient and scalable, but grounded in the physical realities of battery performance over time.

7

Research Proposal

This chapter outlines the research proposal that guides the remainder of the research. It begins by identifying the research gap based on the preceding literature study, after which the central research question is formulated along with several sub-questions and a final research objective. The proposed work aims to integrate battery degradation modeling with uncertainty quantification into a rolling horizon fleet assignment framework for battery-electric aircraft. The outcomes of this research are expected to provide a foundational methodology for battery degradation-aware electric fleet planning, supporting future developments in sustainable and efficient airline operations.

7.1. Research Gap Analysis

A wide range of literature was examined to identify the current state of research on battery-electric aviation. While many studies address either battery degradation or airline operations, few attempt to combine these domains—particularly in the context of electric passenger aircraft. As summarized in Table **??**, each of the most relevant studies contributes to specific areas, but none jointly capture the dynamic interaction between battery ageing and operational decision-making at the fleet level.

Coverage of Key Topics Across Literature and the Research. Symbols indicate: ✓ = addressed, – = mentioned or partially adressed, no mark = not adressed.

	Electric Aviation	**Battery Degradation**	**Uncertainty in Degradation**	**Operational Airline Modelling**	**Range Estimation**
van Oosterom et al. (2023) [10]	✓	–		✓	
Paek et al. (2019) [44]	✓	✓			–
He et al. (2022) [48]		✓	✓		
Hoogreef et al. (2023) [80]	✓			✓	✓
Chan et al. (2025) [94]	✓			✓	
Wolleswinkel et al. (2024) [6] & *de Vries et al. (2024)* [7]	✓	–		–	✓
This Research	✓	✓	✓	✓	✓

The papers by *Wolleswinkel et al. (2024)* [6] and *de Vries et al. (2024)* [7], authored by members of Elysian—who are also collaborators in this research—lay the foundation for the technical feasibility and conceptual design of large battery-electric aircraft. Their work highlights several design and performance challenges but does not address these predictive operational models that account for battery degradation over time in detail. To date, no research integrates both degradation modeling

and operational planning in a manner that systematically propagates battery degradation effects into aircraft performance metrics, such as range, within fleet optimization or scheduling frameworks. While recent advances validate the technical feasibility of large battery-electric passenger aircraft, a critical gap remains in modeling how battery degradation with its uncertainty quantification impacts aircraft performance and fleet-level operational decisions. Addressing this gap is essential to unlock the full environmental and economic potential of electric aviation.

7.2. Research Proposal

Taking the complete Literature Study into consideration, the overarching research question is:

> ***"How can battery degradation and ageing be systematically incorporated into an electric fleet assignment model to optimize realistic operational and economic performance over time?"***

This study aims to develop a fleet assignment framework for battery-electric aircraft that explicitly accounts for battery degradation and ageing processes over time. The resulting model will support strategic and operational decision-making regarding aircraft deployment, battery replacement, and long-term performance forecasting. A rolling horizon methodology will be employed to adjust fleet assignments based on the evolving battery health of the aircraft, thereby enabling ageing-aware optimization of future electric airline operations.

To address this research question, the following research (sub-)questions are proposed:

1. **How can battery degradation be modeled to accurately estimate electric aircraft performance and range over time?**
   Metrics: State of Health (SoH), Achievable Range

2. **What are the main cost drivers of battery systems in electric aircraft, and how do different replacement strategies impact their lifecycle cost per flight hour?**
   Metrics: Lifecycle Cost per Flight Hour (LCC/FH)

3. **What are optimal battery replacement thresholds based on aircraft mission profiles and economic trade-offs?**
   Metrics: End-of-Life (EoL) Threshold

4. **How can predictive models of battery degradation, including uncertainty quantification, be optimally integrated into a rolling horizon fleet assignment framework?**
   Metrics: Computational Performance, Optimal Prediction Horizon, Planning Outcomes

5. **What is the impact of ageing-aware electric fleet assignment on airline-level performance metrics CASK and RASK?**
   Metrics: Revenue per Available Seat Kilometer (RASK), Cost per Available Seat Kilometer (CASK)

6. **How do utilization strategies affect battery longevity and long-term fleet economics in electric operations?**
   Metrics: Battery Cycle Life, % of Flights with >70% DoD, Long-Term Cost Efficiency

Together, these questions span the data-driven modelling of battery degradation, its integration into operational optimization, and the evaluation of system-level and economic impacts. The scope is aligned with the context of electric regional aircraft operations, with specific reference to the 90-passenger concept developed by Elysian Aircraft.

7.3. Research Objective

On the basis of the identified research gap and literature study, the objective of this thesis is:

> ***"To develop a rolling horizon fleet assignment model for battery-electric aircraft that integrates battery degradation and ageing. The model aims to support optimal and realistic operational planning and battery replacement strategies, with a focus on maintaining aircraft performance and maximizing long-term profits."***

8

Research Planning

This chapter outlines the structured planning and timeline for the research presented in chapter 7 It includes key dates for the research process.

Table 8.1: Research Planning Timeline

Calendar Weeks & Key Dates	Phase Title	Description
CW 7–15 *Start: 11 Feb 2025*	Literature Review & Research Proposal	Conduct a comprehensive review of electric aviation, battery ageing, and fleet modeling. Formulate the research gap, objectives, and approach.
CW 16–21	Methodology Development	Design and implement the core model: battery degradation prediction with uncertainty quantification, electric range estimation using the Breguet equation, MILP-based fleet assignment, and rolling horizon integration.
CW 22–23	Module Testing & Verification	Test and validate each model component.
CW 24–26	First Case Study	Apply the complete model to the fictional Italian regional airline scenario. Simulate scheduling, assess model, operational feasibility and gain insights for improvements.
CW 27–29 *Midterm: 14–20 Jul 2025*	Iterative Refinement & Prepare for Midterm Meeting & Report Writing	Enhance model performance and robustness based on the first case study. Improve degradation accuracy, potentially build another prediction model and refine optimization results. Spend time on report writing
CW 30–35	*Research Break*	
CW 36–38	Iterative Refinement & Report Writing	Resume work by further improving core modules and aligning development with research question needs. Continue writing.
CW 39–42	Second Case Study Setup and Testing	Prepare a real-world dataset from Flightradar and test the model on the the dataset to gain insights.
CW 43–45	Model Evaluation and Improvement & Sensitivity Study	Assess model outcomes on real data. Run scenario testing and quantify sensitivities to input parameters.
CW 47–49 *Green Light: 1–7 Dec 2025*	Final Integration & Improvements & Continue Writing	Final model adjustments and prepare data and results for reporting. Prepare for Green Light presentation.
CW 50–52	Final Presentation Preparation & Final Reporting Adjustments	Final minor technical reporting adjustments and final presentation preparation.
CW 1–2 *Finalisation: 5–11 Jan 2026*	Thesis Defense	Thesis Defense and ensuring all documents are submitted.

9

Conclusions

This thesis proposal addresses a key research gap at the intersection of battery degradation modeling and operational fleet planning for electric aviation. As the aviation sector moves toward decarbonization, electric aircraft are gaining attention as a viable solution for short- to medium-range operations. Yet, despite progress in conceptual design and feasibility studies, there is limited understanding of how battery degradation and ageing dynamically influence aircraft range, fleet scheduling, and long-term economic performance in airline operations.

A comprehensive literature review revealed that while battery capacity degradation and electric aircraft conceptual design are active areas of research, most studies remain confined to their isolated technical domains. There is limited integration of battery health modeling with fleet-level optimization frameworks. Furthermore, recent degradation studies increasingly leverage data-driven methods for accurate prediction and uncertainty quantification of battery health. However, these have yet to be systematically connected to operational planning problems in electric aviation.

Recent studies, such as *Wolleswinkel et al. (2024)* [6] and *de Vries et al. (2024)* [7], have challenged long-standing assumptions about the limitations of battery-electric aircraft, demonstrating that larger passenger capacities and longer ranges may be feasible than previously thought. However, these works focus primarily on aircraft-level performance and design parameters, and do not address how battery degradation propagates through time into operational decision-making frameworks.

This research aims to fill that gap by developing a rolling horizon electric fleet assignment model that incorporates data-driven battery health forecasts, uncertainty quantification, and mission-specific range estimation. The proposed framework will support operational decisions by realistically simulating how battery degradation affects fleet performance, airline strategies, and costs.

To evaluate the proposed framework, the research will apply it to two case studies: one fictional and one based on real-world flight data. These studies will assess how degradation and ageing-aware fleet assignment affects aircraft utilization, battery replacement strategies, and airline-level performance metrics under realistic conditions. The resulting methodology aims to support strategic decision-making for electric fleet operations and contribute to the broader transition toward sustainable aviation.

References

[1] Elysian Aircraft. *Elysian Aircraft*. https://www.elysianaircraft.com/.

[2] *Aviation - IEA*. URL: https://www.iea.org/energy-system/transport/aviation.

[3] Marina Kousoulidou and Daniele Violato. “Towards Climate-Neutral aviation”. In: *ResearchGate* (Oct. 2020). URL: https://www.researchgate.net/publication/344953087_Towards_Climate-Neutral_Aviation.

[4] enviro.aero. *AVIATION 2050 GOAL AND THE PARIS AGREEMENT*. Tech. rep. Oct. 2021. URL: https://aviationbenefits.org/media/167476/fact-sheet_4_aviation-2050-and-paris-agreement2.pdf.

[5] Bofan Wang, Zhao Jia Ting, and Ming Zhao. “Sustainable aviation fuels: Key opportunities and challenges in lowering carbon emissions for aviation industry”. In: *Carbon Capture Science Technology* 13 (Aug. 2024), p. 100263. DOI: 10.1016/j.ccst.2024.100263. URL: https://www.sciencedirect.com/science/article/pii/S2772656824000757.

[6] Rob E. Wolleswinkel et al. “A New Perspective on Battery-Electric Aviation, Part I: Reassessment of achievable range”. In: *AIAA SCITECH 2022 Forum* (Jan. 2024). DOI: 10.2514/6.2024-1489. URL: https://doi.org/10.2514/6.2024-1489.

[7] Reynard De Vries et al. “A New Perspective on Battery-Electric Aviation, Part II: Conceptual Design of a 90-Seater”. In: *AIAA SCITECH 2022 Forum* (Jan. 2024). DOI: 10.2514/6.2024-1490. URL: https://doi.org/10.2514/6.2024-1490.

[8] Bright Appiah Adu-Gyamfi and Clara Good. “Electric aviation: A review of concepts and enabling technologies”. In: *Transportation Engineering* 9 (July 2022), p. 100134. DOI: 10.1016/j.treng.2022.100134. URL: https://www.sciencedirect.com/science/article/pii/S2666691X22000032X.

[9] Laxman Timilsina et al. “Battery degradation in electric and hybrid electric vehicles: a survey study”. In: *IEEE Access* 11 (Jan. 2023), pp. 42431–42462. DOI: 10.1109/access.2023.3271287. URL: https://www.researchgate.net/publication/370353801_Battery_Degradation_in_Electric_and_Hybrid_Electric_Vehicles_A_Survey_Study.

[10] Simon Van Oosterom and Mihaela Mitici. “Optimizing the battery charging and swapping infrastructure for electric short-haul aircraft—The case of electric flight in Norway”. In: *Transportation Research Part C Emerging Technologies* 155 (Aug. 2023), p. 104313. DOI: 10.1016/j.trc.2023.104313. URL: https://www.sciencedirect.com/science/article/pii/S0968090X23003029.

[11] *Reducing emissions from aviation*. Accessed April 2025. URL: https://climate.ec.europa.eu/eu-action/transport/reducing-emissions-aviation_en.

[12] *ACARE Goals - Acare*. Accessed April 2025. URL: https://www.acare4europe.org/acare-goals/.

[13] *Investigation of the effects of civil aviation fuel Jet A1 blends on diesel engine performance and emission characteristics*. Accessed April 2025. URL: https://www.researchgate.net/publication/286061182_Investigation_of_the_effects_of_civil_aviation_fuel_Jet_A1_blends_on_diesel_engine_performance_and_emission_characteristics.

[14] *Sustainable Aviation Fuels*. Accessed April 2025. Sept. 2024. URL: https://www.airbus.com/en/innovation/energy-transition/sustainable-aviation-fuels.

[15] *Developing Sustainable Aviation Fuel (SAF)*. Accessed April 2025. URL: https://www.iata.org/en/programs/sustainability/sustainable-aviation-fuels/.

[16] Dawei Xu. “Technologies and challenges of hydrogen powered aviation”. In: *Journal of Physics Conference Series* 2608.1 (Oct. 2023), p. 012003. DOI: 10.1088/1742-6596/2608/1/012003. URL: https://doi.org/10.1088/1742-6596/2608/1/012003.

[17] Armaan Sharma and Mansur M. Arief. *Hydrogen in Aviation: Evaluating the Feasibility and Benefits of a Green Fuel Alternative*. 2024. arXiv: 2412.15137 [eess.SY]. URL: https://arxiv.org/abs/2412.15137.

[18] Ye Xie et al. "Review of hybrid electric powered aircraft, its conceptual design and energy management methodologies". In: *Chinese Journal of Aeronautics* 34.4 (Aug. 2020), pp. 432–450. DOI: 10.1016/j.cja.2020.07.017. URL: https://www.sciencedirect.com/science/article/pii/S1000936120303368.

[19] *History of Aircraft amp; Aviation*. Jan. 2022. DOI: 10.15394/eaglepub.2022.1066.n2. URL: https://eaglepubs.erau.edu/introductiontoaerospaceflightvehicles/chapter/history-of-aircraft-and-aviation/.

[20] Mike Goulette. "The History of Electric Flight - The new RC Soaring Digest - Medium". In: *Medium* (June 2023). URL: https://medium.com/rc-soaring-digest/the-history-of-electric-flight-12a78926ade4.

[21] b777 Driver. *World's first electric flight 21st October 1973 - Complete story*. Video. July 2015. URL: https://www.youtube.com/watch?v=7BY7BtyDsVo.

[22] Martyn Cowley et al. *Exclusive first hand report, of Paul MacCready's solar powered aircraft project*. Tech. rep. URL: https://www.humanpoweredflight.co.uk/hpfMedia/media/7/solar-challenger-aeromodeller-1981.pdf.

[23] NASA Dryden Flight Research Center. *NASA / DFRC: Photo ECN-13413 — Albatross*. https://www.dfrc.nasa.gov/Gallery/Photo/Albatross/HTML/ECN-13413.html.

[24] Akira Yoshino. "Development of the Lithium-Ion battery and recent technological trends". In: *Elsevier eBooks*. Jan. 2014, pp. 1–20. DOI: 10.1016/b978-0-444-59513-3.00001-7. URL: https://www.sciencedirect.com/science/article/abs/pii/B9780444595133000017.

[25] Nazek El-Atab et al. "Solar powered Small Unmanned aerial Vehicles: a review". In: *Energy Technology* 9.12 (Sept. 2021). DOI: 10.1002/ente.202100587. URL: https://www.researchgate.net/publication/354445699_Solar_Powered_Small_Unmanned_Aerial_Vehicles_A_Review.

[26] Pipistrel. *Taurus Electro - Pipistrel*. en-US. Oct. 2024. URL: https://www.pipistrel-aircraft.com/products/taurus-electro/.

[27] Andrew Y. Chen. "Analysis on technical challenges and prospects of electric aircraft". In: *Applied and Computational Engineering* 59.1 (May 2024), pp. 253–259. DOI: 10.54254/2755-2721/59/20240815. URL: https://www.researchgate.net/publication/382369690_Analysis_on_technical_challenges_and_prospects_of_electric_aircraft.

[28] EUROBAT. *BATTERY INNOVATION ROADMAP 2035*. Tech. rep. June 2024. URL: https://www.eurobat.org/wp-content/uploads/2024/09/white-paper-innovation-roadmap-2024-Tech-Annex_web_version.pdf.

[29] Geon-Tae Park et al. "Ultrafine-grained Ni-rich layered cathode for advanced Li-ion batteries". In: *Energy Environmental Science* 14.12 (Jan. 2021), pp. 6616–6626. DOI: 10.1039/d1ee02898g. URL: https://pubs.rsc.org/en/content/articlehtml/2021/ee/d1ee02898g.

[30] George G. Njema, Russel Ben O. Ouma, and Joshua K. Kibet. "A review on the recent advances in battery development and energy storage technologies". In: *Journal of Renewable Energy* 2024 (May 2024), pp. 1–35. DOI: 10.1155/2024/2329261. URL: https://onlinelibrary.wiley.com/doi/10.1155/2024/2329261.

[31] Danielle M. Gendron et al. "A High-Throughput technique for unidirectional critical current density testing of solid electrolyte materials". In: *Journal of the Electrochemical Society* (Jan. 2025). DOI: 10.1149/1945-7111/ada740. URL: https://iopscience.iop.org/article/10.1149/1945-7111/ada740.

[32] Jonas Hellgren et al. *Airport charging system designs and power management for Megawatt-Level charging of Battery-Electric aircraft*. Tech. rep. 2023. URL: https://www.icas.org/icas_archive/icas2024/data/papers/icas2024_0442_paper.pdf.

[33] Z Guo et al. *Aviation to grid: airport charging infrastructure for electric aircraft*. Dec. 2020. URL: https://bura.brunel.ac.uk/handle/2438/23431.

[34] Rekha Narayan et al. “Self□Healing: an emerging technology for Next□Generation smart batteries”. In: *Advanced Energy Materials* 12.17 (Oct. 2021). DOI: 10.1002/aenm.202102652. URL: https://advanced.onlinelibrary.wiley.com/doi/epdf/10.1002/aenm.202102652.

[35] Heart Aerospace. *Heart Aerospace*. https://heartaerospace.com/.

[36] Maeve Aero. *Maeve Aero*. https://maeve.aero/.

[37] Sam H. Finkelstein et al. “How lithium-ion batteries work conceptually: thermodynamics of Li bonding in idealized electrodes”. In: *Physical Chemistry Chemical Physics* 26.36 (Jan. 2024), pp. 24157–24171. DOI: 10.1039/d4cp00818a. URL: https://pubs.rsc.org/en/content/articlehtml/2024/cp/d4cp00818a.

[38] John B. Goodenough. “How we made the Li-ion rechargeable battery”. In: *Nature Electronics* 1.3 (Mar. 2018), p. 204. DOI: 10.1038/s41928-018-0048-6. URL: https://www.nature.com/articles/s41928-018-0048-6.

[39] Ivana Hasa et al. “Ensuring accurate Key Performance Indicators for Battery applications by implementing consistent Reporting Methodologies”. In: *Transportation research procedia* 72 (Jan. 2023), pp. 3625–3632. DOI: 10.1016/j.trpro.2023.11.559. URL: https://doi.org/10.1016/j.trpro.2023.11.559.

[40] Xuebing Han et al. “A review on the key issues of the lithium ion battery degradation among the whole life cycle”. In: *eTransportation* 1 (July 2019), p. 100005. DOI: 10.1016/j.etran.2019.100005. URL: https://www.sciencedirect.com/science/article/abs/pii/S2590116819300050.

[41] Tuhibur Rahman and Talal Alharbi. “Exploring Lithium-Ion Battery Degradation: A Concise Review of Critical Factors, Impacts, Data-Driven Degradation Estimation Techniques, and Sustainable Directions for Energy Storage Systems”. In: *Batteries* 10.7 (2024), p. 220. DOI: 10.3390/batteries10070220.

[42] Battery University. *BU-204: How do Lithium Batteries Work?* Mar. 2022. URL: https://batteryuniversity.com/article/bu-204-how-do-lithium-batteries-work.

[43] Andrew Carnovale and Xianguo Li. “A modeling and experimental study of capacity fade for lithium-ion batteries”. In: *Energy and AI* 2 (Oct. 2020), p. 100032. DOI: 10.1016/j.egyai.2020.100032. URL: https://doi.org/10.1016/j.egyai.2020.100032.

[44] Sung Wook Paek, Sangtae Kim, and Christober Vinoth Raj Rayappan. “Impact of Battery Degradation on Lifetime Ranges of Electric Aircraft and Unmanned Underwater Vehicles”. In: *2019 IEEE Conference on Control Technology and Applications (CCTA)*. IEEE. Hong Kong, China, Aug. 2019.

[45] T. N. V. Krishna et al. “Powering the Future: Advanced Battery Management Systems (BMS) for Electric Vehicles”. In: *Energies* 17.14 (), p. 3360. DOI: 10.3390/en17143360. URL: https://doi.org/10.3390/en17143360.

[46] Data.gov. *National Aeronautics and Space Administration - Li-Ion battery aging datasets*. Dec. 2023. URL: https://catalog.data.gov/dataset/li-ion-battery-aging-datasets.

[47] Iowa State University. *ISU-ILCC Battery Aging Dataset*. Dec. 2023. URL: https://iastate.figshare.com/articles/dataset/_b_ISU-ILCC_Battery_Aging_Dataset_b_/22582234.

[48] Haowei He et al. “EVBattery: a Large-Scale electric vehicle dataset for battery health and capacity estimation”. In: *arXiv (Cornell University)* (Jan. 2022). DOI: 10.48550/arxiv.2201.12358. URL: https://arxiv.org/abs/2201.12358.

[49] George Hawley. *Understanding Tesla’s Lithium-Ion Batteries*. https://evannex.com/blogs/news/understanding-teslas-lithium-ion-batteries/. Evannex blog post. 2023.

[50] Ming-Feng Ge et al. “A review on state of health estimations and remaining useful life prognostics of lithium-ion batteries”. In: *Measurement* 174 (Jan. 2021), p. 109057. DOI: 10.1016/j.measurement.2021.109057. URL: https://www.sciencedirect.com/science/article/pii/S0263224121000890?via%3Dihub.

[51] Shi Li et al. “A comparative study of model-based capacity estimation algorithms in dual estimation frameworks for lithium-ion batteries under an accelerated aging test”. In: *Applied Energy* 212 (Feb. 2018), pp. 1522–1536. DOI: 10.1016/j.apenergy.2018.01.008. URL: https://www.sciencedirect.com/science/article/pii/S0306261918300084?via%3Dihub.

[52] Khushbu Kumari and Suniti Yadav. “Linear regression analysis study”. In: *Journal of the Practice of Cardiovascular Sciences* 4.1 (Jan. 2018), p. 33. DOI: 10.4103/jpcs.jpcs_8_18. URL: https://journals.lww.com/jpcs/fulltext/2018/04010/linear_regression_analysis_study.9.aspx.

[53] Abdul Azis Abdillah et al. “Comparative analysis of regression methods for estimation of remaining useful life of lithium ion battery”. In: *Recent in Engineering Science and Technology* 3.01 (Jan. 2025), pp. 9–18. DOI: 10.59511/riestech.v3i01.93. URL: https://www.mbi-journals.com/index.php/riestech/article/view/93.

[54] Houssem Sifaou, Abla Kammoun, and Mohamed-Slim Alouini. “A Precise Performance Analysis of Support Vector Regression”. In: *CoRR* abs/2105.10373 (2021). arXiv: 2105.10373. URL: https://arxiv.org/abs/2105.10373.

[55] G Naresh and Praveenkumar Thangavelu. “Integrating machine learning for health prediction and control in over-discharged Li-NMC battery systems”. In: *Ionics* (Sept. 2024). DOI: 10.1007/s11581-024-05834-5. URL: https://link.springer.com/article/10.1007/s11581-024-05834-5.

[56] Iqbal H. Sarker. “Machine learning: algorithms, Real-World applications and research directions”. In: *SN Computer Science* 2.3 (Mar. 2021). DOI: 10.1007/s42979-021-00592-x. URL: https://link.springer.com/article/10.1007/s42979-021-00592-x.

[57] Gilles Louppe. *Understanding Random Forests: From Theory to Practice*. 2015. arXiv: 1407.7502 [stat.ML]. URL: https://arxiv.org/abs/1407.7502.

[58] Geng Wang, Zhiqiang Lyu, and Xiaoyu Li. “An optimized random forest regression model for Li-Ion battery prognostics and health management”. In: *Batteries* 9.6 (June 2023), p. 332. DOI: 10.3390/batteries9060332. URL: https://www.mdpi.com/2313-0105/9/6/332.

[59] Man-Fai Ng et al. “Predicting the state of charge and health of batteries using data-driven machine learning”. In: *Nature Machine Intelligence* 2.3 (Mar. 2020), pp. 161–170. DOI: 10.1038/s42256-020-0156-7. URL: https://www.nature.com/articles/s42256-020-0156-7.

[60] Alexey Natekin and Alois Knoll. “Gradient boosting machines, a tutorial”. In: *Frontiers in Neurorobotics* 7 (Jan. 2013). DOI: 10.3389/fnbot.2013.00021. URL: https://www.frontiersin.org/journals/neurorobotics/articles/10.3389/fnbot.2013.00021/full.

[61] Cheng-Chia Huang and Cheng-Chia Huang. *Boosting the Model: The Enhancement in the Forest-based and Boosted Classification and Regression tool*. en-US. Mar. 2024. URL: https://www.esri.com/arcgis-blog/products/arcgis-pro/analytics/boosting-the-model-the-enhancement-in-the-forest-based-and-boosted-classification-and-regression-tool.

[62] Roger Koenker Bassett, Gilbert, and Jr. “Regression quantiles”. In: *Econometrica* 46.1 (1978), pp. 33–50. URL: https://doi.org/10.2307/1913643https://www.jstor.org/stable/1913643.

[63] Mengfan Xu. “Quantile Regression Model and Its Application Research”. In: *Academic Journal of Science and Technology* 8.3 (2023), pp. 172–176. DOI: 10.54097/vt1qpm59.

[64] Hugh A. Chipman, Edward I. George, and Robert E. McCulloch. “BART: Bayesian additive regression trees”. In: *The Annals of Applied Statistics* 4.1 (Mar. 2010). DOI: 10.1214/09-aoas285. URL: https://arxiv.org/abs/0806.3286.

[65] Miriana Quiroga et al. *Bayesian additive regression trees for probabilistic programming*. June 2022. URL: https://arxiv.org/abs/2206.03619.

[66] Antonio R. Linero. *Generalized Bayesian Additive Regression Trees Models: Beyond Conditional Conjugacy*. Feb. 2022. URL: https://arxiv.org/abs/2202.09924.

[67] Leonardo Dal Ronco et al. *ExplainBattery: Enhancing Battery Capacity Estimation with an Efficient LSTM Model and Explainability Features*. Tech. rep. 2024. URL: https://ceur-ws.org/Vol-3839/paper4.pdf.

[68] Pengcheng Xu and Yunfeng Lu. “Predicting Li-ion Battery Cycle Life with LSTM RNN”. In: *Department of Chemical and Biomolecular Engineering, University of California, Los Angeles* (2025). {phoenixfilber, luucla}@ucla.edu.

[69] Luca Biggio et al. *Dynaformer: A Deep Learning Model for Ageing-aware Battery Discharge Prediction*. 2022. arXiv: 2206.02555 [cs.LG]. URL: https://arxiv.org/abs/2206.02555.

[70] Meng Wei et al. “Remaining useful life prediction of lithium-ion batteries based on Monte Carlo Dropout and gated recurrent unit”. In: *Energy Reports* 7 (May 2021), pp. 2862–2871. DOI: 10.1016/j.egyr.2021.05.019. URL: https://www.sciencedirect.com/science/article/pii/S2352484721002973.

[71] Tobias Sterbak. *Model uncertainty in deep learning with Monte Carlo dropout in keras - Depends on the definition*. June 2022. URL: https://www.depends-on-the-definition.com/model-uncertainty-in-deep-learning-with-monte-carlo-dropout/.

[72] David Fagbuyiro. “Guide to Transfer Learning in Deep Learning - David Fagbuyiro - Medium”. In: *Medium* (Nov. 2024). URL: https://medium.com/@davidfagb/guide-to-transfer-learning-in-deep-learning-1f685db1fc94.

[73] Kailong Liu et al. “Transfer learning for battery smarter state estimation and ageing prognostics: Recent progress, challenges, and prospects”. In: *Advances in Applied Energy* 9 (Dec. 2022), p. 100117. DOI: 10.1016/j.adapen.2022.100117. URL: https://www.sciencedirect.com/science/article/pii/S266679242200035X.

[74] Pratham Grover et al. “Ensemble transfer learning for distinguishing cognitively normal and mild cognitive impairment patients using MRI”. In: *Algorithms* 16.8 (Aug. 2023), p. 377. DOI: 10.3390/a16080377. URL: https://www.mdpi.com/1999-4893/16/8/377.

[75] Xiaobo Liu et al. “Ensemble Transfer Learning Algorithm”. In: *IEEE Access* 6 (Dec. 2017), pp. 2389–2396. DOI: 10.1109/access.2017.2782884. URL: https://doi.org/10.1109/access.2017.2782884.

[76] Mahdi Noorafza et al. “Airline network Planning Considering Climate impact: Assessing new operational improvements”. In: *Applied Sciences* 13.11 (May 2023), p. 6722. DOI: 10.3390/app13116722. URL: https://www.mdpi.com/2076-3417/13/11/6722.

[77] Bruno dos Santos. *AE4423 Airline Planning and Optimisation*. Department of Aerospace Engineering, Air Transport Operations, Delft University of Technology, Delft. no date available.

[78] Lei Zhou et al. “Airline Planning and Scheduling: Models and Solution Methodologies”. In: *Frontiers of Engineering Management* 7.4 (2020). DOI: 10.1007/s42524-020-0093-5.

[79] Manoj Lohatepanont and Cynthia Barnhart. “Airline Schedule Planning: Integrated Models and Algorithms for Schedule Design and Fleet Assignment”. In: *Transportation Science* 38.1 (2004), pp. 19–32. DOI: 10.1287/trsc.1030.0026.

[80] Maurice Hoogreef et al. “Coupled Hybrid Electric Aircraft Design and Strategic Airline Planning”. In: *AIAA Aviation 2019 Forum* (June 2023). DOI: 10.2514/6.2023-3869. URL: https://research.tudelft.nl/en/publications/coupled-hybrid-amp-electric-aircraft-design-and-strategic-airline.

[81] Hanif D. Sherali, Ebru K. Bish, and Xiaomei Zhu. “Airline fleet assignment concepts, models, and algorithms”. In: *European Journal of Operational Research* 172.1 (Apr. 2005), pp. 1–30. DOI: 10.1016/j.ejor.2005.01.056. URL: https://www.sciencedirect.com/science/article/pii/S0377221705002109.

[82] Mihaela Mitici, Madalena Pereira, and Fabrizio Oliviero. “Electric Flight Scheduling with Battery-Charging and Battery-Swapping Opportunities”. In: *EURO Journal on Transportation and Logistics* 11.2 (2022), p. 100074. DOI: 10.1016/j.ejtl.2022.100074.

[83] Marius Magnus Krömer, David Topchishvili, and Cornelia Schön. “Sustainable airline planning and scheduling”. In: *Journal of Cleaner Production* 434 (Dec. 2023), p. 139986. DOI: 10.1016/j.jclepro.2023.139986. URL: https://www.sciencedirect.com/science/article/pii/S0959652623041446.

[84] Gurobi Optimization, LLC. *Gurobi Optimizer — Gurobi Solutions*. https://www.gurobi.com/solutions/gurobi-optimizer/. Accessed: 2025-12-08.

[85] Joachim Zietz. “Dynamic Programming: An Introduction by example”. In: *The Journal of Economic Education* 38.2 (Apr. 2007), pp. 165–186. DOI: 10.3200/jece.38.2.165-186. URL: https://doi.org/10.3200/jece.38.2.165-186.

[86] Dhawal Thakkar and Balamurugan Palaniappan. “Aircraft routing using dynamic programming and reinforcement learning: A customer-centric approach”. In: *Journal of the Air Transport Research Society* 2 (May 2024), p. 100018. DOI: 10.1016/j.jatrs.2024.100018. URL: https://www.sciencedirect.com/science/article/pii/S2941198X24000290.

[87] François Vanderbeck. “Implementing mixed integer column generation”. In: *Springer eBooks*. Mar. 2006, pp. 331–358. DOI: 10.1007/0-387-25486-2_12. URL: https://link.springer.com/chapter/10.1007/0-387-25486-2_12.

[88] Sergio Ledesma, Juan Gabriel Aviña-Cervantes, and Raul Sanchez. “Practical Considerations for Simulated Annealing Implementation”. In: *Simulated Annealing*. InTech, 2008. DOI: 10.5772/5560. URL: https://doi.org/10.5772/5560.

[89] Ding Wang et al. “Recent Progress in Reinforcement Learning and Adaptive Dynamic Programming for Advanced Control Applications”. In: *IEEE/CAA Journal of Automatica Sinica* 11.1 (2024), pp. 18–36. DOI: 10.1109/JAS.2023.123843.

[90] Lukas Glomb, Frauke Liers, and Florian Roesel. “A rolling-horizon approach for multi-period optimization”. In: *European Journal of Operational Research* 300.1 (July 2021), pp. 189–206. DOI: 10.1016/j.ejor.2021.07.043. URL: https://www.sciencedirect.com/science/article/pii/S0377221721006536.

[91] A.P. Reijns. *Aircraft maintenance scheduling using engine sensor data*. 2021. URL: https://repository.tudelft.nl/record/uuid:481ae77f-2b50-4bc9-8443-e1849a0f187d.

[92] *Optimizing flexible one-to-two matching in ride-hailing systems with boundedly rational users*. Accessed April 2025. URL: https://www.researchgate.net/publication/351049431_Optimizing_flexible_one-to-two_matching_in_ride-hailing_systems_with_boundedly_rational_users.

[93] Flightradar. *Live flight tracker - Real-Time flight tracker Map*. Accessed April 2025. URL: https://www.flightradar24.com/51.88,-9.57/6.

[94] Ben Chan. *Optimizing Fleet Assignment Decisions for Regional Airlines with Hybrid Electric Aircraft Uptake*. Feb. 2025. URL: https://www.gokcincinar.com/publication/c-2024-icas/.